3-11-2011

High Frequency Direction Finding Using Structurally Integrated Antennas on a Large Airborne Platform

Clair F. Corbin

High Frequency Direction Finding Using Structurally Integrated Antennas On a Large Airborne Platform

THESIS

Clair F. Corbin, First Lieutenant, USAF

AFIT/GE/ENG/11-06

DEPARTMENT OF THE AIR FORCE
AIR UNIVERSITY

AIR FORCE INSTITUTE OF TECHNOLOGY

Wright-Patterson Air Force Base, Ohio

AFIT/GE/ENG/11-06

High Frequency Direction Finding Using Structurally Integrated Antennas On a Large Airborne Platform

THESIS

Presented to the Faculty

Department of Electrical and Computer Engineering

Graduate School of Engineering and Management

Air Force Institute of Technology

Air University

Air Education and Training Command

In Partial Fulfillment of the Requirements for the

Degree of Master of Science in Electrical Engineering

Clair F. Corbin, B.S.E.E.

First Lieutenant, USAF

March 2011

AFIT/GE/ENG/11-06

High Frequency Direction Finding Using Structurally Integrated Antennas On a Large Airborne Platform

Clair F. Corbin, B.S.E.E.
First Lieutenant, USAF

Approved:

/signed/	8 Mar 2011
Maj Geoffrey A. Akers, PhD (Chairman)	date
/signed/	8 Mar 2011
Dr. Michael A. Temple (Member)	date
/signed/	8 Mar 2011
Dr. Julie A. Jackson (Member)	date

Abstract

Estimating the angle of arrival (AOA) of a high frequency (HF) signal in the 2-32 MHz band is challenging, especially if the antenna array is installed on a platform with dimensions on the order of one wavelength. Accurate AOA estimates are necessary for search and rescue operations and geolocating RF emitters of interest.

This research examines the performance of a high frequency direction finding (HFDF) system using structurally integrated (SI) antennas installed on an airborne platform which allows the aircraft structure to become the receiving element. Two simulated HFDF systems are analyzed at center frequencies of $f_c = 4$ MHz and $f_c = 11$ MHz. The relationship between the number of SI antennas used and the AOA accuracy is examined by simulating systems using $N_A = 4$, $N_A = 8$, and $N_A = 16$ antennas. Simulation is performed using the SI array to synthesize the pattern of a 3-loop cube, or vector, antenna. The maximum likelihood algorithm is used to produce AOA estimates.

An array of SI antennas, with a dedicated receiver channel for each antenna, produce more accurate AOA estimates at $f_c = 11$ MHz versus $f_c = 4$ MHz. The accuracy improves as N_A increases, regardless of center frequency. Linearly combining the outputs of the feed points to match an arbitrary antenna pattern in order to perform AOA estimation is an unnecessary step resulting in a suboptimal array for HFDF purposes.

Acknowledgements

My sincere thanks go to my advisor, Maj Geoff Akers, for his ability to keep me pointed in the right direction throughout this research effort and being there to entertain my numerous questions. You helped make this experience much more enjoyable than I could have hoped. I would also like to thank my committee members, Dr. Michael Temple and Dr. Julie Jackson, for their enthusiasm for this subject and their willingness to share their technical expertise.

This project would not have been possible without the support of my research sponsors, Dr. Charles Cerny and Dr. Philip Mumford, at AFRL. Thank you for ensuring I understood the purpose of this project and for putting me in contact with the outside agencies necessary for a successful outcome. I wish you the best with your future research efforts.

I would like to thank the researchers at BerrieHill Research Corporation, especially Dr. Tri Van, for all the assistance (and data) you provided during this effort. Your willingness to answer my numerous, often repetitive, questions on antenna data was a tremendous help in completing this effort.

Finally, I must acknowledge the tremendous sacrifice and support of my beautiful wife and our wonderful children. Without your love and unwavering support I would not have been able to complete this research. Thank you for always being there to melt away the stress with a smile and a hug. You are truly the source of my motivation.

Clair F. Corbin

Table of Contents

Page

List of Figures

List of Tables

List of Symbols

List of Abbreviations

High Frequency Direction Finding Using Structurally Integrated Antennas On a Large Airborne Platform

I. Introduction

1.1 Introduction

This research is part of a larger project managed by the Sensors Directorate of the Air Force Research Laboratory. The overall research goal is to extend accurate direction finding (DF) to the high frequency (HF) band using a single, airborne platform. The HF band is generally defined as spanning 3-32 MHz [1]. This research considers center frequencies of f_c= 4 MHz and f_c = 11 MHz which are in the HF band. There are several airborne assets currently used for DF missions, including an extensively modified C-135 aircraft shown in Fig. 1.1 used by the the US Air Force, the US Navy's EP-3E Aries II, and the RAF's NIMROD R1. The long wire antenna seen in Fig. 1.1 allows detection of HF signals but current DF capability of these aircraft in the HF band is not publicly available. As of 2002, a low-band DF subsystem for use on large airborne platforms was still under development [2].

Accurate DF allows for precise geolocation of the emitter. This is necessary for identifying and locating friendly, hostile, and unknown radio frequency emitters. Search and rescue operations are one common application of this technology. High frequency radios are commonly found on ships and may be used to transmit distress signals. By identifying and geolocating the source of the distress signal, rescuers will know where to focus their efforts, increasing the probability of survival.

This research explores the use of structurally integrated (SI) antennas combined with modern signal processing techniques, including superresolution techniques, as a possible way to extend the airborne DF capability to the HF band. Structurally integrated antennas result in the aircraft structure being used as the radiating element.

Figure 1.1: Variants of the RC-135 are currently used to detect and analyze signals throughout the EM spectrum. The long wire antenna is used to detect HF signals. (U.S. Air Force photo/Tech. Sgt. Deborah Davis)

Computer simulations are performed using various combinations of structurally integrated antennas and the results are analyzed to determine if the simulated ensemble provides accurate angle of arrival (AOA) estimates. The AOA is an estimate of the direction, in terms of elevation and azimuth, from which the signal is emitted; AOA is not an estimate of the *(x,y,z)*-coordinates of the emitter.

Two potential methods of combining and processing the outputs of the structurally integrated antennas are explored. One method assumes each antenna feed point has a dedicated, independent receiver channel. The second method uses the structurally integrated antennas to synthesize the pattern of a 3-loop cube antenna, also known as a vector antenna, which requires 3 receiver channels regardless of the number of antennas used, because each channel synthesized 1 loop of the cube antenna. The 3-loop cube antenna is discussed in more detail in Section 3.2.

This research builds on the work of Akers [3] and Dixon [4], which focused on using SI antennas for DF on unmanned aerial vehicle(UAV)-sized platforms. The center frequency of the incident signals in these previous works was to a higher frequency band ($f_c = 20$ MHz to $f_c = 100$ MHz) and the number of SI antennas was limited to $N_A = 4$. The dimensions of the UAV-sized aircraft with respect to wavelengths (λ) of the incident signals are shown in Table 1.1.

Table 1.1: Dimensions of UAV-sized aircraft with respect to signal wavelengths (λ) as used in previous research.

meters (approximate)	Wavelengths at 20 MHz	Wavelengths at 150 MHz
35 (wingspan)	2.33	17.5
14 (length)	0.93	7

1.2 Research Goals

The primary purpose of this research is to determine if an ensemble of SI antennas can function in a DF system on a large, airborne platform. The accuracy of azimuth AOA estimation using incident signals of two center frequencies, $f_c = 4$ MHz and $f_c = 11$ MHz, is used as the primary analysis measurement. The Maximum Likelihood Method (MLM) DF algorithm is used to generate the AOA estimates. A range of signal-to-noise ratios (SNR) are simulated to explore the effect of interference on the accuracy of the AOA estimates. The simulated SNR is achieved by adding complex, white Gaussian noise to each sample of the received incident signal.

A secondary goal is to determine the relationship between the number of SI antennas such a High Frequency Direction Finding (HFDF) system would require and the effect of input impedance and feed point location on the performance of the system. The results of this research will reveal the relationship between the location of SI antenna feed points, the number of feed points comprising the DF system, and resulting AOA estimation error.

1.2.1 Scope. The scope of this research is limited to evaluating a fixed number of SI antenna configurations for use in a DF system. The scope of this research is limited to:

1. Antenna radiating characteristics for a maximum of 16 SI antennas, whose radiated fields are provided by BerrieHill Research Corporation (BRC) for $f_c = 4$ MHz and $f_c = 11$ MHz,
2. Using a single-signal DF algorithm,
3. Ideal operational conditions, i.e. no atmospheric or multipath effects, no intentional jamming, perfectly calibrated DF system, etc.,
4. DF of a single, stationary emitter.

1.2.2 Assumptions. The purpose of this research is related to the feasibility of a system of SI antennas to perform as a HFDF system on an airborne platform. Optimization of the system is not addressed. The following assumptions are made throughout this research:

1. A single signal with known polarization is incident on the platform,
2. Noise is characterized as complex, additive, white Gaussian,
3. The true AOA of the incident signal is known exactly,
4. Environmental and operational conditions are ideal: atmospheric and multipath effects do not exist, and antennas and receivers are perfectly matched and calibrated.

1.3 Resources

The resources required to complete this research include:

1. simulated antenna radiation characteristics provided by BRC,
2. a copy of `Matlab`® software for performing the DF algorithm,
3. an 8 core workstation with 48 GB of RAM to facilitate parallel `Matlab`® processing and minimize computational time.

1.4 Overview

This thesis contains an analysis of two implementations of SI antenna ensembles to determine the feasibility for use in a HFDF system at two center frequencies, $f_c = 4$ MHz and $f_c = 11$ MHz. Statistical analysis of resulting AOA estimation errors is the primary method of reporting the results. Chapter II contains background on DF theory and details common techniques of AOA estimation as well as providing background information on SI antennas and one method used to determine where to place the antennas on a structure. Chapter III contains a description of the simulated antenna data used in this research, details the method used to estimate AOA, as well as providing the parameters used in the simulation environment. Chapter IV contains the results and analysis of the simulations. Finally, Chapter V presents the conclusions and recommendations for future research.

II. Background

Direction finding (DF) systems are used to determine the relative direction to an energy source (emitter) based on estimates of the angle of arrival (AOA) of an incident electromagnetic (EM) wave [4]. This chapter contains a review of the literature covering traditional methods used to perform DF such as amplitude and phase comparison, as well as modern signal processing techniques commonly applied to DF. Section 2.4 reviews the research of Penno and Pasala [5], including the Maximum Likelihood Method (MLM), which is used as the primary estimation technique in this research. Additional key components of this research, Structurally Integrated (SI) antennas and the Theory of Characteristic Modes (TCM), are described in Section 2.5.

2.1 Introduction

Applications of DF are numerous in both civilian and military environments and include tasks such as search and rescue, frequency management, tracking and recovery of stolen vehicles, military intelligence gathering, and homing systems, to include precision guided munition systems [6].

Advances in digital signal processing methods and the increase of computational power has led to improved DF system accuracy, as well as, relaxing of system design requirements. Antenna selection has especially benefited from these advances. Many early forms of AOA estimation required each antenna comprising the system to have identical radiation patterns. Overall, DF systems continue to grow in complexity. According to Schmidt [7], techniques used in DF systems usually fit into one of four categories:

1. Traditional beamsteering - Physically or electrically steering an antenna or antenna array with known main lobe (or beam) characteristics to maximum perceived power. The main lobe is defined by Balanis [8] as the radiation lobe containing the direction of maximum radiation. The direction of the main beam is

used to determine the AOA of an incident EM wave. Beamsteering is the basis of radar tracking systems.

2. Nullsteering - Similar concept as traditional beamsteering except a null is steered in the direction of maximum perceived power, which is then used to determine the AOA.

3. Computational Signal Processing - Computation of sensor voltages is used to determine AOA using statistical methods. DF algorithms are further broken down into classes such as correlation-based, eigen-structured, and root-finding. Capon, Bartlett, Pisarenko, MLM, and multiple signal characterization (MUSIC), are a few well-known DF algorithms commonly applied [9].

4. Interferometrics - Array of antennas used to estimate AOA through phase and amplitude comparison between antenna responses due to the incoming signal characteristics [6]. Interferometrics assumes all antenna elements are identical.

2.2 AOA Estimation Methods

Research related to AOA estimation has focused on robust DF algorithms relying on minimization of AOA estimation errors to achieve the most accurate results. Traditionally, DF systems have been developed under the assumption that only one signal is being radiated in the operating environment. Recent emphasis has been placed on development of systems and algorithms assuming multiple signals are present in the operating environment [7].

The essential components of a DF system are shown in Fig. 2.1 and include:

1. The antenna array to collect energy from the arriving signal of interest.

2. A receiving system consisting of one receive channel per antenna used to measure the response of the antenna array. Modern systems use analog-to-digital converters to represent signal measurements in digital format.

3. DF processor to extract information such as azimuth and elevation AOA.

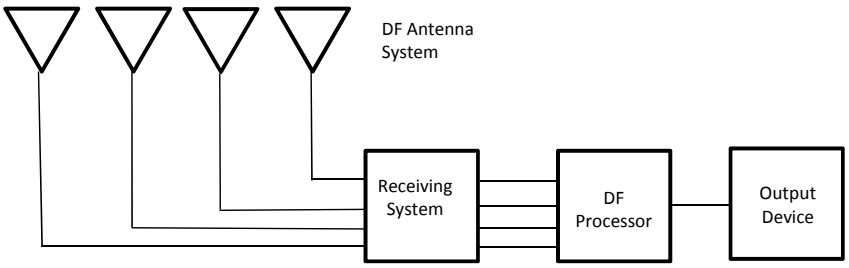

Figure 2.1: Essential components of a DF system.

4. User interface displaying information such as emitter location estimates and error ellipses on a geographical information system [6].

Techniques for estimating AOA include amplitude comparison, phase comparison, and time difference of arrival (TDOA). These techniques may be used individually, or in combination. TDOA is typically implemented using multiple platforms, as opposed to a single platform consisting of multiple antennas, and is not applicable to this research effort.

2.2.1 Amplitude Comparison. Amplitude comparison is often used in monopulse radar systems. Monopulse is also known as simultaneous lobe comparison [10]. The word "target", as used here, refers to the radiated signal of interest. The distinctive characteristic of an amplitude comparison antenna is a single reflector with a cluster of feed horns resulting in a beam pattern that is squinted on opposite sides of the axis and having a coincident phase center, as shown in Fig. 2.2.

A system using the amplitude comparison method collects wavefront information simultaneously from multiple, overlapping beams. AOA estimates obtained from an amplitude comparison system are based on the ratio of the magnitudes of the phasor voltage responses of the antenna array. AOA is referenced between boresight (main axis) and the target. It is often required that the antennas used for the amplitude comparison method produce identical beam patterns [4]. The radiated signal produces voltages that are in phase but have different amplitudes within each beam at the receiver. Received amplitudes are dependent on target AOA. The amplitude

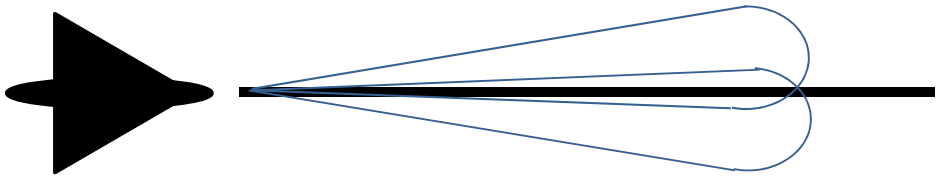

Figure 2.2: Squinted beam pattern used in amplitude comparison DF systems

comparison is a complex ratio such that

$$V_{DF} \equiv \frac{|\bar{v}_2| - |\bar{v}_1|}{|\bar{v}_2| + |\bar{v}_1|} = \frac{\Delta v}{\Sigma v}, \tag{2.1}$$

where V_{DF} is the voltage magnitude ratio of the sum and difference of system responses. A target on the boresight of the system results in equal voltage amplitudes and the ratio is zero. All the information required to determine the direction of the signal is contained in V_{DF} [10]. However, the AOA is not estimated directly from V_{DF}. An amplitude comparison system is characterized by a plot of V_{DF} versus AOA. The relationship between V_{DF} and AOA is approximately linear over some range of AOA depending on system characteristics. This nearly linear relationship allows an AOA estimate to be determined based on the measured ratio.

For a system of antennas having identical patterns, the antenna producing the strongest response is used to determine a coarse AOA estimate. Comparing amplitude responses of adjacent antennas provide refined AOA estimates. If the system has a dedicated receiver channel for each antenna, the amplitude responses can be measured simultaneously resulting in monopulse DF accuracies of 3.0 to 10.0 degrees [11]. Compared to the accuracy of other AOA estimation techniques, the performance of amplitude comparison DF systems is considered poor and is unable to provide an accurate estimate of the emitter range. Additionally, amplitude comparison systems are sensitive to multipath effects. The accuracy of amplitude comparison systems typically increases as the number of antennas increase and pattern beamwidth decreases [11].

2.2.2 Phase Comparison. Phase comparison, also known as phase interferometry, is another method of AOA estimation that is commonly used in monopulse radar systems [10]. In phase comparison monopulse systems, the antenna beams are parallel and identical. The phase centers are displaced slightly on each side of system boresight. The identical antenna beam pattern requirement remains. It is difficult to produce identical beams in practice due to differences in hardware and the difficulty in producing antennas with exact placement of phase centers. Modern digital signal processing techniques can compensate for some of these shortcomings in design and manufacture [3].

Antennas that are not identical cause both amplitude comparison and phase comparison systems to become hybrid to some extent. Elements of phase comparison exist in an amplitude comparison system and elements of amplitude comparison exist in a phase comparison system. These effects can generally be considered negligible [10]. Careful calibration of DF systems is required to ensure maximum accuracy in estimating AOA.

Phase comparison systems measure the relative phase response between antennas in an array. The phase response is proportional to the incident wave AOA. The geometry of a two-element phase interferometer is shown in Fig. 2.3. The phase difference between the response of each antenna is proportional to the propagation path length difference, a. The difference in propagation path length results from antenna one being physically located closer to the emitter and receiving the planar phase front earlier in time than antenna two. The path length difference for a pair of antennas separated by distance d is

$$a = dsin(\theta)(\text{units of length}). \tag{2.2}$$

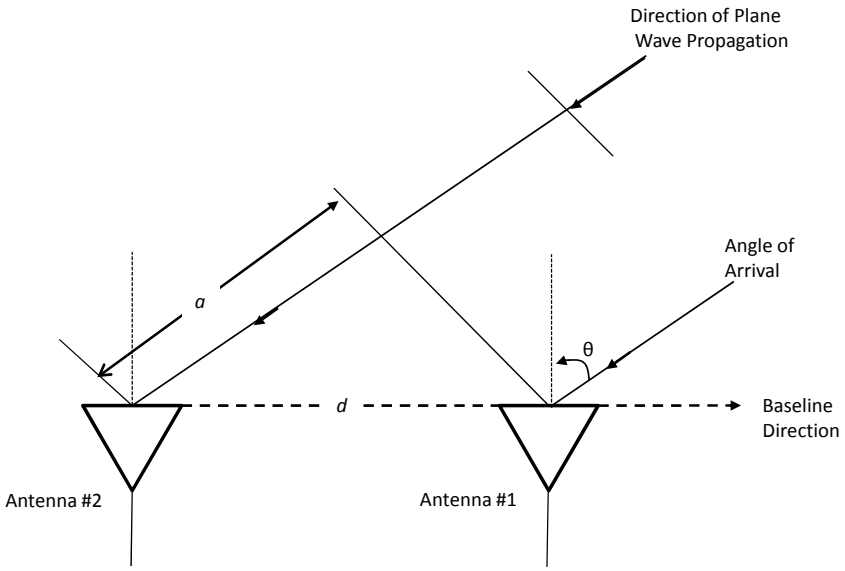

Figure 2.3: Geometry of two antenna phase comparison DF system

The relative electrical phase difference, $\Delta\phi$, is mapped from AOA for antenna separation d and incident wavelength λ by

$$\Delta\phi = \left(\frac{2\pi d}{\lambda}\right) sin(\theta)(\text{radians}). \tag{2.3}$$

The physical separation, d, of antenna elements in a phase interferometry antenna array must be chosen carefully. When d is greater than the wavelength of the incident signal, the phase difference will be sufficiently large to allow for phase difference resolution, however, the phase difference will be ambiguous. Ambiguities, also called grating lobes, occur whenever d is larger than $\frac{\lambda}{2}$ [6]. Multiple AOAs can produce the same phase difference in multiples of 2π [3]. Nonuniform placement of antennas within an array may be used to resolve such ambiguities. By spacing some antenna elements in the array less than $\frac{\lambda}{2}$ apart, the (smaller) phase difference measured by these antennas may be used to resolve the ambiguity and determine an accurate AOA [6]. Not all system design requirements allow for such spacing due to having a limited

number of antenna elements or limitations on the extent of the antenna array. Such is the case when airborne platforms are considered for high frequency DF systems.

The phase comparison method of AOA estimation can achieve a 10:1 increase in accuracy over the amplitude comparison method spanning the same range of frequencies, and phase comparison systems are relatively resistant to multipath effects [11]. Accuracy is dependent upon identical antenna responses and careful system calibration, which may eliminate phase comparison systems from consideration in some applications [4].

2.2.3 Signal Processing Techniques. Amplitude and phase comparison methods of AOA estimation have been developed under the assumption that a single signal is being received by the DF system. In actual operation, multiple sources may be radiating. Direction finding systems developed using the single source assumption may operate effectively in a multi-source environment if one of the following conditions is true [7]:

1. The signals are well separated in frequency; i.e. by more than the reciprocal of the observation time.
2. The signals are well separated in time; i.e. by more than the reciprocal of the bandwidth of the data.
3. The signals are well separated in direction of arrival; i.e. by more radians than the reciprocal of the diameter (in wavelengths) of the array collecting data.

If the system is operating in an environment where signals from several sources with overlapping frequency, overlapping time, and AOAs within an array beamwidth are received, more robust processing techniques are required for accurate AOA estimation.

Recent DF research has focused on signal processing techniques. The expansion of computational power has allowed for the development and implementation of advanced signal processing techniques and algorithms that previously were too complex

for real-time system application. Additionally, the need for electrically or mechanically scanned beams has been diminished by array processing techniques [4]. The implementation of superresolution algorithms, such as MLM, MUSIC, and Estimation of Signal Parameter via Rotational Invariance Techniques (ESPRIT) has resulted in an increase in AOA estimation accuracy and a relaxing of the requirement for identical antennas in traditional DF systems [3].

Butler matrix beamforming is an array signal processing technique that has been explored for AOA estimation on an airborne platform [4]. A multi beam, multi channel receiver is used to implement either amplitude or phase comparison AOA estimation, as presented above, without the use of electrically or mechanically scanned beams.

A Butler matrix beamforming device may be used with either linear or circular antenna arrays. The Butler matrix was first discussed by Butler in 1960 [12] and is summarized here.

An $n \times n$ element Butler matrix, when connected to an n-element array, produces the correct excitation for the corresponding spatially-orthogonal set of n possible phase modes [4]. The Butler matrix has the form of

$$\mathbf{B} = \frac{1}{n} \begin{bmatrix} \varepsilon^0 & \varepsilon^0 & \varepsilon^0 & \cdots & \varepsilon^0 \\ \varepsilon^0 & \varepsilon^1 & \varepsilon^2 & \cdots & \varepsilon^{(n-1)} \\ \varepsilon^0 & \varepsilon^2 & \varepsilon^4 & \cdots & \varepsilon^{2(n-1)} \\ \vdots & \vdots & \vdots & \vdots & \vdots \\ \varepsilon^0 & \varepsilon^{(n-1)} & \varepsilon^{2(n-1)} & \cdots & \varepsilon^{(n-1)(n-1)} \end{bmatrix} \tag{2.4}$$

where

$$\varepsilon = \exp\left(-j\frac{2\pi}{n}\right) \tag{2.5}$$

and n is the number of elements in the antenna array. Given an input vector of excitation voltages $\bar{\mathbf{v}}$ and output vector $\bar{\mathbf{u}}$, the Butler transformation is expressed as

$$\bar{\mathbf{u}} = \mathbf{B}\bar{\mathbf{v}} \tag{2.6}$$

where output vector $\bar{\mathbf{u}}$ contains the n modal output voltages, M_i for $i = 0, 1, 2, \ldots, (n-1)$. This allows 2.6 to be expressed as

$$\begin{bmatrix} M_0 \\ M_1 \\ M_2 \\ \vdots \\ M_{n-1} \end{bmatrix} = \frac{1}{n} \begin{bmatrix} \varepsilon^0 & \varepsilon^0 & \varepsilon^0 & \cdots & \varepsilon^0 \\ \varepsilon^0 & \varepsilon^1 & \varepsilon^2 & \cdots & \varepsilon^{(n-1)} \\ \varepsilon^0 & \varepsilon^2 & \varepsilon^4 & \cdots & \varepsilon^{2(n-1)} \\ \vdots & \vdots & \vdots & \vdots & \vdots \\ \varepsilon^0 & \varepsilon^{(n-1)} & \varepsilon^{2(n-1)} & \cdots & \varepsilon^{(n-1)(n-1)} \end{bmatrix} \begin{bmatrix} V_0 \\ V_1 \\ V_2 \\ \vdots \\ V_{n-1} \end{bmatrix}. \tag{2.7}$$

Mode 0 (M_0) is produced by exciting all elements in the array in-phase and Mode 1 (M_1) is produced by exciting the elements such that there is a phase progression of one wavelength. Mode i is produced by exciting the elements such that there are i wavelengths of phase progression and 360° of phase difference between adjacent elements.

A linear antenna array connected to a Butler matrix beam former is capable of providing up to 180 degrees of coverage for AOA estimation but requires that the incident wave frequency either be known or estimated [4].

2.3 Sources of Error in AOA Estimates

Many factors affect AOA estimation accuracy. Careful consideration of error sources and mitigation methods must be taken during the design of a DF system. The following is a list of common error sources in DF systems [4, 6]:

1. Emitter-to-receiver geometry - system geometry can greatly affect AOA estimation accuracy. Best accuracy is obtained when the emitter is in the center of an equilateral triangle of receivers.
2. Signal-of-interest frequency - AOA accuracy degradation is inversely proportional to frequency, i.e. estimate of higher frequency emitter AOA is more accurate than low frequency emitter estimates. Most wideband arrays span a range

of frequencies such that estimated AOA is possible for emitters with frequencies between 100-500 MHz or 500-4000 MHz for VHF/UHF systems, for example.

3. Signal-to-noise ratio (SNR) - SNR is affected by emitter power, propagation distance and propagation medium, as well as atmospheric and man made noise such as power lines.
4. Instrumentation - System noise may be increased by manufacture defects or errors in the implementation of the AOA estimation techniques. System noise figure errors may be manifested in a number of ways:
   (a) Lowering effective SNR,
   (b) Creation of amplitude/phase imbalance in the receiver channels,
   (c) Induce time/frequency errors,
   (d) Calibration inaccuracies.
5. Observation - Errors may be made at the operator interface. Human factors play a significant role in observation-induced errors.

This is not intended to be an exhaustive list of error sources in AOA estimation and DF systems. There are many additional sources of error cited throughout the literature, including quantization error due to the resolution of the analog to digital converter (ADC) used in digital receivers. This list highlights a few key error sources that should be considered during system design.

2.4 Comparison of Three AOA Estimation Techniques

Prior DF research examines antenna ensembles on unmanned aerial vehicles (UAV) for DF purposes. The MLM algorithm implemented in previous research efforts is based on an algorithm developed by Penno and Pasala [5]. A summary of their findings is presented here.

Penno and Pasala demonstrate that AOA estimates can be obtained from a multiarm spiral antenna. A multiarm spiral antenna has a single aperture and multiple

ports. Multiple modes of excitation are achievable from such an antenna. If a multi-arm spiral antenna can be employed for AOA estimation as part of a DF system, the amount of physical space required for such a system can be reduced and DF systems can potentially be placed on airborne platforms.

Other changes may be possible if accurate AOA estimates are realizable. A multi mode antenna is typically followed by a mode former, such as the Butler matrix presented earlier, and phase comparison of the different modal voltage outputs are used to estimate the azimuth of the incident radiation. The research of Penno and Pasala attempts to eliminate the need for the mode former and replace it with a multi channel digital receiver, saving cost, weight, and bulk [5].

A key assumption is that the N-terminal output voltages of the antenna are coupled into an N-channel receiver. The development of the MLM algorithm is aimed to operate on the N signal voltages to produce estimates of azimuth and elevation. The approach allows for modern parameter-based estimation techniques of AOA to be applied in addition to traditional comparison methods. A development of the comparison method, the MLM algorithm, and the MUSIC algorithm are presented. All three methods are simulated and results are compared.

2.4.1 Phase Comparison Method. The comparison method, as presented previously, uses the discrete Fourier transform (DFT) to transform the N terminal voltages to N modal outputs, for which closed-form expressions exist and are derived by the authors. The phase of the mode-1 signal is used to obtain a coarse estimate of azimuth. Recognizing that higher rates of phase change with respect to azimuth produce more accurate estimates, a higher-order mode is desirable. The mode-1 phase is used to resolve ambiguities associated with higher-order phase. Amplitude comparison of the modal output voltages is used for elevation angle estimates. The modal output voltage ratios are treated as a look-up table to estimate elevation angle. As presented previously, areas with small amplitude ratio change produce less accurate elevation estimates.

2.4.2 The Maximum Likelihood Method. The MLM algorithm may be applied to the terminal voltages directly or to the modal output voltages obtained after taking the DFT of the terminal voltages. Application of the MLM AOA estimation algorithm requires an array of steering vectors for each potential emitter location. The array is comprised of steering vectors resulting from ideal received terminal voltages (E_h and/or E_v) for all possible emitter locations. Each steering vector contains the output of the multimode antenna excited by a unit-amplitude plane wave for a particular AOA [5]. The MLM algorithm correlates a received noisy signal vector with each possible steering vector. The AOA associated with the steering vector most parallel to the received vector is determined to be the estimated AOA of the incident signal [4]. Noise is considered zero-mean Gaussian for the simulations performed by Penno and Pasala. The accuracy of the MLM algorithm is dependent upon the indexing of the steering vector, that is, the step size between possible AOAs contained in the array. The method of interpolation among possible steering vectors when the correlation does not result in an exact match also affects the accuracy of the estimation [7].

2.4.3 Multiple Signal Classification (MUSIC). Penno and Pasala also examined the MUSIC approach to AOA estimation. MUSIC is an algorithm based on a signal subspace approach. MUSIC is designed to operate with DF systems in a multiple-signal environment. The algorithm may be applied to either the output terminal voltages directly or the modal output voltages. MUSIC requires the data space to be decomposed into a signal-plus-noise subspace and a noise subspace. It must be recognized that the steering vector corresponding to the true direction of arrival is orthogonal to the noise subspace [5]. The algorithm consists mostly of geometric calculations such as vector dot products, matrix transformations, and projections onto subspaces [7]. The accuracy of AOA estimates from MUSIC, as in MLM, is dependent upon the indexing of the steering vector array and the interpolation method used.

2.4.4 Analysis of Results. The comparison method tends to breakdown for elevation-angle estimates when AOA is greater than 65 degrees. This breakdown is

potentially due to the "flat" voltage ratios the comparison method uses to estimate the elevation angle in this region. A "flat" voltage ratio indicates that (2.1) has started to converge, i.e. a change in AOA does not produce a significant change in V_{DF} for AOAs greater than 65 degrees using the multiarm spiral antenna [5]. The MLM and MUSIC algorithms provide comparably more accurate estimates in the same region of elevation AOA. The three methods examined result in poor elevation-angle estimates near the horizon, i.e. near 90 degrees elevation AOA. This performance is attributed to the presence of nulls for all modes of operation near 90 degrees [5]. Penno and Pasala conclude that MLM and MUSIC algorithms extend acceptable elevation-angle estimate coverage from 0 to 60 degrees. The three methods provide similar azimuth AOA estimates. Azimuth is the only angle estimate required in some applications, including location estimation [13]. The traditional comparison method is shown to be successful when azimuth AOA is sufficient.

An accurate steering vector and a properly calibrated DF system are key to achieving the most accurate results [5]. Despite showing accurate AOA estimates are possible from a multiarm spiral antenna, Penno and Pasala acknowledge that a long baseline interferometer will produce more accurate estimates [5].

2.5 Structurally Integrated Antennas and the Theory of Characteristic Modes

Electrically small antennas are known to be inefficient when used for wideband operation. Wideband operations generally require antennas with electrical sizes of one-quarter wavelength or more [14]. The use of SI antennas is one method that has been explored to overcome these inefficiencies. The small antenna may be viewed as a probe used to excite a current on the surface of the structure. The structure is usually not considered electrically small and may be effectively used as a radiator [15]. Granger [16, 17] demonstrated in the early 1950s that the structure of an aircraft could be used to radiate signals in a predictable manner when the wavelength is on the order of twice the wingspan. Structural antennas have also been proposed, and

demonstrated, for communication purposes on aircraft [18], and in more recent times, on naval vessels [19, 20]. Akers [3] and Dixon [4] examined DF using structurally integrated antennas on aircraft with maximum structural extent on-the-order of one wavelength with favorable AOA estimation results. The difficulty in applying Si antennas stems from the low input impedance of the feeds and the resulting poor radiating characteristics. The low input impedance is a result of the long wavelength with-respect-to the size of the radiating structure.

The Theory of Characteristic Modes was introduced by Garbacz and Turpin [21] in 1971. The theory was refined by Harrington and Mautz [22] later that year and applied to bodies of revolution and wire objects [23]. TCM has since been applied to determining antenna feedpoint location on aircraft and ships. The TCM states that multiple, orthogonal transmit and receive channels may be realized on a single structure, analogous to modes in a waveguide. Near optimal arrangement of small antennas may be determined from the mode current or voltage distribution on the surface of the structure, as seen in Fig. 2.4. TCM may be used to significantly improve the efficiency of the small antennas by placing the antennas near a maximum of the characteristic mode of the structure. Characteristic modes may also be used to synthesize a desired antenna pattern [15].

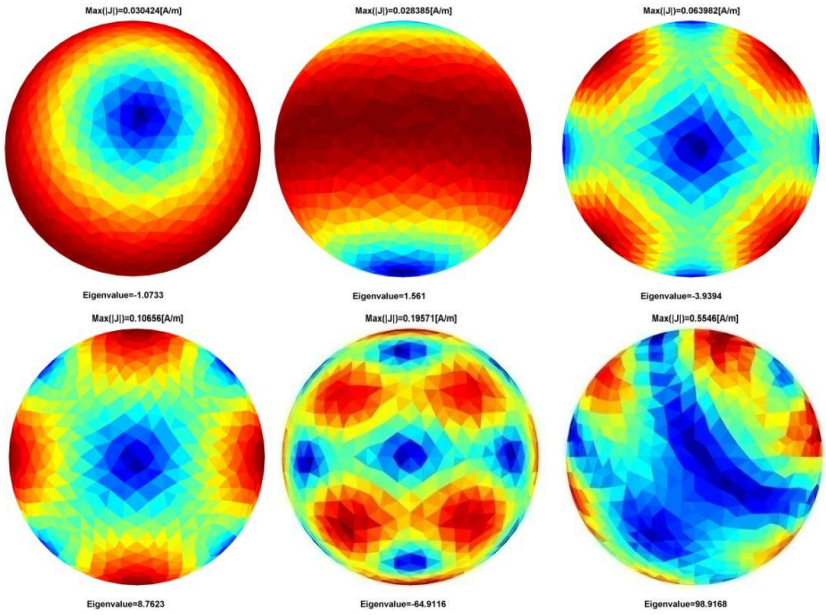

Figure 2.4: An example of surface current distributions similar to those used to determine near optimal feed point placement using the Theory of Characteristic Modes [15]. Image used with permission by Dr. Van in an email dated 12/30/2010.

III. Methodology

Implementing a High Frequency direction finding (HFDF) system on an airborne platform is challenging due to the size of the structure with respect to the wavelength of the complex incident signals. In the HF frequency band (3 MHz to 32 MHz) the aircraft structure is on the order of, or smaller than, one wavelength. Beamforming using a linear array of half-wavelength antenna elements is not possible in this scenario. The problem to be solved is one of creating a receive array using the aircraft as the receiving structure and then using this array to estimate the angle of arrival (AOA) of a signal of interest.

3.1 Research Goals

The goals of this research are to determine the relationship between the number of feed points comprising the direction finding (DF) system, the location of structurally integrated antenna feed points, and the resulting AOA estimation error when using a conceptual HFDF system on a large airborne platform. Given simulated, radiated, far-field data, computer simulations conducted in `Matlab`® are the primary method used to examine these relationships. The research goals were achieved by taking the following steps:

- Implementing the maximum likelihood method (MLM) AOA estimation technique for center frequencies of $f_c = 4$ MHz and $f_c = 11$ MHz incident waves
- Determining the relationship between AOA estimation error and number of feed points comprising the DF system
- Determining the four feed point locations resulting in minimum estimation error for each frequency

A platform-based spherical coordinate system is used in this research, as illustrated in Fig. 3.1, where the nose of the aircraft acts as the origin of the coordinate system. To limit the computational complexity, the elevation AOA is set to aircraft waterline, $\theta = 90$ degrees, for all simulations conducted in this research. In the HF

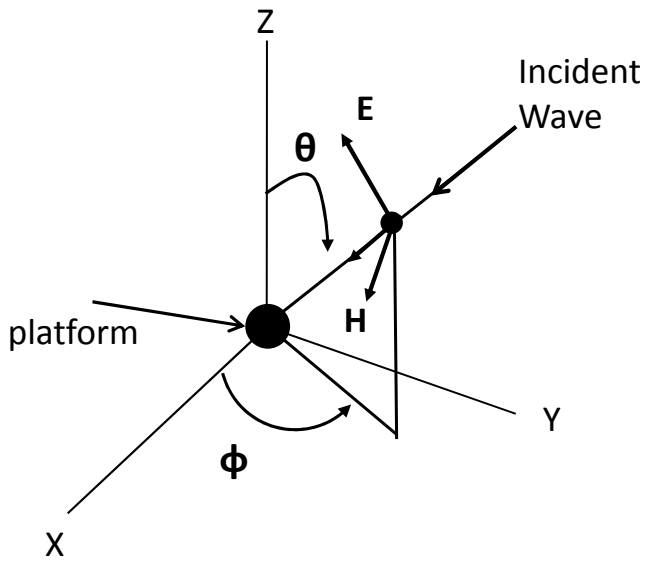

Figure 3.1: Platform based spherical coordinate system with azimuth and elevation AOA.

range, it is expected that skywaves, waves reflected from the Earth's atmosphere, will be received by an airborne system. Elevation angles ranging from 0° to 180° can realistically be expected in the operating environment. Azimuth AOA are simulated from 0° to 345° in 15° increments. Only azimuth AOA estimation for horizontally, or ϕ-polarized incident plane waves are considered. For airborne applications, aircraft have little vertical extent, and therefore poor response to vertically polarized incident fields.

3.2 Antenna Data

Antenna data for use in the simulations are provided by BerrieHill Research Corporation (BRC). BRC has been awarded a contract by the Air Force Research Laboratory Sensors Directorate (AFRL) to determine the optimal feed point locations on a large conducting airframe. The data provided by BRC includes complex far-field radiated voltages, physical feed locations, complex input impedance, and induced complex current for each feed point. The data is provided for a total of 16 feed points based on both $f_c = 4$ MHz and $f_c = 11$ MHz complex incident signals. The physical location of the feed points is dependent on the frequency of interest; the location of

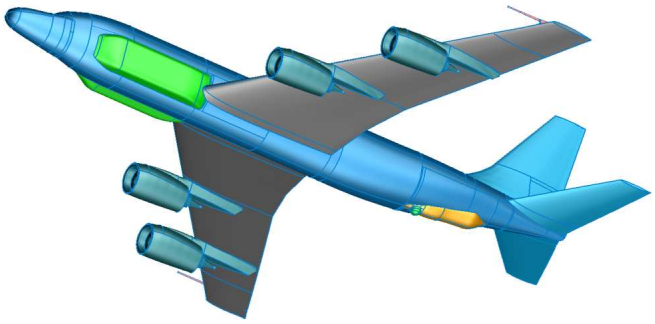

Figure 3.2: Simplified model of large aircraft used for electromagnetic simulations to determine optimal feed point locations [15]. Image used with permission by Dr. Van in an email dated 12/30/2010.

the feed points for the $f_c = 4$ MHz data are not the same as the location of the feed points for the $f_c = 11$ MHz data.

BRC used a simplified model of the aircraft to determine the optimal feed point locations. The model is simplified by removing the numerous blade antennas typically found on the fuselage of such an aircraft in order to reduce computational burden. Before removing the blade antennas, BRC verified that the blade antennas had minimal impact on the surface currents in the simulations [15]. The model is shown in Fig. 3.2. Additionally, it is assumed that the aircraft is perfectly conducting.

Two sets of data have been provided for each center frequency. One data type treats each of the 16 feed points as having an independent receiver channel. One receiver channel is required for each feed point used in the DF system. Simulations are conducted using combinations of $N_A = 4$, $N_A = 8$, and $N_A = 16$ feed points and the AOA estimation performance is analyzed. This data type will be referred to as individual feed data.

The second data type contains antenna data synthesized to closely match the radiation pattern of a 3-loop cube antenna, also known as a vector antenna. This data type will be referred to as synthesized data. A cube antenna is comprised of 3 identical orthogonal loops as depicted in Fig. 3.3. The loops are referenced as the XY-

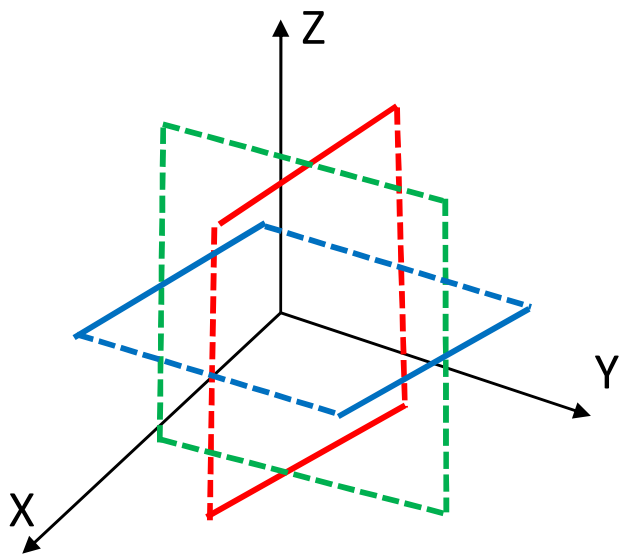

Figure 3.3: Cube antenna consisting of three identical orthogonal square loops.

loop, parallel to the xy-plane; the YZ-loop, parallel to the yz-plane; and the XZ-loop, parallel to the xz-plane. The data are generated by exciting combinations of $N_A = 4$, $N_A = 8$, or $N_A = 16$ feed points on the surface of the platform. The synthesized data are valid for the primary (xy-plane) cut, i.e. aircraft waterline. The synthesized cube antenna data set requires three receiver channels, each channel synthesizes one loop of a cube antenna (XY, XZ, YZ).

The antenna feed locations have been determined using the theory of characteristic modes (TCM) as described in Section 2.5. Short monopoles used as feeds are placed at the maximum of the characteristic voltage on the structure as determined by calculating the characteristic modes. A detailed explanation of the process used to determine feed locations is contained in [15]. The feed point input impedance is small, often $\ll 1\ \Omega$, resulting in poor radiating characteristics for the frequencies of interest. The poor radiating characteristics are a result of low input impedances and are to be expected due to the poor mutual coupling between the aircraft structure and the feeds as noted by Granger [17] and detailed by Tanner [18].

3.3 The Maximum Likelihood Method for AOA Estimation

The MLM algorithm is used as the primary AOA estimator for this research. The MLM process is well-known and accepted as a valid algorithm for DF applications. The MLM algorithm is based on maximizing the likelihood of a steering vector being matched to the received data. Conceptually, the MLM AOA algorithm correlates a received noisy vector with each steering vector in an array manifold. The lag of the correlation is then used to determine the estimated AOA.

Each complex incident signal is coherently integrated over 1024 samples in order to increase SNR. The received signal contains both amplitude and phase data. According to Friedlander [24], in a single signal model with no multipath effects, all of the direction information is contained in the phase, not the amplitude. The sampling frequency is set at 10 times the frequency of the signal of interest. The number of samples translates to an integration time of T_i= 25.6 μseconds at f_c = 4 MHz and T_i = 9.31 μseconds at f_c = 11 MHz. A total of N_I= 200 iterations of the MLM algorithm are performed for each simulated AOA in order to provide a robust Monte Carlo simulation. The final reported AOA estimate and associated error statistics for each AOA is an average of all Monte Carlo observations for a given AOA.

Source code originally designed for use with a multiarm spiral antenna DF system described by Penno and Pasala [5] and used previously by Akers [3] and Dixon [4] has been adapted for use in this research. The code was previously used for AOA estimation research using SI antennas on UAV-sized platforms. The `Matlab`® code for modeling and simulation of the proposed HFDF system is an adaptation of these previous works. The MLM is a computationally intense algorithm, and since the goal of this research is to evaluate whether the proposed DF system is feasible, a single, stationary emitter model is used in all simulations. This greatly reduces the computation time required to complete this research effort.

3.3.1 Array Manifold. The array manifold is a key component necessary to accurately estimate the AOA using MLM. The array manifold may be visualized as

a look-up table of steering vectors. The steering vector is the ideal complex response, i.e. terminal voltage (V_r) for the individual feed data or far-field radiated voltage (E^{rad}) in the synthesized data, of the SI antenna array to a given signal arriving from a given direction (AOA). The steering vectors are ideal in the sense that the response is not corrupted by noise, and the exact AOA is known. The steering vectors contain an entry for each feed point for a given AOA for the individual feed data. The steering vectors contain an entry for each synthesized loop of the cube antenna for a given AOA for the synthesized data.

The array manifold is indexed in one degree increments in both azimuth and elevation. Azimuth angles from 0° to 359° are included in the array manifold and elevation angles from 0° to 179° are included. In all simulations, the elevation AOA of the simulated complex incident signal is set equal to 90°, known as aircraft waterline. The array manifold for the individual feed data has size $360 \times 180 \times N$ where N is the number of feed points comprising the HFDF system being simulated. HFDF systems comprised of $N_A = 4$, $N_A = 8$, and $N_A = 16$ feed points are simulated. The array manifold for the synthesized data has size $360 \times 180 \times 3$. Combinations of $N_A = 4$, $N_A = 8$, and $N_A = 16$ feed points are used to closely match the pattern of the cube antenna. Researchers at BRC determined which feed points to combine in order to achieve the match.

3.3.2 Received Voltage via the Reciprocity Theorem. The antenna data contain the radiated far-field voltages for each feed point or synthesized loop of a cube antenna. The steering vectors and array manifold are comprised of the complex terminal voltage response to the received signal. The received voltage at each feed point is determined by applying the reciprocity theorem as outlined in a research note by Van [25] using the radiated far-field voltages provided by BRC. The received voltage is defined as

$$V_r = -\frac{j4\pi}{k_o \eta_o I_o} E^{rad} e^{-j\vec{k}^{inc} \cdot \vec{R}_o} \ , \tag{3.1}$$

where $k_o = \frac{2\pi}{\lambda}$ is the freespace wavenumber, $\eta_o = 376.73$ (ohms) is the freespace impedance, I_o (amps) is the complex current at the feed point, E^{rad} (volts) is the radiated far-field voltage, which accounts for the directive gain of the feed point by appropriately scaling the unit amplitude plane wave $e^{-j\vec{k}^{inc}\cdot\vec{R}_o}\left(\frac{\text{volts}}{\text{meter}}\right)$ where $\vec{R}_o$ (meters) is the feed point location in space and $\vec{k^{inc}}$ is the incident wave vector defined by (3.2) where (θ_i, ϕ_i) are the incident angles

$$\vec{k}^{inc} = k_o \left(\sin\theta_i \cos\phi_i, \sin\theta_i \sin\phi_i, \cos\theta_i\right). \tag{3.2}$$

The reciprocity theorem is applied directly for the DF system made up of independent feed points. The reciprocity theorem is not able to be applied directly to the synthesized data. The exact method used to linearly combine the far-field voltages of the individual feed points to produce the synthesized data was not available before this research effort concluded. The simulations using the synthesized data were completed using the far-field radiated voltage, not a received voltage value. Due to the differences in the types of data used to generate the complex incident signal, the results cannot be compared directly.

3.3.3 Development of the MLM AOA Estimation Algorithm. The ideal voltage output vector, or steering vector, may be expressed as

$$\vec{V} = [v_1, v_2, \cdots, v_N]^T = \vec{g}, \tag{3.3}$$

where v_1 to v_N is the received voltage at each feed point in the HFDF system and $\vec{g}$ denotes the steering vector.

The received voltage, V_r, defined in (3.1) is used to scale a sinusoidal signal which, when combined with the complex, additive, white Gaussian noise (AWGN), becomes the complex, received incident signal

$$\vec{x}[k] = V_r e^{j2\pi \frac{f_c}{f_{samp}} k} + \vec{n}[k], \tag{3.4}$$

where f_{samp} is the sampling frequency, k is the discreet sample number, and $\vec{n}[k]$ is the zero-mean, complex AWGN vector with covariance C_n.

The probability density function (pdf) of the received signal $\vec{x}$ is Gaussian with a mean of $\vec{V}(\theta_0, \phi_0)$ and covariance C_n, such that

$$f_X\left(\vec{x}|\theta_0, \phi_0\right) = \frac{e^{-\left(\vec{x}-\vec{V}(\theta_0,\phi_0)\right)^H C_n^{-1}\left(\vec{x}-\vec{V}(\theta_0,\phi_0)\right)}}{\pi^N |C_n|}. \tag{3.5}$$

For a given received signal, $\vec{x}_0$ with the values to be estimated as variable parameters (θ, ϕ), the likelihood function is

$$L\left(\vec{x}_0|\theta, \phi\right) = \frac{e^{-Q}}{\pi^N |C_n|}, \tag{3.6}$$

where

$$Q = \left(\vec{x_0} - \vec{V}(\theta, \phi)\right)^H \left[{C_n}^{-1}\right] \left(\vec{x_0} - \vec{V}(\theta, \phi)\right). \tag{3.7}$$

The estimates of the parameters θ_0, ϕ_0 are the values (θ, ϕ) that maximize (3.6), which is the same as the minimization of Q. Using a process described by Penno and Pasala [5], it can be shown that the minimization of Q may be reduced to maximizing the surface Q_2 to determine the AOA estimate, where Q_2 is defined as

$$Q_2 = \frac{|\vec{x}_0^H C_n^{-1} \vec{g}|^2}{\vec{g}^H C_n^{-1} \vec{g}}. \tag{3.8}$$

The noise is modeled as complex AWGN, so the covariance matrix is given by

$$C_n = E(\vec{n}\vec{n}^H) = \sigma^2 I \tag{3.9}$$

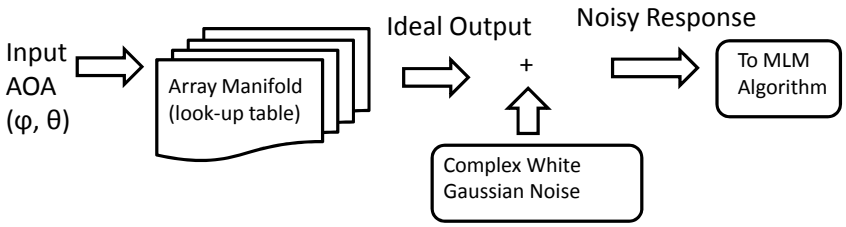

Figure 3.4: Graphical representation of complex incident signal generation process.

so that the Q_2 surface is given by

$$Q_2 = \frac{|\vec{x}_0^H \hat{g}|^2}{\sigma^2} \tag{3.10}$$

where

$$\hat{g} = \frac{\vec{g}}{\|\vec{g}\|}. \tag{3.11}$$

The AOA estimates reported in this research are based on the expected value of the Q_2 surface, $E[Q_2]$, defined as

$$E[Q_2] = \frac{\hat{g}^H R_x \hat{g}}{\sigma^2}. \tag{3.12}$$

3.3.4 Signal Generation. An idealized signal model is used in this research and closely matches the models used in previous research efforts [3, 4]. The complex incident signal is generated using the ideal steering vector for the AOA being simulated. Zero-mean, complex, AWGN is added to each sample of the signal to achieve a user-defined SNR. A detailed description of SNR is contained in Section 3.3.5. The autocorrelation of the noisy signal is then input to the MLM algorithm and an estimated AOA is determined. A graphical representation of the signal generation process is shown in Fig. 3.4.

This signal model produces results based on a "best-case scenario". The array response is known exactly for the simulated AOA as a result of the steering vectors

being used to generate the complex incident signal. All simulated AOAs are chosen such that no interpolation is required, that is, whole-number values are selected as simulated AOAs, eliminating the granularity of the array manifold as a source of estimation error. Without the addition of complex AWGN, the complex incident signal and the steering vectors are identical.

The complex incident signal is composed of in-phase and quadrature (I-Q) data components. The complex signal contains amplitude and phase data at each antenna feed point. The phase reference of the feed point configuration is set to the nose of the aircraft which is the origin of the coordinate system. This method requires an appropriate phase delay for each of the feed points and results in the phases "lining up" so they may be integrated coherently. The phase delay is accounted for in the BRC-provided far-field data.

Additionally, as a result of using the steering vectors as the basis for the complex incident signal, the array manifold is ideally calibrated. Array manifold calibration is a common topic in the literature because the calibration plays a significant role in the accuracy of the AOA estimates.

3.3.5 Signal-to-Noise Ratio. The SNR is defined as the average power in the received signal divided by the average noise power as shown in (3.13), where V_r is the complex received voltage defined in (3.1), and σ^2 is the noise variance which is equal to the noise power because the simulated noise is modeled as zero-mean,

$$SNR = \frac{|V_r|^2}{\sigma^2}. \tag{3.13}$$

Complex AWGN is generated using the pseudo-random number generator, *randn*, in `Matlab`® . The resulting noise vector is added to the ideal received complex voltage vector (steering vector for simulated AOA) as in (3.4) to achieve an average SNR defined per signal sample. The noise includes both external environmental noise as well as internal receiver noise. The magnitude of the complex AWGN is determined based

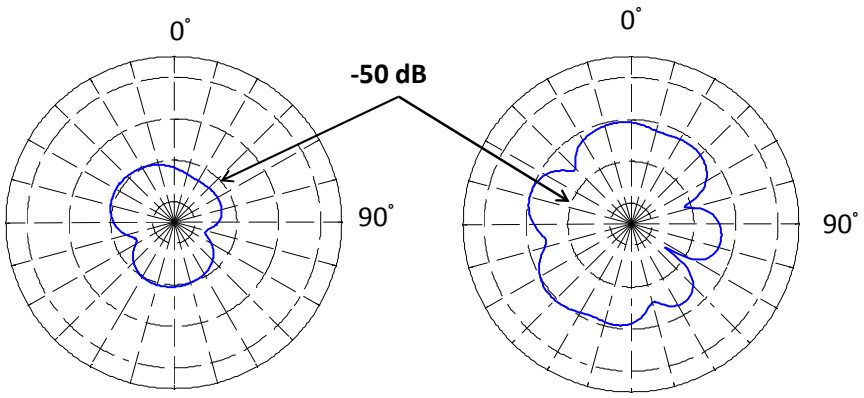

Figure 3.5: Two representative gain patterns for the SI feed points: (left) feed point #1 for the $f_c = 4$ MHz HFDF system, and (right) feed point #1 for the $f_c = 11$ MHz HFDF system.

on the average power of the received signal. The signal power is averaged over all possible azimuth angles. The magnitude of the noise required to achieve the desired SNR is calculated as

$$\sqrt{\frac{(P_{avg}) \cdot 10^{\left(\frac{-SNR_{dB}}{10}\right)}}{2}} \tag{3.14}$$

where SNR_{dB} is the user-defined per-sample SNR expressed in decibels and P_{avg} is the received signal power averaged over all azimuth angles defined as

$$P_{avg} \approx \frac{1}{N_A} \cdot \sum_{i=1}^{N} v_i^2, \tag{3.15}$$

where N_A is the number of feed points, and v_i is the voltage at the ith feed point averaged over all azimuth angles.

This method for generating the complex AWGN ensures the antenna gain patterns are accounted for in the simulations. The antenna gain patterns, examples of which are shown in Fig. 3.5, are not uniform over all azimuth angles. Gain patterns for all feed points are shown in Appendix A. The poor directive gain is a result of the low input impedance of the feed points, which is attributed to the poor mutual coupling between the aircraft structure and the SI antenna feed.

Due to coherently integrating over 1024 samples of each noisy, complex incident signal, the effective SNR is significantly higher than the per-sample SNR defined previously. The integration is coherent because the samples are complex, i.e. magnitude and phase are included [26] and the phases are matched. This increase in SNR is known as *integration gain* or *processing gain*. The power in a single sample is defined as

$$P_{sig} = |V_r|^2 \tag{3.16}$$

where V_r is the amplitude of the received signal. If the ideal, complex incident signal is sampled N_s times, the signal power becomes

$$P_{sig} = N_s^2 |V_r|^2. \tag{3.17}$$

The complex AWGN is modeled as I-Q data

$$n(t) = n_I(t) + n_Q(t) \tag{3.18}$$

where the I-Q components are independent, identically distributed (iid) with zero mean and each component has noise power $\frac{\sigma^2}{2}$ so that the total power in each complex noise sample is σ^2. The power in N_s samples of noise is

$$P_{noise} = N_s \sigma^2. \tag{3.19}$$

This results in a realized SNR of

$$SNR = \frac{P_{sig}}{P_{noise}} = \frac{N_s^2 |V_r|^2}{N_s \sigma^2} = \frac{N_s |V_r|^2}{\sigma^2} = N_s SNR_s, \tag{3.20}$$

where SNR_s is the per-sample SNR. Processing 1024 samples of each complex incident signal, as is done in this research, results in an effective SNR which is approximately 30.1 dB greater than the user-defined per-sample SNR. The gain in SNR achieved by processing many samples of the complex incident signal significantly impacts the

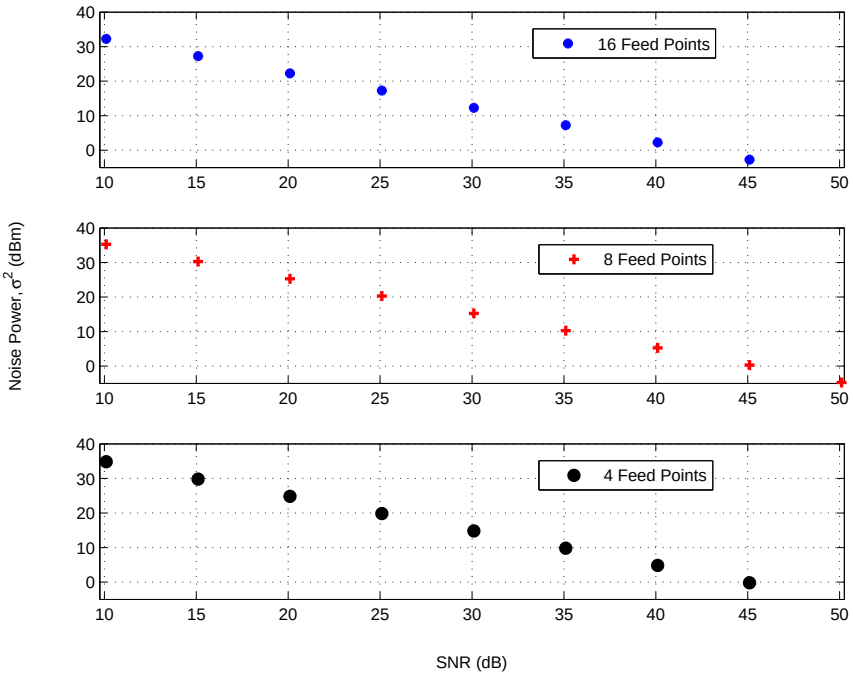

Figure 3.6: Average noise power in dBm added to each sample of a $f_c = 4$ MHz complex incident signal to achieve the desired SNR using $N_A = 4$, $N_A = 8$, or $N_A = 16$ feed points.

ability of the DF system to provide reliable AOA estimates in the presence of noise. The integration gain effectively results in an increase in the received signal power while the noise power remains constant, regardless of the number of samples available.

The operational noise and interference environment is not characterized in this research and the complex AWGN is the only source of interference. The noise power added to each sample in order to achieve the desired average SNR using the individual feed point DF system model is shown in Fig. 3.6 and Fig. 3.7.

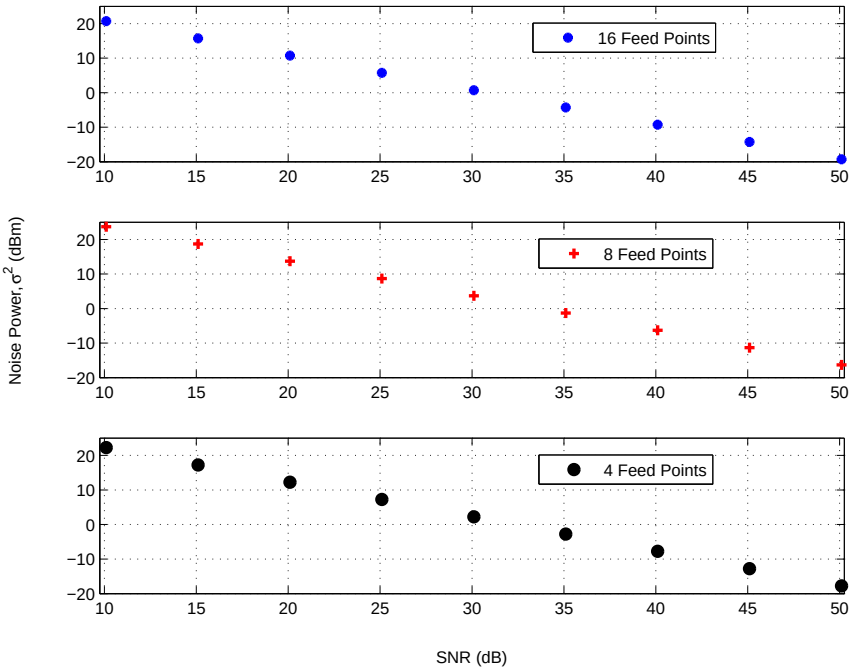

Figure 3.7: Average noise power in dBm added to each sample of an $f_c = 11$ MHz complex incident signal to achieve the desired SNR using $N_A = 4$, $N_A = 8$, or $N_A = 16$ feed points.

IV. Presentation and Analysis of Results

4.1 Introduction

This chapter contains the results and analysis of computer simulations of a proposed high frequency direction finding (HFDF) system modeled on a large airframe. The system uses short, monopole feeds placed in diverse locations over the airframe. The feeds are used to excite currents on the surface of the structure allowing the structure to be used as the radiating element, and using reciprocity, as the receiving element.

The angle of arrival (AOA) estimation results are based on two distinct treatments of the modeled HFDF system. One model treats each feed point as having an independent receiver channel. In the second model, the feed point responses are combined to synthesize the pattern of a cube antenna, which requires three receiver channels, regardless of the number of feed points combined. Each receiver channel synthesizes one loop of a cube antenna, as discussed in Section 3.2. Simulations are performed using a single, horizontally(ϕ)-polarized incident signal transmitted from a continuous wave (CW) emitter. Simulations are performed using transmitter frequencies of $f_c = 4$ MHz and $f_c = 11$ MHz. The frequencies are chosen such that the larger dimension of the modeled aircraft is less than one wavelength at $f_c = 4$ MHz and greater than one wavelength at $f_c = 11$ MHz. The relationships between aircraft dimensions and signal wavelength are shown in Table 4.1. This choice of frequencies allows for analysis of the relative platform size with respect to the signal wavelength on the accuracy of angle of arrival (AOA) estimation.

A range of signal-to-noise ratio (SNR) is simulated and the results are used to qualitatively determine the threshold SNR required to perform AOA estimation. The SNR threshold is found by examining the standard deviation of the estimation error for the range of SNR values, as described by Friedlander [24]. SNR is the primary factor affecting the accuracy of AOA estimates. As SNR increases, the accuracy of the estimate improves. Estimation results from both models and frequencies are presented and analyzed to determine the feasibility of the modeled HFDF system. The goal is

Table 4.1: Dimensions of the modeled Aircraft with respect to signal wavelength (λ).

meters (approximate)	Wavelengths at 4 MHz	Wavelengths at 11 MHz
40 (wingspan)	0.59	1.63
41.53 (length)	0.62	1.71

to achieve acceptable AOA estimation accuracy while minimizing system complexity. System complexity may be minimized by reducing the number of feed points and/or receiver channels required to perform AOA estimation.

Simulations are performed using system models comprised of $N_A = 4$, $N_A = 8$ and $N_A = 16$ feed points for both individual feed point channels and synthesized cube antenna channels. Magnitude of the input impedance, without regard to feed location, is used to determine which feed points to include in the $N_A = 4$ and $N_A = 8$ individual feed point models. The larger the input impedance of the feed point, the larger the electrical response to the incident signal. Researches at BerrieHill Research Corporation (BRC) determined which feed points to use for the synthesized cube antenna data models. Simulations of random combinations of $N_A = 4$ individual feed points at a given SNR are also performed and the results are presented. The random combinations are used to examine the effect of feed point location on AOA estimation accuracy, as well as to test the assumption that input impedance is the critical factor in determining which feed points to use.

The received complex incident signal is sampled at 10 times the incident signal frequency and coherently integrated over 1024 samples to achieve an increase in SNR. Two hundred iterations at each azimuth angle are performed to provide a robust Monte Carlo simulation and to take advantage of the asymptotic properties of the maximum likelihood estimator. As the number of iterations increase, the mean value of the estimate will approach the actual value. It has been experimentally determined

in this research that 200 iterations are sufficient for convergence of the AOA estimates to occur for the system models used.

Results are reported for estimated azimuth AOA only. An elevation angle of 90°, or aircraft waterline, is used in all simulations in order to reduce simulation run time. For some applications of AOA estimation, such as emitter localization, the estimated azimuth AOA is often sufficient, according to Torrieri [13].

Analysis of each simulated HFDF system focuses primarily on the AOA estimation error and the standard deviation of the estimation errors for the range of simulated SNR values. The AOA estimation error is found by calculating the mathematical difference between the estimated AOA and the true AOA. Estimation error values are limited to the range ±180°. The standard deviation is calculated using the 200 iterations of estimation error and then averaged over the 24 azimuth angles for each simulated SNR.

Results and analysis are presented for simulated individual feed point HFDF systems comprised of $N_A = 4$, $N_A = 8$, and $N_A = 16$ feed points. Results are based on simulations of both $f_c = 4$ MHz and $f_c = 11$ MHz incident signals. The results of 25 random configurations of $N_A = 4$ feed points are presented. Next, results and analysis of simulations using synthesized cube antenna data are presented for both $f_c = 4$ MHz and $f_c = 11$ MHz incident signals.

4.2 Results and Analysis of 4 MHz Individual Feed Point HFDF System

This section presents the results and analysis of AOA estimation using a system of individual feed points. In this model, each feed point has an independent receiver channel. There is a maximum of $N_A = 16$ feed points comprising the modeled HFDF system.

4.2.1 AOA Results Using 16 Individual Feed Points. This section presents the results and analysis of the individual feed point HFDF system comprised of $N_A = 16$ feed points. The directive gain patterns associated with these feed points are

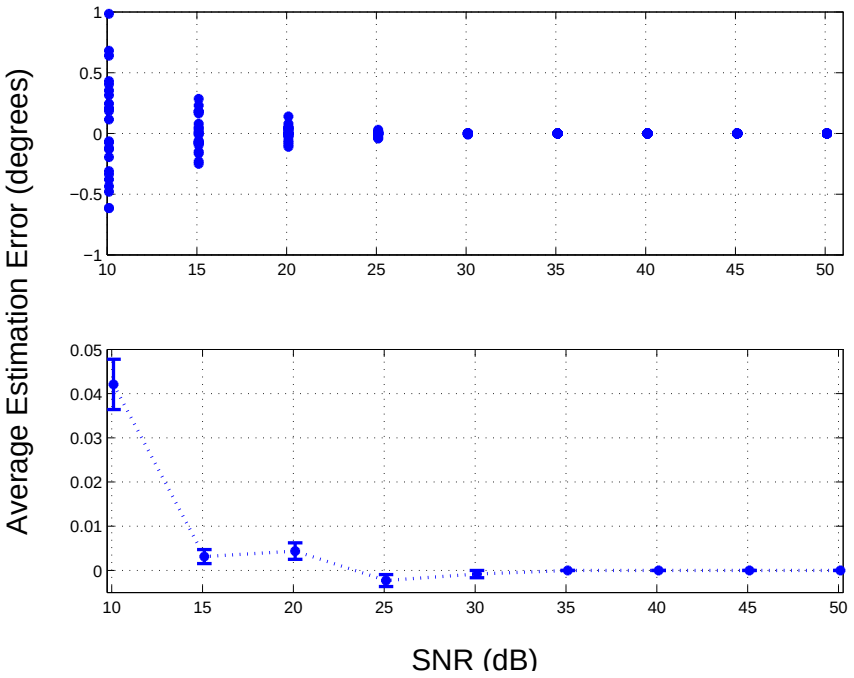

Figure 4.1: Azimuth estimation error vs. SNR for a $f_c = 4$ MHz incident signal and $N_A = 16$ individual feed points. Top: Average estimation error of 24 azimuth angles based on 200 Monte Carlo iterations. Bottom: Estimation error averaged over 200 Monte Carlo iterations and 24 azimuth angles with 95% confidence intervals.

contained in Appendix A. The top plot of Fig. 4.1 shows the average AOA estimation error as a function of SNR. The estimation error averaged over 200 Monte Carlo iterations at each of the 24 simulated azimuth angles is plotted for each simulated SNR. As the SNR increases, the estimation error approaches zero, as expected. The bottom plot of Fig. 4.1 shows the average estimation error versus SNR with the estimation error averaged over the 24 azimuth angles. The error bars represent the 95% confidence interval of the average estimation error. The average estimation error is less than 1° at the lowest SNR simulated, as the estimation errors are distributed almost evenly about 0°. Average estimation error improves only slightly as SNR increases beyond $SNR = 20$ dB.

The standard deviation of the estimation error is often used to measure the accuracy of AOA estimates [24]. The standard deviation of the AOA estimation

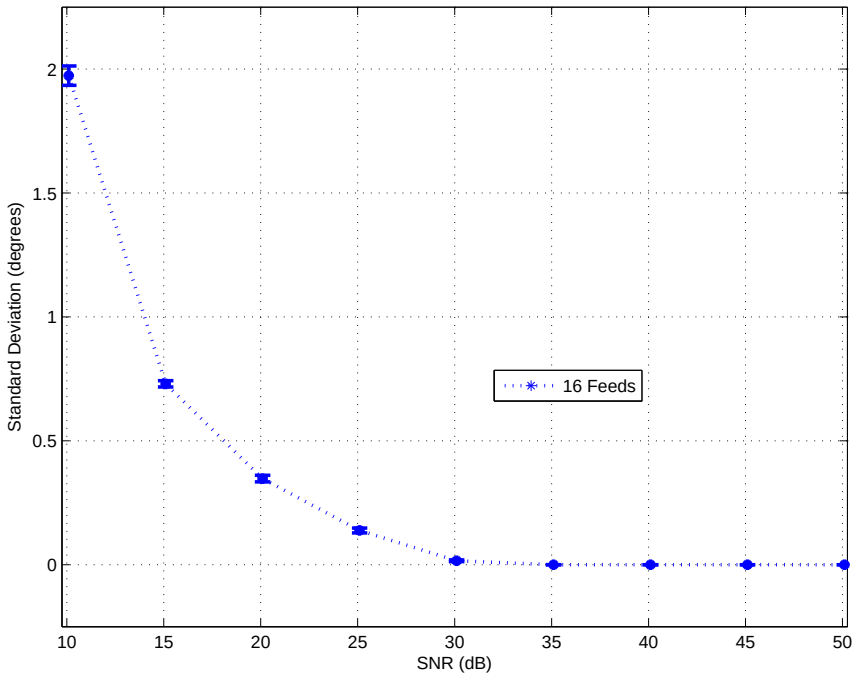

Figure 4.2: Standard deviation of AOA estimation error vs. SNR for a $f_c = 4$ MHz incident signal and $N_A = 16$ individual feed points with 95% confidence intervals.

error for a $f_c = 4$ MHz incident signal using a HFDF system comprised of $N_A = 16$ individual feed points is shown in Fig. 4.2. The standard deviation is determined using 200 Monte Carlo iterations at each azimuth angle and averaged over 24 azimuth angles for each simulated SNR value. The threshold SNR for accurate HFDF is defined as the SNR beyond which minimal reduction in the standard deviation is realized by increasing the SNR. The threshold SNR for the simulated $f_c = 4$ MHz HFDF system using $N_A = 16$ individual feed points and integrating over 1024 samples is approximately $SNR = 30$ dB. The standard deviation is less than 0.5° at $SNR = 20$ dB and approximately 0° for values above the threshold.

As stated in Section 3.3.5, a value of $SNR = 13$ dB or greater is often required to achieve accurate AOA estimates in operational DF systems. As Fig. 4.2 shows, the standard deviation begins to approach the minimum value when the SNR is between $SNR = 20$ dB and $SNR = 30$ dB. The average estimation error has begun to approach 0° but the estimation errors have some distribution about the mean.

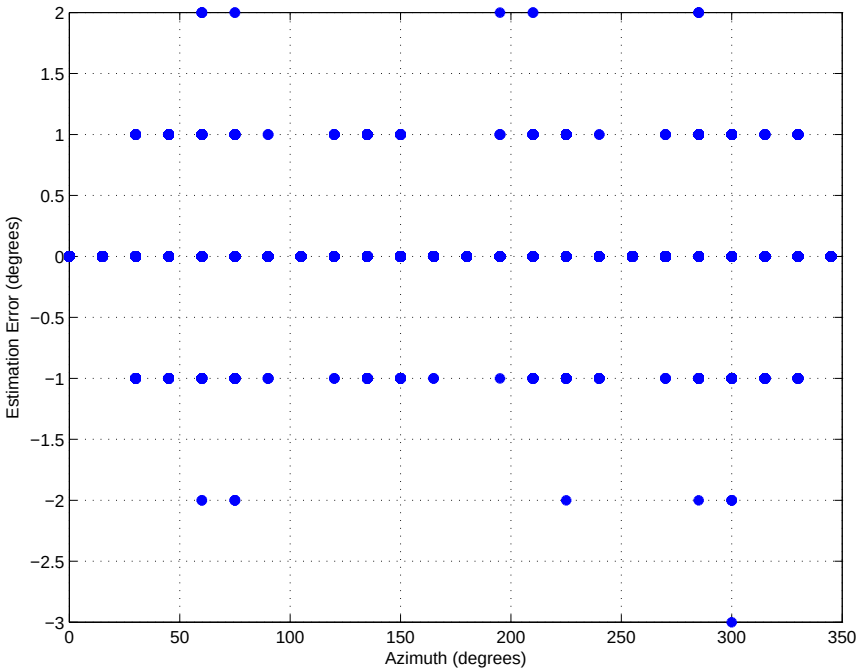

Figure 4.3: Azimuth estimation error vs. true azimuth angle for a $f_c = 4$ MHz incident signal with $SNR = 20$ dB using $N_A = 16$ individual feed points.

The extent of the estimation error distribution over 200 iterations at each azimuth angle is shown in Fig. 4.3. Error distribution plots resulting from simulations using additional SNR values are contained in Appendix B. Recall that the estimation error will be an integer value due to the array manifold resolution. The envelope of the error distribution expands and contracts across the range of azimuth angles. This trend is likely due to symmetry in the location of feed points on the aircraft.

4.2.2 AOA Results Using 8 Individual Feed Points. The results and analysis of the individual feed point, $f_c = 4$ MHz HFDF system comprised of $N_A = 8$ feed points are contained in this section. The $N_A = 8$ feed points comprising the simulated HFDF system are a subset of the $N_A = 16$ total feed points available. The $N_A = 8$ feed points with the highest input impedance are used to generate the modeled HFDF system. The location of the feed points on the aircraft is not taken into consideration during selection of the feed points. The $N_A = 8$ feed points used in the simulated

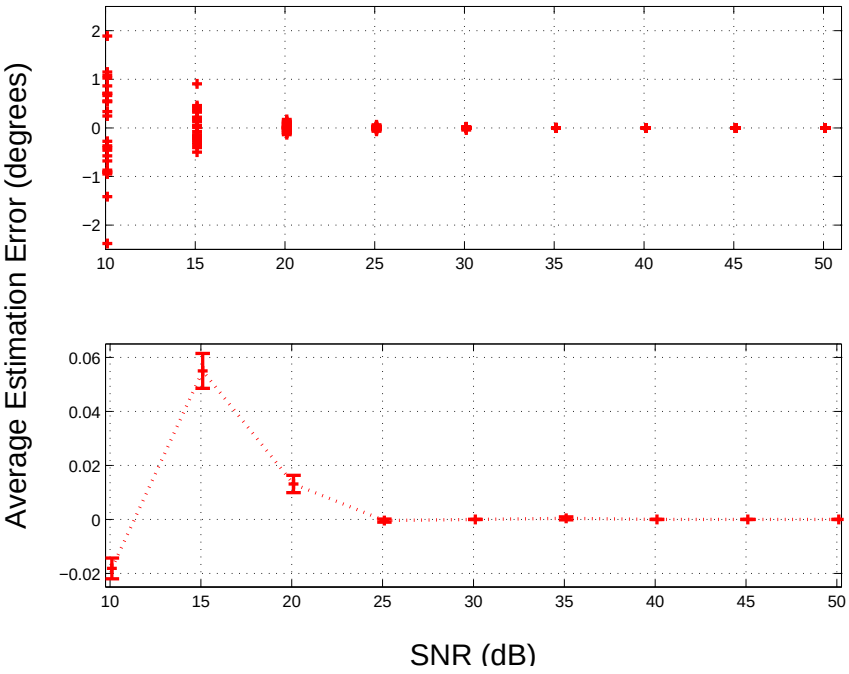

Figure 4.4: Azimuth estimation error vs. SNR for a $f_c = 4$ MHz incident signal and $N_A = 8$ individual feed points. Top: Average estimation error of 24 azimuth angles based on 200 Monte Carlo iterations. Bottom: Estimation error averaged over 200 Monte Carlo iterations and 24 azimuth angles with 95% confidence intervals.

HFDF system are numbered 9-16 in the BRC-provided data. The directive gain patterns associated with these feed points are contained in Appendix A.

The average azimuth estimation error as a function of SNR is shown in Fig. 4.4. The top plot shows the average AOA estimation error as a function of SNR. The estimation error averaged over 200 Monte Carlo iterations at each of the 24 simulated azimuth angles is plotted for each simulated SNR. At the lowest simulated SNR values, $SNR = 10$ dB and $SNR = 15$ dB, the estimation errors are distributed over a wider range when the simulated HFDF system is comprised of $N_A = 8$ feed points compared to the simulated HFDF system comprised of $N_A = 16$ feed points. At $SNR = 10$ dB, the average estimation error for all simulated azimuth angles is within approximately 2° of the true azimuth angle. As the SNR increases, the estimation error approaches 0°. The bottom plot of Fig. 4.4 shows the average estimation error versus SNR

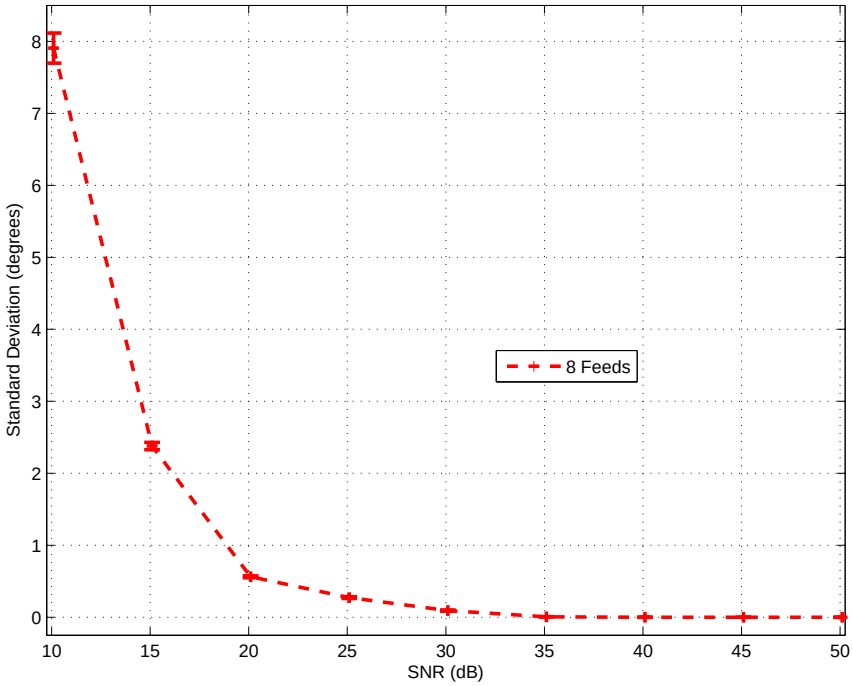

Figure 4.5: Standard deviation of AOA estimation error vs. SNR for a $f_c = 4$ MHz incident signal and $N_A = 8$ individual feed points with 95% confidence intervals.

where the estimation error has been averaged over 24 azimuth angles. The error bars represent the 95% confidence interval of the average estimation error. The average estimation error at $SNR = 10$ dB is negative due to the uneven distribution of the errors about 0°. Similar to the performance of the $N_A = 16$ feed point HFDF system, the average estimation error averaged over 24 azimuth angles and 200 iterations is very near 0° due to the almost even distribution of the errors about 0°.

As is the case with the simulated HFDF system comprised of $N_A = 16$ feed points, the average estimation error performance improves only slightly as SNR increases beyond $SNR = 20$ dB. The threshold SNR for the simulated $f_c = 4$ MHz HFDF system using $N_A = 8$ individual feed points is approximately $SNR = 20$ dB to $SNR = 25$ dB, as shown in Fig. 4.5. The standard deviation at $SNR = 10$ dB has increased to approximately 8°, an increase of nearly 6° compared to the HFDF system comprised of $N_A = 16$ feed points. The threshold SNR is approximately the

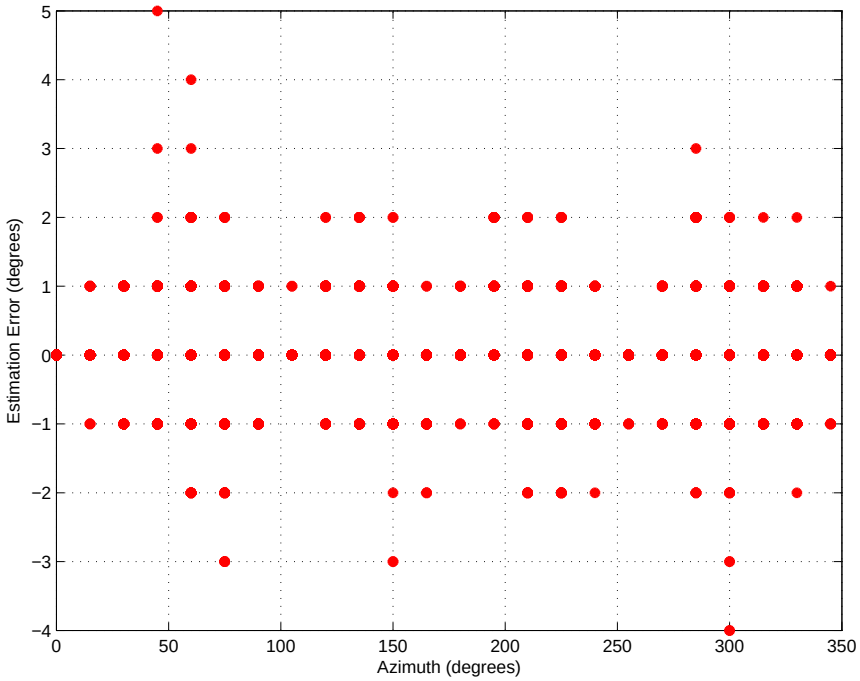

Figure 4.6: Azimuth estimation error vs. true azimuth angle for a $f_c = 4$ MHz incident signal with $SNR = 20$ dB using 8 individual feed points.

same as the threshold SNR for the HFDF system comprised of $N_A = 16$ feed points. The estimation errors at $SNR = 20$ dB are more widely distributed when $N_A = 8$ feed points are used compared to the error distribution of the $N_A = 16$ feed point system, as seen in Fig. 4.6. The trend of the error distribution envelope to expand and contract remains present.

4.2.3 AOA Results Using 4 Individual Feed Points. The results and analysis of the individual feed point, $f_c = 4$ MHz HFDF system comprised of $N_A = 4$ feed points are described in this section. The $N_A = 4$ feed points are a subset of the total of $N_A = 16$ feed points available and have been selected based on the input impedance of the feed point. The $N_A = 4$ feed points with the highest input impedance are used to generate the simulated HFDF system. The location of the feed points on the aircraft is not considered during selection. The $N_A = 4$ feed points used in the simulated

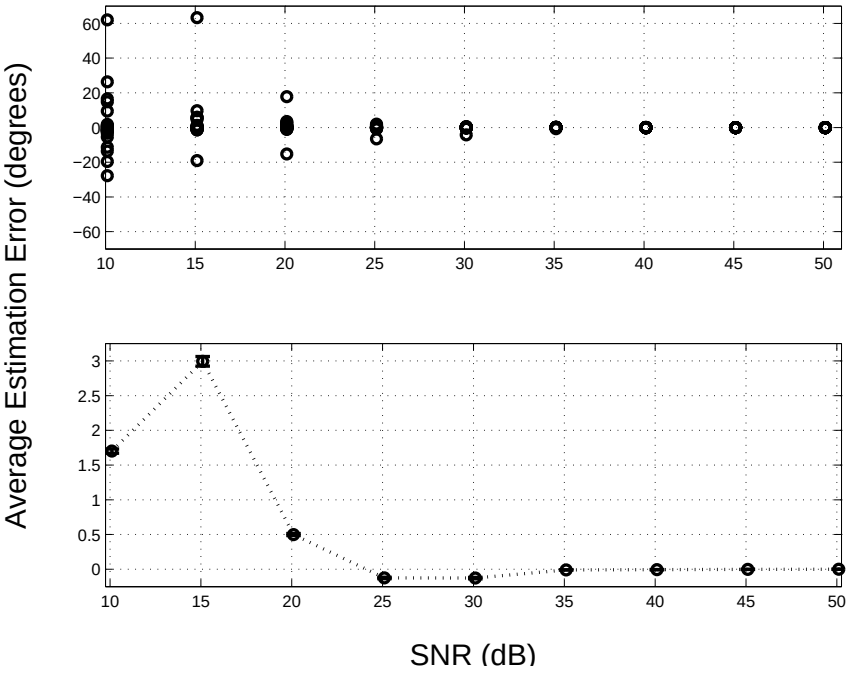

Figure 4.7: Azimuth estimation error vs. SNR for a $f_c = 4$ MHz incident signal and $N_A = 4$ individual feed points. Top: Average estimation error of 24 azimuth angles based on 200 Monte Carlo iterations. Bottom: Estimation error averaged over 200 Monte Carlo iterations and 24 azimuth angles with 95% confidence intervals.

HFDF system are labeled 10, 14, 15, and 16 in the BRC-provided data. The directive gain patterns associated with these feed points are contained in Appendix A.

The average azimuth estimation error as a function of SNR is shown in Fig. 4.7. The top plot shows the average AOA estimation error as a function of SNR. The estimation error averaged over 200 Monte Carlo iterations at each of the 24 simulated azimuth angles is plotted for each simulated SNR. As the SNR increases, the estimation error approaches zero. The bottom plot of Fig. 4.7 shows the average estimation error versus SNR where the estimation error has been averaged over 24 azimuth angles. The error bars represent the 95% confidence interval of the average estimation error. Similar to the performance of the $N_A = 8$ and $N_A = 16$ feed point HFDF systems, the average estimation error approaches 0°, but the range of average estimation errors is greater than the range of errors resulting from the $N_A = 8$ and

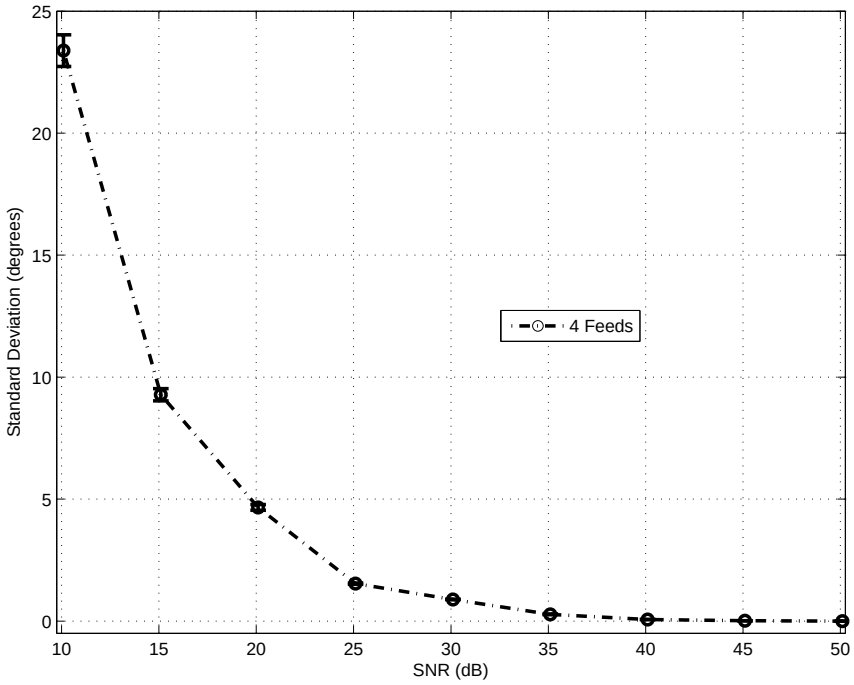

Figure 4.8: Standard deviation of AOA estimation error vs. SNR for a $f_c = 4$ MHz incident signal and $N_A = 4$ individual feed points with 95% confidence intervals.

$N_A = 16$ feed point HFDF systems at the lowest values of SNR. The errors are not as evenly distributed around 0°, causing the average estimation error to be significantly greater when compared to the estimation error of the $N_A = 8$ and $N_A = 16$ feed point systems. The uneven distribution of errors also explains why the average error at $SNR = 10$ dB is lower than the average error at $SNR = 15$ dB. This uneven distribution of errors indicates some angles are more accurately estimated, which is likely due to the patterns of the SI antennas used to create this array.

A significant decrease in estimation accuracy occurs when the simulated HFDF system is reduced from $N_A = 8$ feed points to $N_A = 4$ feed points. The average estimation error eventually approaches 0°, as shown in Fig. 4.7, but an increase of approximately 10 dB in SNR is necessary to achieve this performance when compared to HFDF systems comprised of $N_A = 8$ or $N_A = 16$ feed points. The standard deviation of the estimation errors, shown in Fig. 4.8, has also increased significantly when compared to the standard deviation of the estimation errors when $N_A = 8$ or

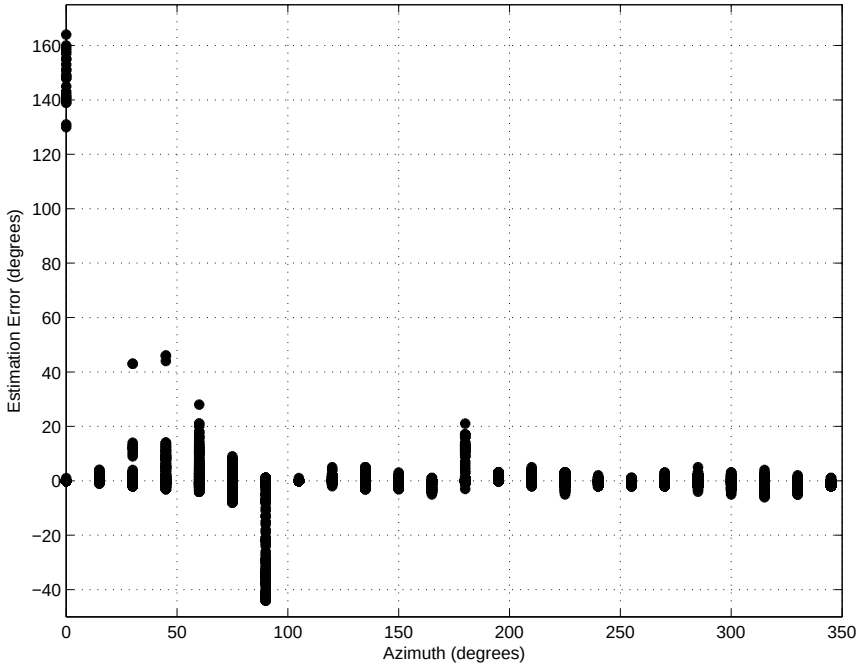

Figure 4.9: Azimuth estimation error vs. true azimuth angle for a $f_c = 4$ MHz incident signal with $SNR = 20$ dB using $N_A = 4$ feed points.

$N_A = 16$ feed points are used. The threshold SNR is between $SNR = 25$ dB and $SNR = 35$ dB for the HFDF system comprised of $N_A = 4$ feed points. The increases in average estimation error and standard deviation are a result of larger estimation errors which occur for all simulated azimuth angles, and particularly at 0° and 90° as seen in Fig. 4.9. These larger estimation errors are likely a result of the relatively small gain of the $N_A = 4$ feed points comprising this system at 0° and 90°, as seen in Appendix A. The standard deviation has also increased significantly at the lowest simulated SNR values. The reduced number of feed points result in a smaller amount of data being available, leading to a decrease in estimation performance.

4.2.4 Comparison of AOA Estimation Performance Using 4, 8, and 16 Feed Points. A comparison of individual feed point HFDF system performance based on the previously presented results using $N_A = 4$, $N_A = 8$, and $N_A = 16$ feed points for a $f_c = 4$ MHz incident signal has been performed. The data in this section may be used to analyze the trade-space between system complexity in terms of receiver

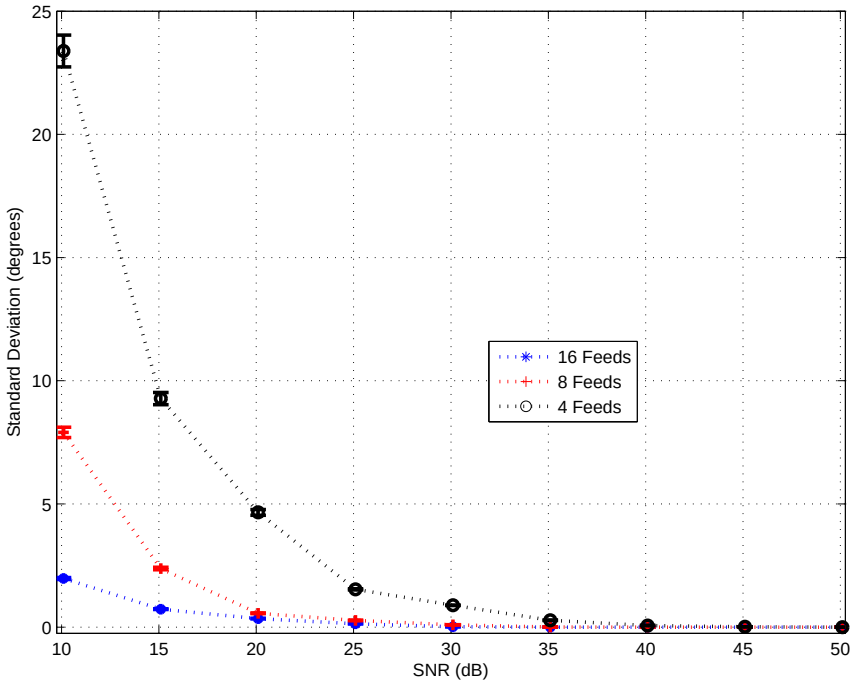

Figure 4.10: Comparison of standard deviation of azimuth estimation error vs. SNR for a $f_c = 4$ MHz incident signal using $N_A = 4$, $N_A = 8$, and $N_A = 16$ feed points.

channels required and AOA estimation accuracy. Results are presented in terms of average estimation error at a given SNR and standard deviation of the estimation error based on 200 Monte Carlo iterations at each azimuth angle.

The standard deviations of the AOA estimation error using $N_A = 4$, $N_A = 8$, and $N_A = 16$ feed points are shown in Fig. 4.10. As was seen previously, the standard deviation resulting from a $N_A = 4$ feed point HFDF system is significantly higher than the standard deviation values resulting from the use of $N_A = 8$ or $N_A = 16$ feed points. At $SNR = 20$ dB or greater, the performance of the systems using $N_A = 8$ and $N_A = 16$ feed points are statistically the same. The $N_A = 4$ feed point HFDF system matches the performance of the $N_A = 8$ or $N_A = 16$ feed point systems in terms of standard deviation for $SNR = 35$ dB and greater. At $SNR = 13$ dB, the value cited as the minimum for accurate AOA estimation, the HFDF system comprised of $N_A = 16$ feed points results in a standard deviation approximately 3° less than the HFDF system comprised of $N_A = 8$ feed points.

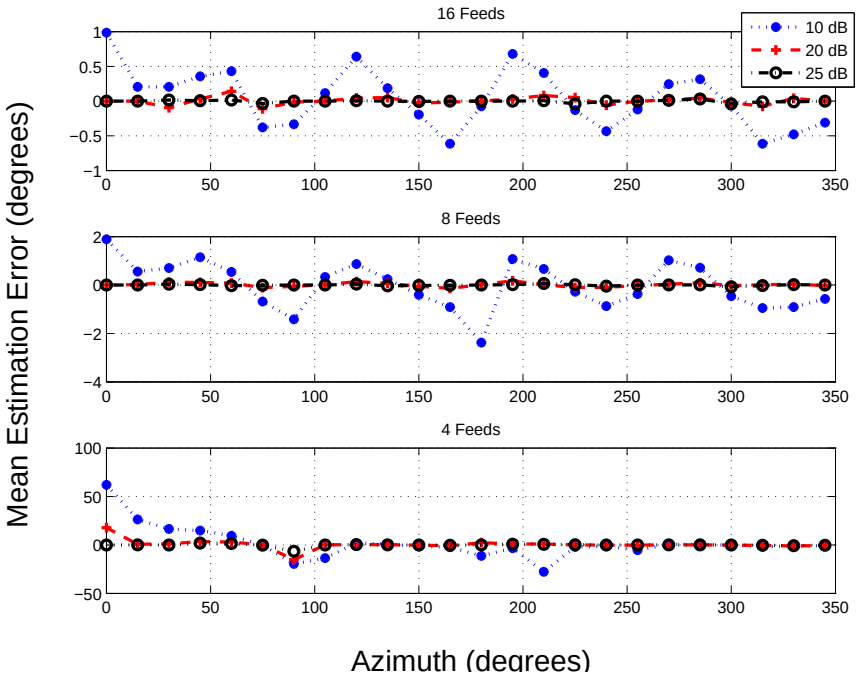

Figure 4.11: Average estimation error vs. SNR for a $f_c = 4$ MHz incident signal. Results based on multiple values of SNR using combinations of $N_A = 4$, $N_A = 8$, and $N_A = 16$ feed points. NOTE: Error scales (y-axis) are different for each plot.

The plots of Fig. 4.11 show the average AOA estimation error for 3 different values of SNR using $N_A = 16$ feed points in the top plot, $N_A = 8$ feed points in the middle plot, and $N_A = 4$ feed points in the bottom plot. The average estimation error decreases as the SNR increases. The greatest difference between a HFDF system comprised of $N_A = 16$ feed points and a system comprised of $N_A = 8$ feed points is apparent at the lowest SNR values simulated. The magnitude of the estimation errors for the HFDF system comprised of $N_A = 4$ feed points is significantly higher with the large errors appearing at certain azimuth angles.

A HFDF system comprised of $N_A = 4$ individual feed points selected based on input impedance as the sole determining factor is not suitable for HFDF at $f_c = 4$ MHz based on the large average estimation error and standard deviation of the error. Other factors to consider when selecting feed points to include in a HFDF system are discussed in Section 4.4. A HFDF system comprised of $N_A = 8$ individual feed points

results in a substantial gain in estimation accuracy over the $N_A = 4$ feed point HFDF system, and the estimation accuracy is similar to that of a HFDF system comprised of $N_A = 16$ feed points at $f_c = 4$ MHz for $SNR = 20$ dB and greater. It is important to recall that the SNR values in this research are based on coherently integrating over 1024 samples of the incident signal. Coherent integration results in an increase of 30.1 dB compared to the per-sample SNR value.

4.3 Results and Analysis of an 11 MHz Individual Feed Point HFDF System

This section presents the results of AOA estimation using a system of individual feed points with each feed point having an independent receiver channel. The maximum number of feed points comprising the HFDF system is $N_A = 16$. It is important to note that the physical location of the $N_A = 16$ feed points comprising the simulated $f_c = 11$ MHz HFDF system is not the same as the location of the feed points comprising the simulated $f_c = 4$ MHz HFDF system.

4.3.1 AOA Results Using 16 Individual Feed Points. This section contains the results and analysis of the individual feed point HFDF system comprised of $N_A = 16$ feed points. The method of analysis is the same as that used for the $f_c = 4$ MHz HFDF system. The directive gain patterns associated with these feed points are contained in Appendix A. The top plot of Fig. 4.12 shows the average AOA estimation error as a function of SNR. The estimation error averaged over 200 Monte Carlo iterations at each of the 24 simulated azimuth angles is plotted for each simulated SNR. As the SNR increases, the estimation error approaches 0°. At the lowest SNR value, $SNR = 10$ dB, the average estimation error of all 24 azimuth angles is less than 0.1°. The bottom plot of Fig. 4.12 shows the average estimation error versus SNR with the estimation error averaged over 24 azimuth angles. The error bars represent the 95% confidence interval of the average estimation error. Average estimation error improves only slightly as SNR increases beyond $SNR = 20$ dB, though the average

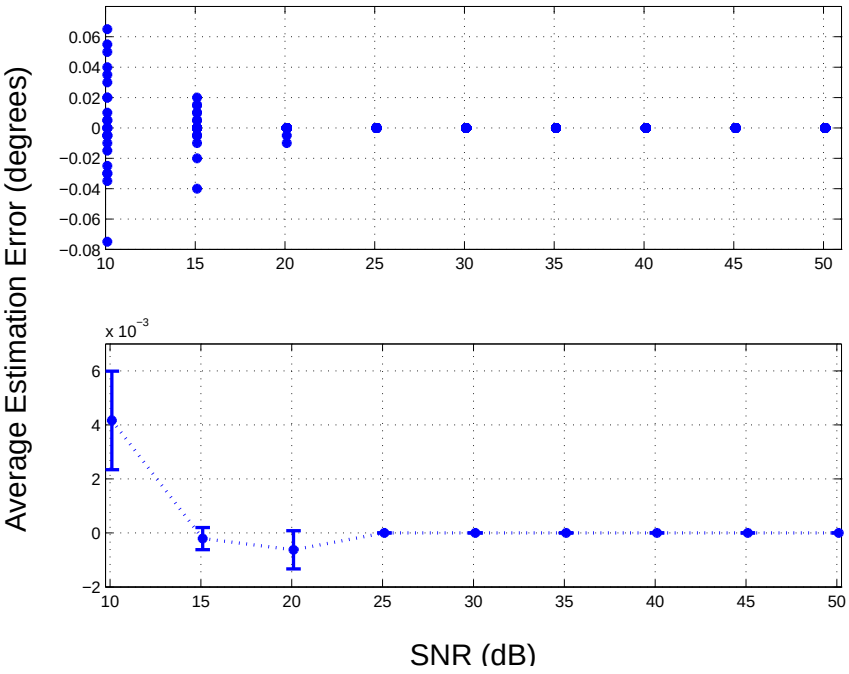

Figure 4.12: Azimuth estimation error vs. SNR for an $f_c = 11$ MHz incident signal and $N_A = 16$ individual feed points. Top: Average estimation error of 24 azimuth angles based on 200 Monte Carlo iterations. Bottom: Estimation error averaged over 200 Monte Carlo iterations and 24 azimuth angles with 95% confidence intervals.

error is less than 0.06° at $SNR = 10$ dB. The 95% confidence interval includes 0° for values above $SNR = 15$ dB.

The standard deviation of the AOA estimation error for an $f_c = 11$ MHz incident signal using a HFDF system comprised of $N_A = 16$ individual feed points is shown in Fig. 4.13. The standard deviation is determined using 200 iterations at each azimuth angle and averaged over 24 azimuth angles for each simulated SNR value. The threshold SNR for the simulated $f_c = 11$ MHz HFDF system using $N_A = 16$ individual feed points is approximately $SNR = 15$ dB to $SNR = 20$ dB. The standard deviation is approximately 0.4° at the lowest simulated SNR and is approximately 0° for all values greater than $SNR = 20$ dB.

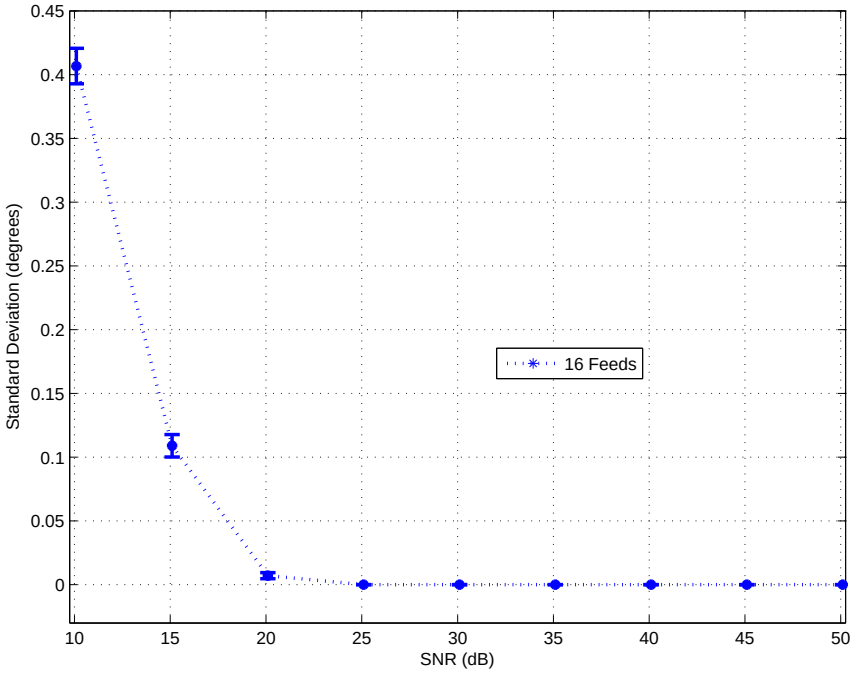

Figure 4.13: Standard deviation of AOA estimation error vs. SNR for an $f_c = 11$ MHz incident signal and $N_A = 16$ individual feeds with 95% confidence intervals.

The distribution of the estimation errors is shown in Fig. 4.14. The average estimation error is negative due to the only errors present at $SNR = 20$ dB being $-1°$. No errors with magnitude greater than $1°$ occurred at $SNR = 20$ dB.

4.3.2 AOA Results Using 8 Individual Feed Points. The results and analysis of the individual feed HFDF system comprised of $N_A = 8$ feed points are shown in this section. The $N_A = 8$ feed points comprising the simulated HFDF system are a subset of the $N_A = 16$ feed points available. The feed points are selected based on the magnitude of the input impedance. The $N_A = 8$ feed points with the highest input impedance are used to generate the simulated HFDF system. The location of the feed points on the aircraft is not considered during selection. The $N_A = 8$ feed points used in the simulated HFDF system are numbered 9-16 in the BRC-provided data. The directive gain patterns associated with these feed points are contained in Appendix A.

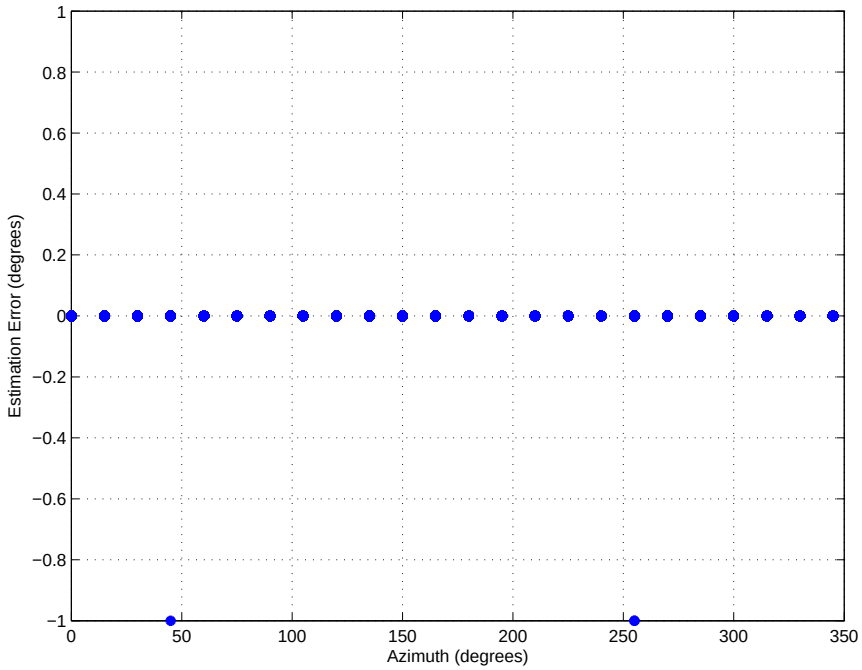

Figure 4.14: Azimuth estimation error vs. true azimuth angle for an $f_c = 11$ MHz incident signal with $SNR = 20$ dB using $N_A = 16$ feed points.

The top plot of Fig. 4.15 shows the average AOA estimation error as a function of SNR. The estimation error averaged over 200 Monte Carlo iterations at each of the 24 simulated azimuth angles is plotted for each simulated SNR. As the SNR increases, the average estimation error converges to 0°. At the lowest SNR value, $SNR = 10$ dB, the average estimation error of all 24 azimuth angles is less than 0.15°. The bottom plot of Fig. 4.15 shows the average estimation error versus SNR with the estimation error averaged over 24 azimuth angles. The error bars represent the 95% confidence interval of the average estimation error. Average estimation error improves only slightly as SNR increases beyond $SNR = 20$ dB. The average estimation error is near 0° for all simulated SNR values, as the average estimation error 0.015° at $SNR = 10$ dB and decreases as SNR increases.

The standard deviation of the AOA estimation error for an $f_c = 11$ MHz incident signal using a HFDF system comprised of $N_A = 8$ individual feed points is shown in Fig. 4.16. The threshold SNR for the simulated $f_c = 11$ MHz HFDF system using

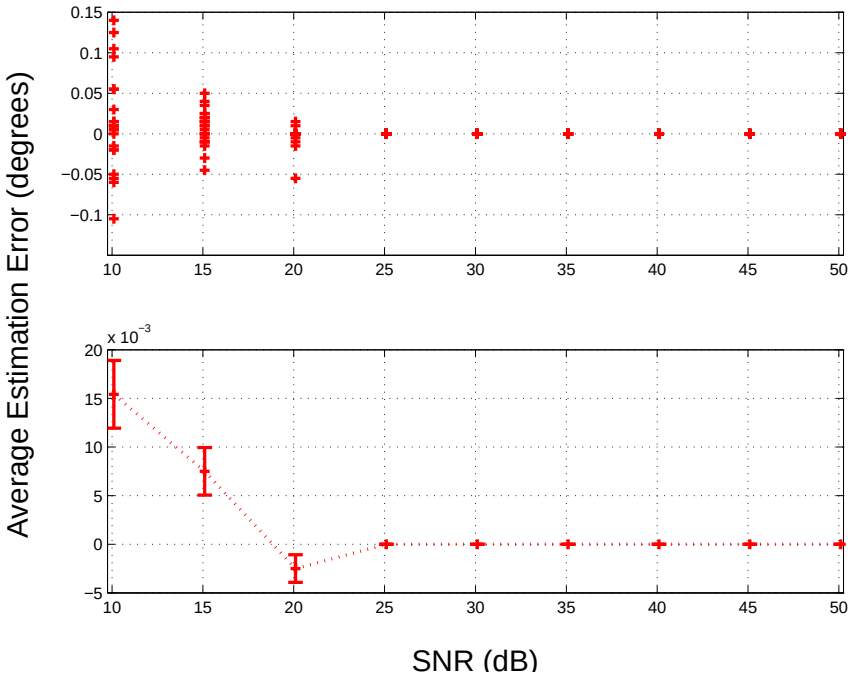

Figure 4.15: Azimuth estimation error vs. SNR for an $f_c = 11$ MHz incident signal and $N_A = 8$ individual feed points. Top: Average estimation error of 24 azimuth angles based on 200 Monte Carlo iterations. Bottom: Estimation error averaged over 200 Monte Carlo iterations and 24 azimuth angles with 95% confidence intervals.

$N_A = 8$ individual feed points is approximately $SNR = 20$ dB. The standard deviation of the estimation errors is less than 0.7° for the lowest SNR simulated. The standard deviation is 0° for all simulated values greater than $SNR = 25$ dB.

The distribution of the estimation errors is shown in Fig. 4.17. The majority of azimuth angles were estimated exactly and the largest estimation error at $SNR = 20$ dB is 1°.

4.3.3 AOA Results Using 4 Individual Feed Points. This section contains the results and analysis of the $f_c = 11$ MHz individual feed HFDF system comprised of $N_A = 4$ feed points. The $N_A = 4$ feed points comprising the simulated HFDF system are a subset of the $N_A = 16$ feed points available. The feed points are selected based on the magnitude of the input impedance. The $N_A = 4$ feed points with the highest

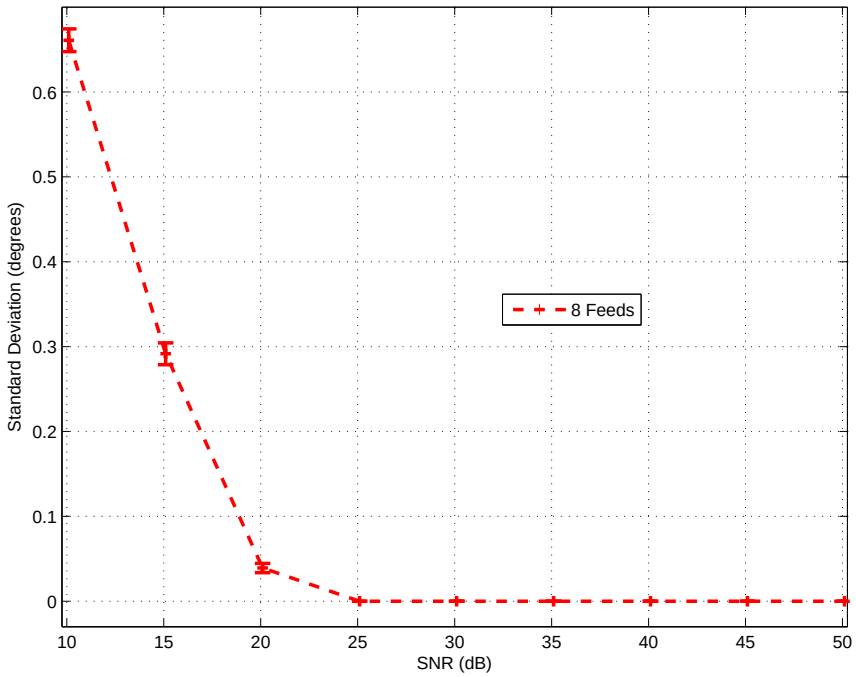

Figure 4.16: Standard deviation of AOA estimation error vs. SNR for an $f_c = 11$ MHz incident signal and $N_A = 8$ individual feed points with 95% confidence intervals.

input impedance are used to generate the simulated HFDF system. The location of the feed points on the aircraft is not considered during selection. The $N_A = 4$ feed points used in the simulated HFDF system are numbered 11, 12, 13, and 16 in the BRC-provided data. The directive gain patterns associated with these feed points are contained in Appendix A.

A significant decrease in AOA estimation accuracy occurs when the $f_c = 11$ MHz individual feed point system is comprised of $N_A = 4$ feed points. The top plot in Fig. 4.18 shows the average AOA estimation error as a function of SNR. The estimation error averaged over 200 Monte Carlo iterations at each of the 24 simulated azimuth angles is plotted for each simulated SNR. As the SNR increases, the average estimation error decreases toward 0°. The average estimation errors are widely distributed for values lower than $SNR = 25$ dB with some distribution of errors evident even at $SNR = 30$ dB. The bottom plot of Fig. 4.18 shows the average estimation error versus SNR with the estimation error averaged over 24 azimuth

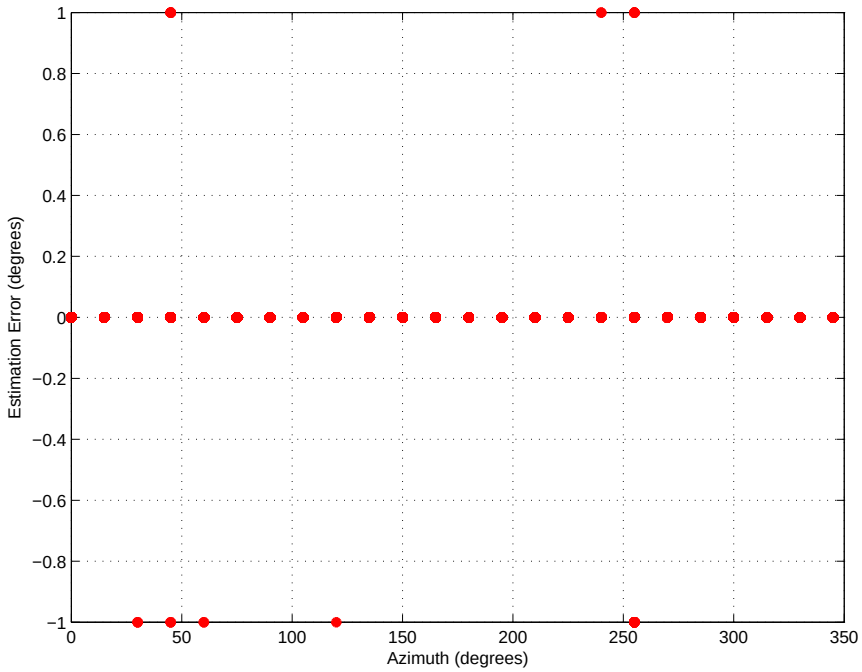

Figure 4.17: Azimuth estimation error vs. true azimuth angle for a $f_c = 11$ MHz incident signal with $SNR = 20$ dB using $N_A = 8$ feed points.

angles. The error bars represent the 95% confidence interval of the average estimation error. Average estimation error trends toward negative values due to the distribution of the errors at certain azimuth angles, as seen in the top plot. The average estimation error approaches 0° for values greater than $SNR = 30$ dB.

The standard deviation of the AOA estimation error for an $f_c = 11$ MHz incident signal using a $N_A = 4$ individual feed point simulated HFDF system is shown in Fig. 4.19. The standard deviation increases significantly when the number of feed points comprising the simulated HFDF system is reduced to $N_A = 4$. The threshold SNR for the simulated $f_c = 11$ MHz HFDF system using $N_A = 4$ individual feed points is approximately $SNR = 30$ dB to $SNR = 35$ dB, though the standard deviation is approximately 0° for all values greater than $SNR = 35$ dB.

The distribution of the estimation errors is shown in Fig. 4.20 for $SNR = 20$ dB. The true azimuth angle is estimated exactly for the majority of angles simulated. Large estimation errors occur when the azimuth AOA is 0° and 180°. Errors of ±180°

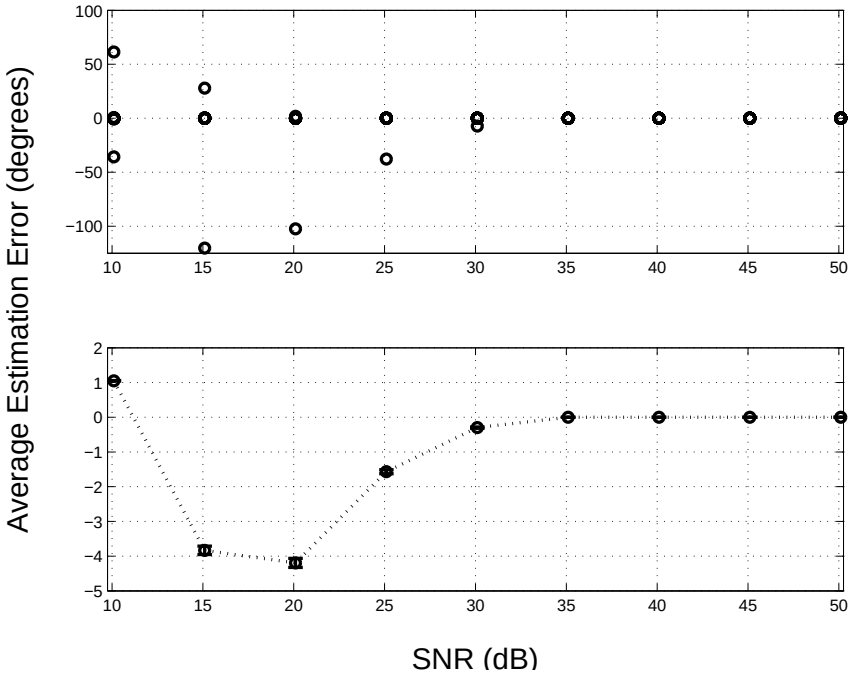

Figure 4.18: Azimuth estimation error vs. SNR for an $f_c = 11$ MHz incident signal and $N_A = 4$ individual feed points. Top: Average estimation error of 24 azimuth angles based on 200 Monte Carlo iterations. Bottom: Estimation error averaged over 200 Monte Carlo iterations and 24 azimuth angles with 95% confidence intervals.

occur and are the leading contributor to the relatively large standard deviation. The distribution of the errors show that the behavior of the average azimuth estimation error and standard deviation is caused by the large magnitude of the errors occurring at a limited number of azimuth angles, namely 0° and 180°. Error distribution plots for other values of SNR are contained in Appendix B.

4.3.4 Comparison of AOA Estimation Performance Using 4, 8, and 16 Feed Points. A comparison of individual feed point HFDF system performance using $N_A = 4$, $N_A = 8$, and $N_A = 16$ feed points for an $f_c = 11$ MHz incident signal is contained in this section. The data in this section may be used to analyze the trade-space between system complexity in terms of receiver channels required and AOA estimation accuracy. Results are presented in terms of average estimation error at a given SNR and standard deviation of the estimation error.

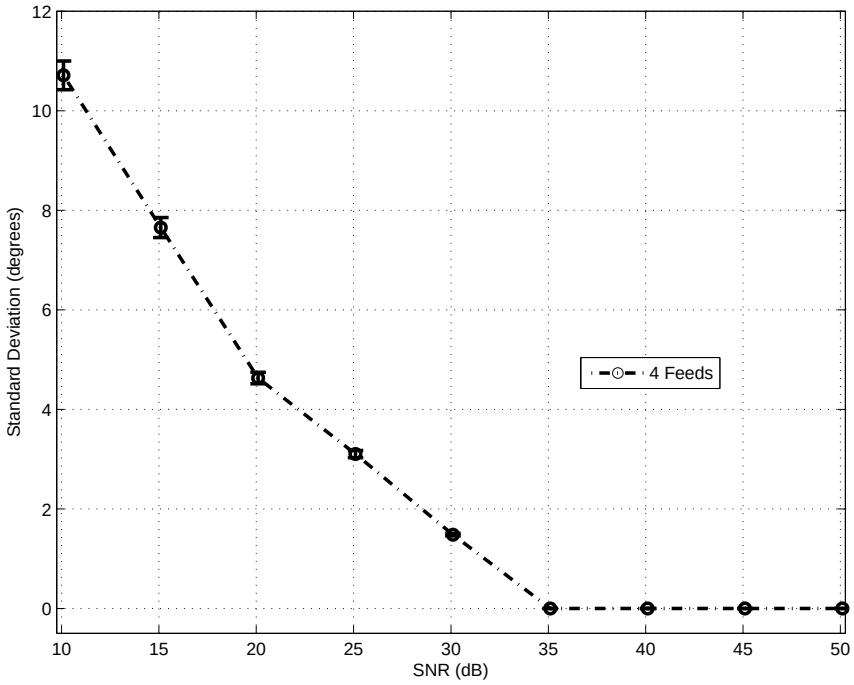

Figure 4.19: Standard deviation of AOA estimation error vs. SNR for an $f_c = 11$ MHz incident signal and $N_A = 4$ individual feed points with 95% confidence intervals.

The standard deviations of the AOA estimation error using $N_A = 4$, $N_A = 8$, and $N_A = 16$ feed points are shown in Fig. 4.21. As seen previously, the standard deviation resulting from a $N_A = 4$ feed point HFDF system is significantly higher than the standard deviations resulting from the use of $N_A = 8$ or $N_A = 16$ feed points for values below $SNR = 35$ dB. At values of $SNR = 20$ dB or greater, the standard deviation of the estimation error of the systems using $N_A = 8$ and $N_A = 16$ feed points are statistically the same. Modest improvement occurs in terms of standard deviation of estimation error when a HFDF system is comprised of $N_A = 8$ feed points as compared to $N_A = 16$ feed points for values less than $SNR = 20$ dB.

The plots of Fig. 4.22 show the average AOA estimation error for 3 different values of SNR using $N_A = 16$ feed points in the top plot, $N_A = 8$ feed points in the middle plot, and $N_A = 4$ feed points in the bottom plot. This figure shows that the average estimation error decreases as the SNR increases. In terms of average estimation error, the simulated HFDF systems using $N_A = 8$ and $N_A = 16$ feeds are

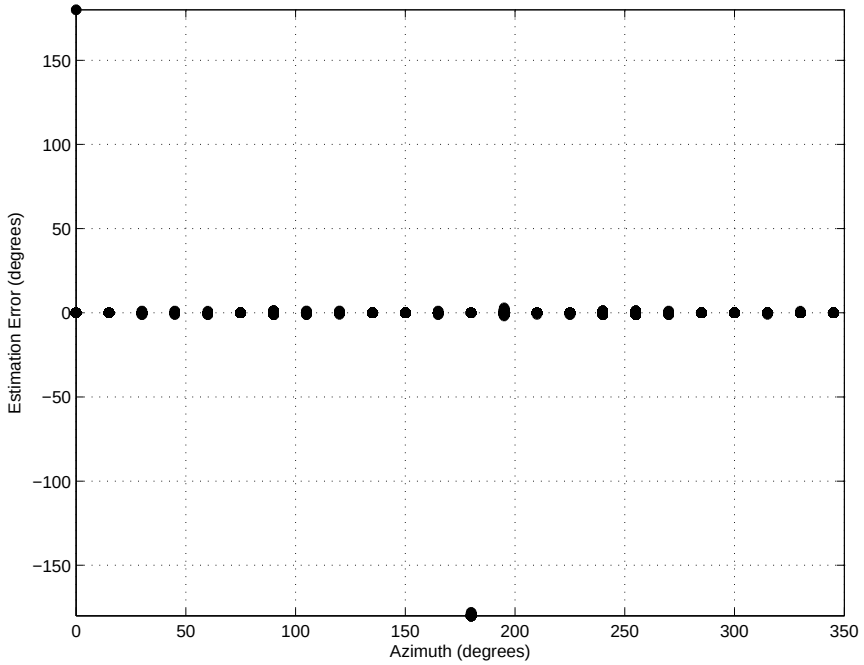

Figure 4.20: Azimuth estimation error vs. true azimuth angle for an $f_c = 11$ MHz incident signal with $SNR = 20$ dB using $N_A = 4$ feed points.

within 0.1° of each other at the lowest SNR value simulated. The plot of average estimation error for the HFDF system comprised of $N_A = 4$ feed points show large errors occur at 0° and 180° azimuth AOA. It is possible that a combination of $N_A = 4$ feed points selected using additional factors, such as diversity of location in addition to input impedance, may result in average estimation error performance more closely matching that achieved using $N_A = 8$ or $N_A = 16$ feed points. The effect of feed point location is investigated in Section 4.4.

4.4 Results and Analysis of 25 Random Configurations of 4 Feed Points

This section contains the results and analysis of AOA estimation error from 25 random configurations of $N_A = 4$ feed points. Random combinations of $N_A = 4$ feed points are used to examine the role of spatial distribution on estimation accuracy. The spatial distribution of antenna elements is crucial in a beamforming AOA estimation system. However, the spatial diversity of feed points in a structurally integrated

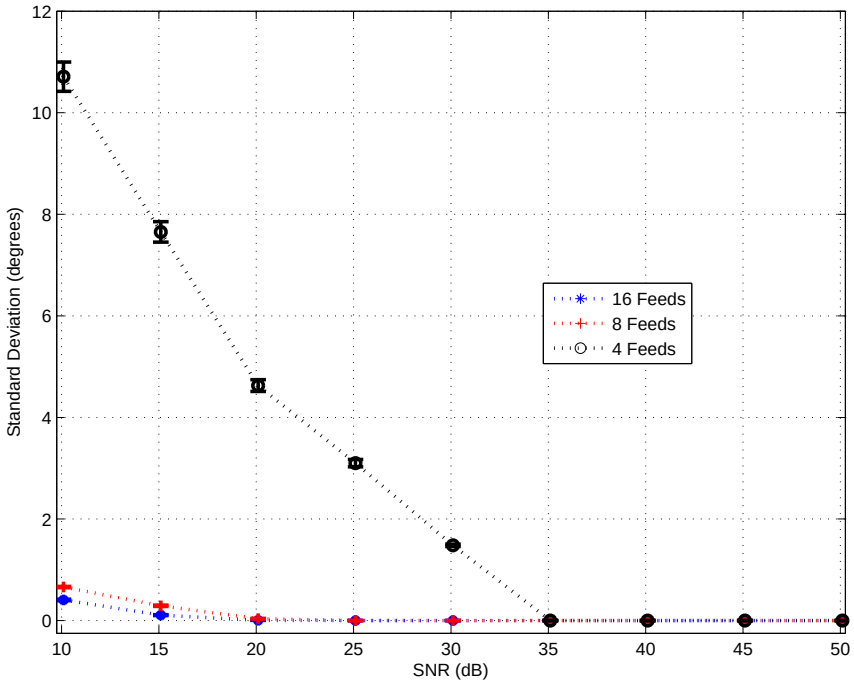

Figure 4.21: Standard deviation of azimuth estimation error vs. SNR for an $f_c = 11$ MHz incident signal. Standard deviation based on average estimation error over 200 iterations of 24 azimuth angles.

system may not have the same impact on the performance of a superesolution AOA estimation algorithm such as MLM.

The role of SNR in estimation accuracy is well-known and is evident in the results presented in this research. The SNR value for the random configuration simulations is chosen based on the results of the $N_A = 4$ feed point configuration based on input impedance. The SNR value is chosen such that some estimation error remains. The SNR value is the same for each random configuration for a given frequency so that only the spatial distribution of the feed points is varying. The average noise power is set based on the received signal power averaged across all azimuth angles.

4.4.1 4 MHz Random Feed Point Configurations. The standard deviation of the estimation error resulting from 25 random combinations of $N_A = 4$ feed points for a $f_c = 4$ MHz incident signal is shown in Fig. 4.23. It is evident that care must be

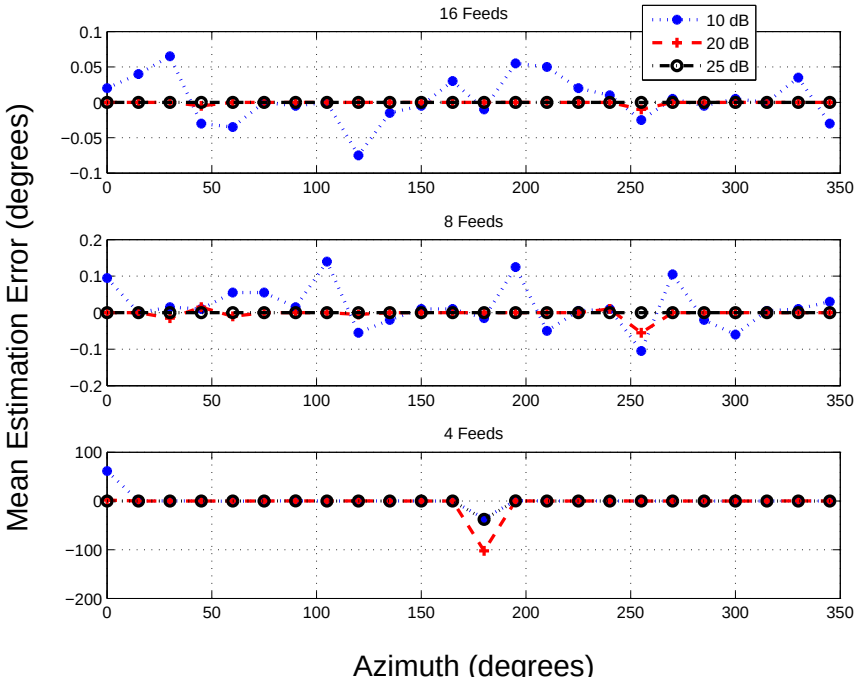

Figure 4.22: Average estimation error vs. SNR for an $f_c = 11$ MHz incident signal. Results based on multiple values of SNR. NOTE: Error scales (y-axis) are different for each plot.

taken when selecting which feed points to include in a reduced array, as the standard deviation of the resulting estimation error varies greatly. While some combinations result in standard deviation near 0° across all azimuth angles, others exceed 50° at numerous azimuth angles. The $N_A = 16$ feed point locations on the aircraft, as well as the $N_A = 4$ feed points from the best random configuration and the four feed points with the highest input impedance, are shown in Appendix C.

The mean standard deviation resulting from the 25 random configurations is shown in Fig. 4.24 where it is compared to the standard deviation of the random configuration resulting in the lowest standard deviation and the standard deviation of the $N_A = 4$ feed points with the highest input impedance. The mean standard deviation of the 25 random configurations is greater than the standard deviation of the high input impedance configuration at all but one azimuth angle.

The best performing random configuration results in a lower standard deviation than the high impedance configuration for all azimuth angles simulated. The feed

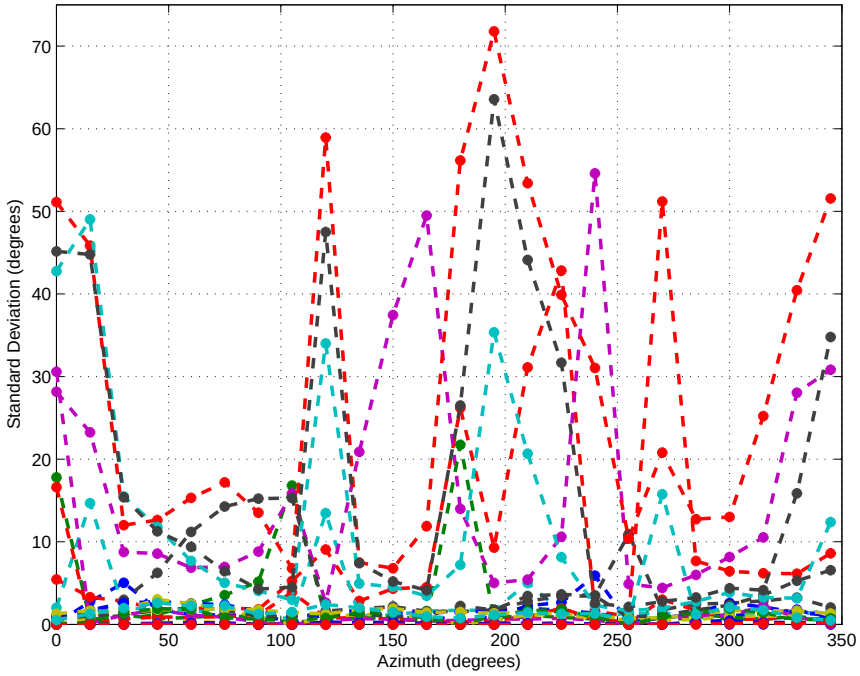

Figure 4.23: Standard deviation vs. azimuth for 25 random configurations of $N_A = 4$ feed points using a $f_c = 4$ MHz incident signal. Results based on $SNR = 25$ dB.

points used in the best random configuration are 6, 11, 13, and 14 in the BRC-provided data. Feed point 14 is also one of the 4 highest input impedance feed points and is physically located on the upper portion of the tail of the aircraft. Feed point 13 also has some vertical displacement, as it is physically located near the base of the tail of the aircraft. Feed points 6 and 11 are located on opposite wings.

4.4.2 11 MHz Random Feed Point Configurations. The standard deviation of the estimation error resulting from 25 random combinations of $N_A = 4$ feed points for an $f_c = 11$ MHz incident signal is shown in Fig 4.25. The standard deviation does not vary as greatly for random configurations of $N_A = 4$ feed points for an $f_c = 11$ MHz incident signal as it does for a $f_c = 4$ MHz incident signal even with an SNR that is 5 dB lower. There are several feed point combinations which result in standard deviation near 0° across all azimuth angles, while there are some configurations that exceed 50° at certain azimuth angles and one configuration results in a large standard

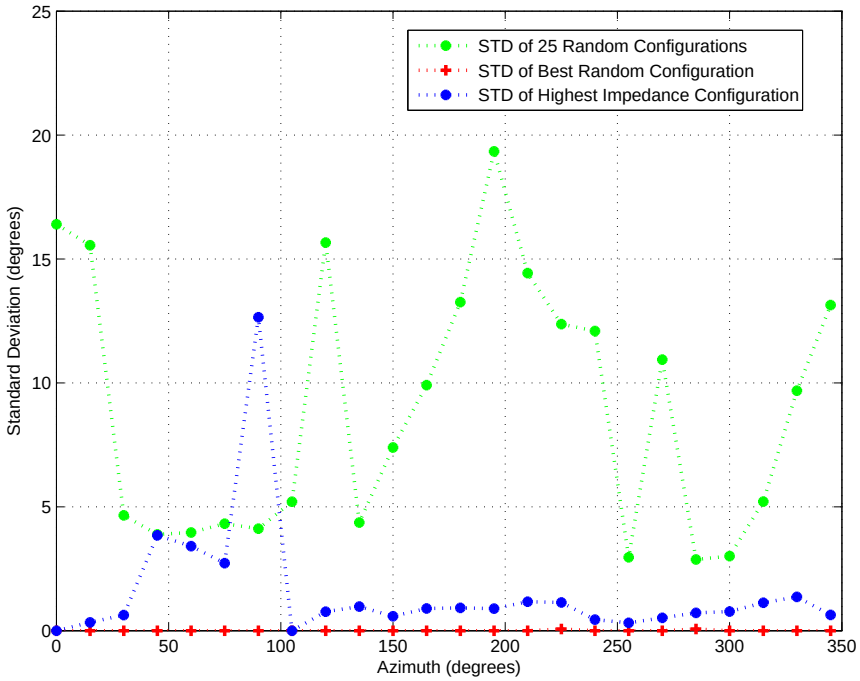

Figure 4.24: Standard deviation vs. Azimuth. Performance of the best $N_A = 4$ random feed point configuration compared to the mean standard deviation of 25 random configurations and $N_A = 4$ feed point configuration with highest input impedance. Results based on a $f_c = 4$ MHz incident signal with $SNR = 25$ dB.

deviation near an azimuth angle of 75°. The $N_A = 16$ feed point locations on the aircraft, as well as the $N_A = 4$ feed points from the best random configuration and the four feed points with the highest input impedance, are shown in Appendix C.

The mean standard deviation resulting from the 25 random configurations is shown in Fig. 4.26 where it is compared to the standard deviation of the random configuration resulting in the lowest standard deviation and the standard deviation of the $N_A = 4$ feed points with the highest input impedance. The mean standard deviation of the 25 random configurations is much closer to the standard deviation of the high input impedance configuration at most azimuth angles compared to the results with a $f_c = 4$ MHz incident signal. The best performing random configuration results in a lower standard deviation than the high impedance configuration for all azimuth angles. The feed points used in the best random configuration are labeled

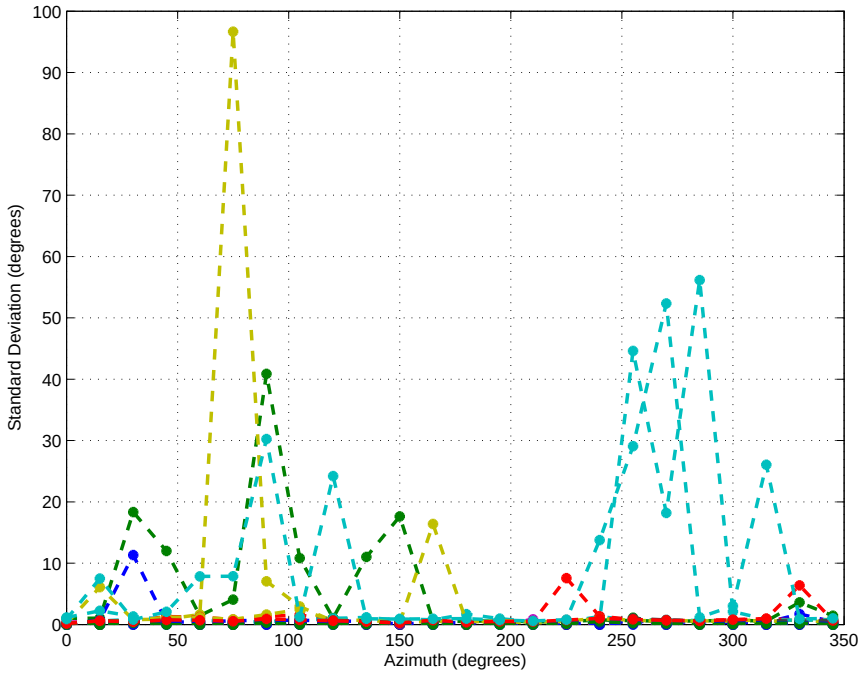

Figure 4.25: Standard Deviation vs. Azimuth for 25 random configurations of $N_A = 4$ feed points. Results based on an $f_c =$ 11 MHz incident signal with $SNR = 20$ dB.

1, 3, 5, and 16 in the BRC-provided data. Feed point 16 is also one of the 4 highest input impedance feed points and is physically located on the upper portion of the tail of the aircraft. Feed points 1 and 3 are located on approximately the same portion of the aircraft near the joint of the fuselage and the wing. Feed point 5 is located on the opposite wing also near the joint of the fuselage and wing. It is likely that placing the feed points near the wing-fuselage junction results in electromagnetic properties similar to a folded dipole antenna as discussed by Granger [17].

4.5 Summary of Individual Feed Point AOA Estimation Results

The results using combinations of $N_A = 4$, $N_A = 8$, and $N_A = 16$ feed points, each with an independent receiver channel, show that accurate AOA estimation of HF signals from an airborne platform using the MLM algorithm is difficult to achieve. The simulations used to generate the results in this research are based on a "best-case"' scenario where the antenna response to the incident signal is known exactly, resulting

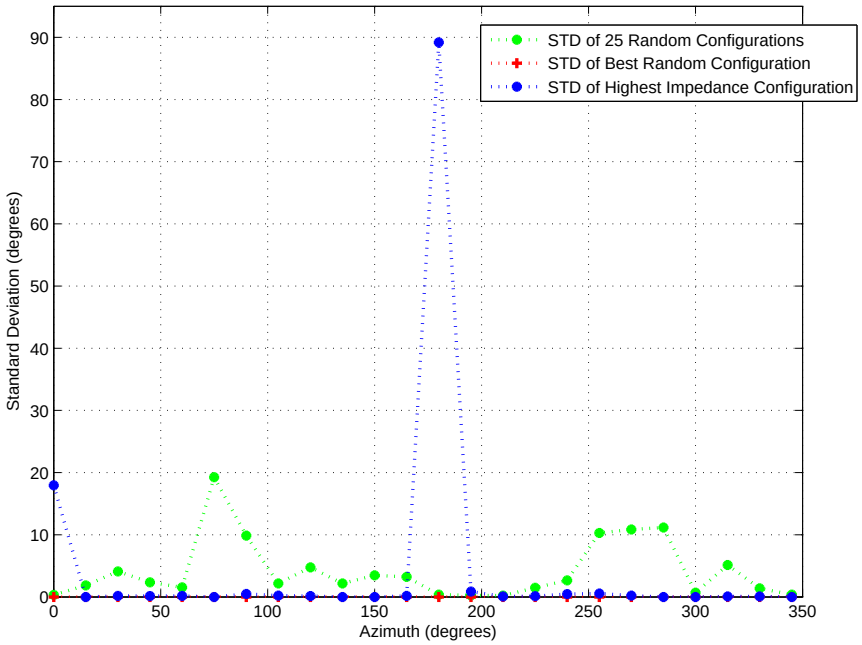

Figure 4.26: Standard deviation vs. Azimuth. Performance of best $N_A = 4$ random feed point configuration compared to the mean standard deviation of 25 random configurations and $N_A = 4$ feed point configuration with highest input impedance. Results based on an $f_c = 11$ MHz incident signal with $SNR = 20$ dB.

in a perfectly calibrated array manifold. All simulated incident signals are incident on the array at angles for which the response is in the array manifold, eliminating any interpolation. Additionally, only one signal is present in the simulated environment, and the signal is free from multipath effects. The only source of interference is complex, additive, white Gaussian noise. Given these ideal parameters, AOA estimation errors remain, especially at the lowest SNR values simulated. Additionally, the SNR has been improved by coherently integrating over 1024 samples of the incident signal, resulting in a 30.1 dB increase in SNR compared to the per-sample SNR.

The number of feed points used in the HFDF system had an affect on the estimation accuracy. As the number of feed points is reduced, the amount of error increases. The increase in estimation error is most noticeable when the number of feed points is reduced from $N_A = 8$ to $N_A = 4$ for both $f_c = 4$ MHz and $f_c = 11$

MHz incident signals. For an $f_c = 11$ MHz system, the performance of the $N_A = 16$ and $N_A = 8$ feed point systems is similar between $SNR = 10$ dB and $SNR = 20$ dB and performance is statistically the same for values greater than $SNR = 20$ dB. The increase in estimation error is more pronounced for a $f_c = 4$ MHz incident signal when reducing the feed points from $N_A = 16$ to $N_A = 8$.

The results of 25 random configurations of $N_A = 4$ feed points show that parameters other than input impedance must be considered when selecting which feed points to include in a reduced feed point system. The spatial distribution of the feed points as well as the directive gain patterns must be considered in addition to the input impedance when selecting which feed points to include. The results of the 25 random configurations show that the selection of the feed point locations had a larger impact on standard deviation of estimation accuracy for the $f_c = 4$ MHz system than the $f_c = 11$ MHz system. More random configurations resulted in standard deviation near zero degrees for the $f_c = 11$ MHz system and the feed points of the best random configuration at $f_c = 11$ MHz has relatively little spatial diversity. The gain patterns for the $f_c = 11$ MHz feed points overall have larger gain and more diversity of pattern shape. The finding that spatial diversity is not as large a factor in selecting feed points for the $f_c = 11$ MHz system agree with the results reported by Newman [27]: as the electrical size of the structure increases, the feed point location is not as critical as it is when the electrical size of the structure is small.

4.6 Results and Analysis of a 4 MHz Synthesized Array HFDF System

This section presents the results and analysis of HFDF system performance using combinations of $N_A = 4$, $N_A = 8$, and $N_A = 16$ feed points to synthesize the radiation pattern of an orthogonal, 3-loop cube antenna for a $f_c = 4$ MHz incident signal. The patterns are synthesized by linearly combining the feed points used in the individual feed point simulations. The results of simulations in this section are based on the far-field radiated voltage, not the received voltage. The incident signals, steering vectors, and array manifolds are based directly on the complex, far-field,

radiated voltages provided by BRC, as it is not possible to apply the reciprocity theorem outlined in Chapter III to the synthesized data. The resulting synthesized patterns of each loop are contained in Appendix A.

! Direct comparison of synthesized array and individual feed point HFDF system results is not valid because the format of the antenna data used to generate the results are not equivalent.

4.6.1 AOA Results Using 16 Feed Points to Synthesize a Cube Antenna Pattern. This section contains the results and analysis of HFDF system simulations using synthesized cube antenna patterns resulting from the linear combination of $N_A = 16$ feed points and a $f_c = 4$ MHz incident signal.

The top plot of Fig. 4.27 shows the average AOA estimation error as a function of SNR. The estimation error averaged over 200 Monte Carlo iterations at each of the 24 simulated azimuth angles is plotted for each simulated SNR. As the SNR increases, the average estimation error converges to 0°. At the lowest SNR value, $SNR = 10$ dB, the average estimation errors are distributed between ±10°. The bottom plot of Fig. 4.27 shows the average estimation error versus SNR where the estimation error is averaged over 200 Monte Carlo iterations and 24 azimuth angles. The error bars represent the 95% confidence interval of the average estimation error. Average estimation error is approximately 0° for all values beyond $SNR = 25$ dB. The synthesized patterns associated with this linear combination of feed points are contained in Appendix A.

The standard deviation of the AOA estimation error resulting from a $f_c = 4$ MHz incident signal on a simulated HFDF system with a synthesized pattern using $N_A = 16$ feed points is shown in Fig. 4.28. The standard deviation is determined using 200 Monte Carlo iterations at each azimuth angle and averaged over 24 azimuth angles for each simulated SNR value. The threshold SNR for accurate DF is defined as the SNR beyond which minimal reduction in the standard deviation is realized as the SNR increases. The threshold SNR is determined to be approximately $SNR = 20$ dB

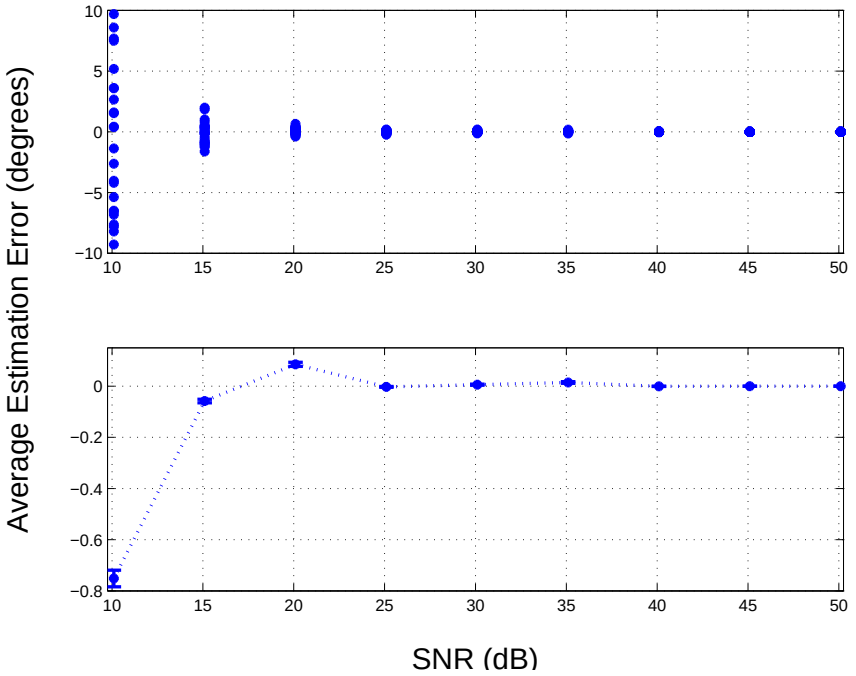

Figure 4.27: Azimuth estimation error vs. SNR for a $f_c = 4$ MHz incident signal using $N_A = 16$ feed points to synthesize a cube antenna pattern. Top: Average estimation error of 24 azimuth angles based on 200 Monte Carlo iterations. Bottom: Estimation error averaged over 200 Monte Carlo iterations and 24 azimuth angles with 95% confidence intervals.

to $SNR = 25$ dB. The standard deviation decreases significantly, by approximately 50°, as the SNR increases from $SNR = 10$ dB to $SNR = 15$ dB.

The distribution of the estimation errors as a function of azimuth with $SNR = 20$ dB is shown in Fig. 4.29. The nearly even distribution of the errors around 0° for all azimuth angles leads to the average estimation error being near 0°. Most of the errors are between ±10° with some errors approaching 15°. There is minimal expanding and contracting of the error envelope across all azimuth angles due to the near-equal directive gain of the synthesized antenna pattern across all azimuth angles.

4.6.2 AOA Results Using 8 Feed Points to Synthesize a Cube Antenna Pattern.

This section contains the results and analysis of HFDF system simulations using synthesized cube antenna patterns resulting from the linear combination of $N_A = 8$

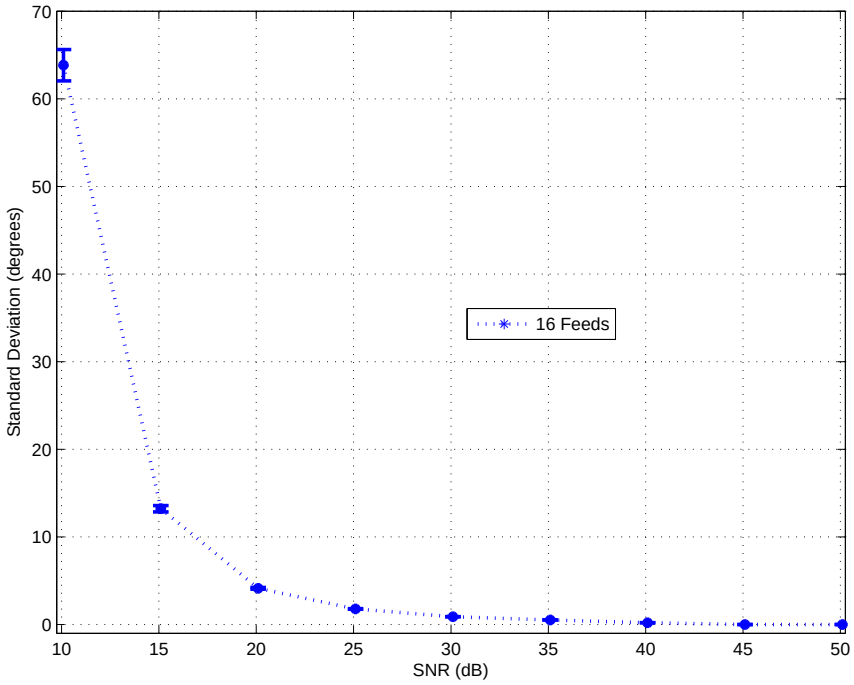

Figure 4.28: Standard deviation of AOA estimation error vs. SNR for a $f_c = 4$ MHz incident signal with 95% confidence intervals using $N_A = 16$ feed points to synthesize a cube antenna pattern.

feed points and a $f_c = 4$ MHz incident signal. The synthesized patterns associated with this linear combination of feed points are contained in Appendix A.

The top plot of Fig. 4.30 shows the average AOA estimation error as a function of SNR. The estimation error averaged over 200 Monte Carlo iterations at each of the 24 simulated azimuth angles is plotted for each simulated SNR. As the SNR increases, the average estimation error converges to 0°. For SNR values between $SNR = 10$ dB and $SNR = 20$ dB, the average estimation error at some azimuth angles is noticeably greater than the average. At the lowest SNR value, $SNR = 10$ dB, the average estimation errors are distributed between ±60°. This distribution of errors is much greater than the results using $N_A = 16$ feed points to synthesize the pattern. The bottom plot of Fig. 4.30 shows the average estimation error versus SNR where the estimation error is averaged over 200 Monte Carlo iterations and 24 azimuth angles.

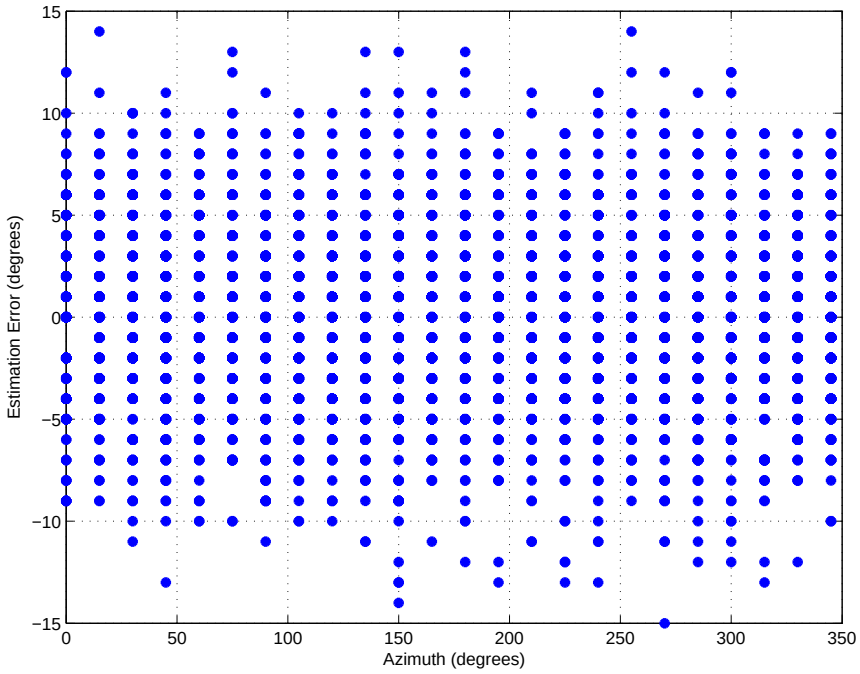

Figure 4.29: Azimuth estimation error vs. true azimuth angle for a $f_c = 4$ MHz incident signal with $SNR = 20$ dB using $N_A = 16$ feed points to synthesize a cube antenna pattern.

The error bars represent the 95% confidence interval of the average estimation error. Average estimation error is approximately 0° for all values o$SNR = 25$ dB.

The standard deviation of the AOA estimation error resulting from a $f_c = 4$ MHz incident signal on a simulated HFDF system with a synthesized pattern using $N_A = 8$ feed points is shown in Fig. 4.31. The threshold SNR is determined to be approximately $SNR = 20$ dB to $SNR = 25$ dB. The reduction in standard deviation from $SNR = 10$ dB to $SNR = 15$ dB is approximately 40° and the standard deviation decreases an additional 30° between $SNR = 15$ dB and $SNR = 20$ dB. The standard deviation at the lowest SNR values are higher using $N_A = 8$ feed points compared to $N_A = 16$ indicating a wider distribution of estimation errors over the 200 iterations and 24 azimuth angles. The standard deviation is approximately 0° for all values greater than $SNR = 30$ dB.

The distribution of the estimation errors as a function of azimuth with $SNR =$ 20 dB is shown in Fig. 4.32. Again, the estimation errors are near evenly distributed

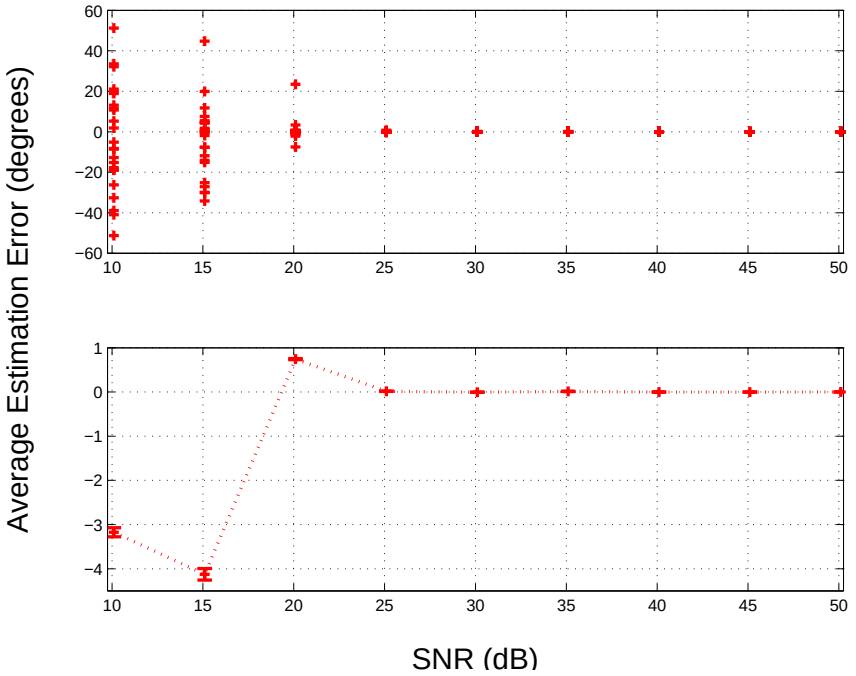

Figure 4.30: Azimuth estimation error vs. SNR for a $f_c = 4$ MHz incident signal using $N_A = 8$ feed points to synthesize a cube antenna pattern. Top: Average estimation error of 24 azimuth angles based on 200 Monte Carlo iterations. Bottom: Estimation error averaged over 200 Monte Carlo iterations and 24 azimuth angles with 95% confidence intervals.

around 0° for most azimuth angles resulting in an average error near 0°. Most of the errors are between ±25°. There are more large estimation errors present, some approaching ±180°, as compared to the results using $N_A = 16$ feed points to synthesize the cube antenna pattern. The expanding and contracting of the errors across all azimuth angles is more pronounced here and is due to the synthesized antenna patterns, especially the xz and yz-loops, having greater gain fluctuations than is present in the $N_A = 16$ feed point synthesized patterns.

4.6.3 AOA Results Using 4 Feed Points to Synthesize a Cube Antenna Pattern.

The results and analysis of HFDF system simulations using synthesized cube antenna patterns resulting from the linear combination of $N_A = 4$ feed points and a $f_c = 4$

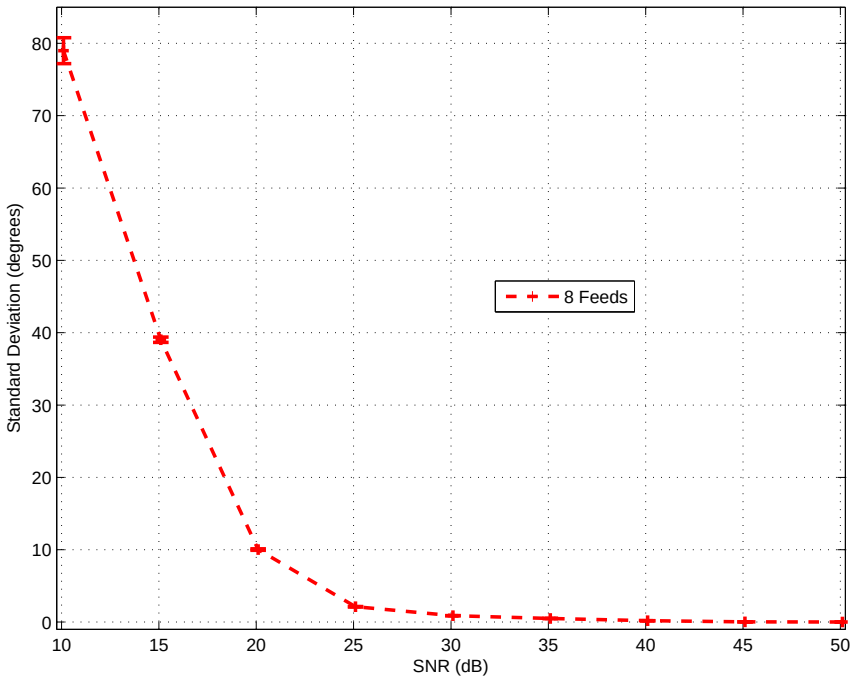

Figure 4.31: Standard deviation of AOA estimation error vs. SNR for a $f_c = 4$ MHz incident signal with 95% confidence intervals using $N_A = 8$ feed points to synthesize cube antenna pattern.

MHz incident signal are contained in this section. The synthesized patterns associated with this linear combination of feed points are contained in Appendix A.

The top plot of Fig. 4.33 shows the average AOA estimation error as a function of SNR. The estimation error averaged over 200 Monte Carlo iterations at each of the 24 simulated azimuth angles is plotted for each simulated SNR. As the SNR increases, the average estimation error converges to 0°, though it does not appear to reach 0° until SNR values are greater than $SNR = 35$ dB. The estimation errors at $SNR = 10$ dB are distributed between $\pm 40°$, but the distribution is not even. This range of errors is less than the error distribution when $N_A = 8$ feeds are used to synthesize the pattern. Similar to the distribution of errors for the synthesized pattern using $N_A = 8$ feed points, there are errors noticeably outside the mean of the distribution for values up to $SNR = 30$ dB. The bottom plot of Fig. 4.33 shows the average estimation error versus SNR where the estimation error is averaged over

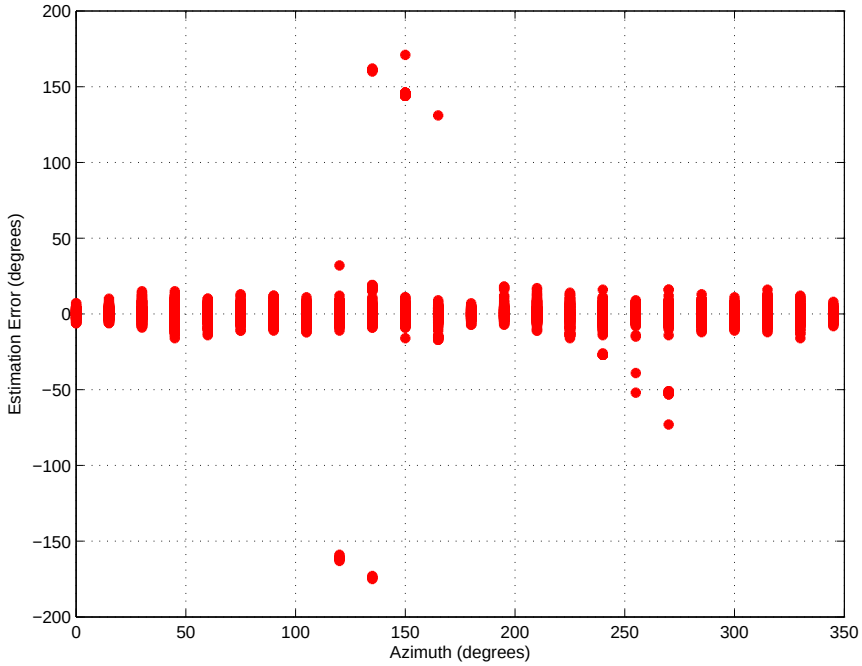

Figure 4.32: Azimuth estimation error vs. true azimuth angle for a $f_c = 4$ MHz incident signal with $SNR = 20$ dB.

200 Monte Carlo iterations and 24 azimuth angles. The error bars represent the 95% confidence interval of the average estimation error. Average estimation error does not reach 0° until the SNR value is $SNR = 35$ dB. An additional 10 dB of SNR is required to achieve 0° error when compared to the $N_A = 16$ or $N_A = 8$ feed point HFDF system using synthesized pattern data.

The standard deviation of the AOA estimation error resulting from a $f_c = 4$ MHz incident signal on a simulated HFDF system with a synthesized pattern using $N_A = 4$ feed points is shown in Fig. 4.34. The threshold SNR is determined to be approximately $SNR = 25$ dB to $SNR = 30$ dB. The standard deviation at $SNR = 10$ dB is approximately 5° less than the corresponding value when $N_A = 8$ feed points are used to synthesize the cube antenna pattern, indicating that the estimation errors are not as widely distributed at this SNR value. The standard deviation is approximately 0° for all values greater than $SNR = 35$ dB.

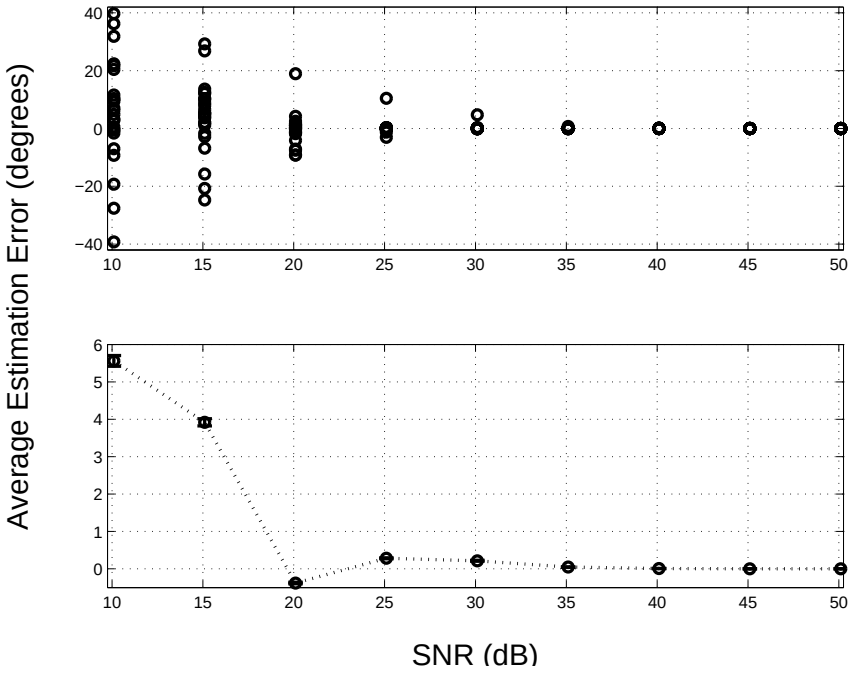

Figure 4.33: Azimuth estimation error vs. SNR for a $f_c = 4$ MHz incident signal using $N_A = 4$ feed points to synthesize a cube antenna pattern. Top: Average estimation error of 24 azimuth angles based on 200 Monte Carlo iterations. Bottom: Estimation error averaged over 200 Monte Carlo iterations and 24 azimuth angles with 95% confidence intervals.

The distribution of the estimation errors as a function of azimuth with $SN = 20$ dB is shown in Fig. 4.35. The estimation errors are not evenly distributed around 0° for azimuth angles between 240° and 75° resulting in an average error that is slightly negative. There are large estimation errors present with some near ±180°. These larger errors effect the average calculation by skewing the result away from 0°. The expanding and contracting of the error envelope across all azimuth angles is present, similar to the results when $N_A = 8$ feed points are used to synthesize the cube antenna pattern.

4.6.4 Comparison of AOA Estimation Performance Using 4, 8, and 16 Feed Points. This section contains a comparison of the AOA estimation results obtained when $N_A = 4$, $N_A = 8$, and $N_A = 16$ feed points are linearly combined to synthesize

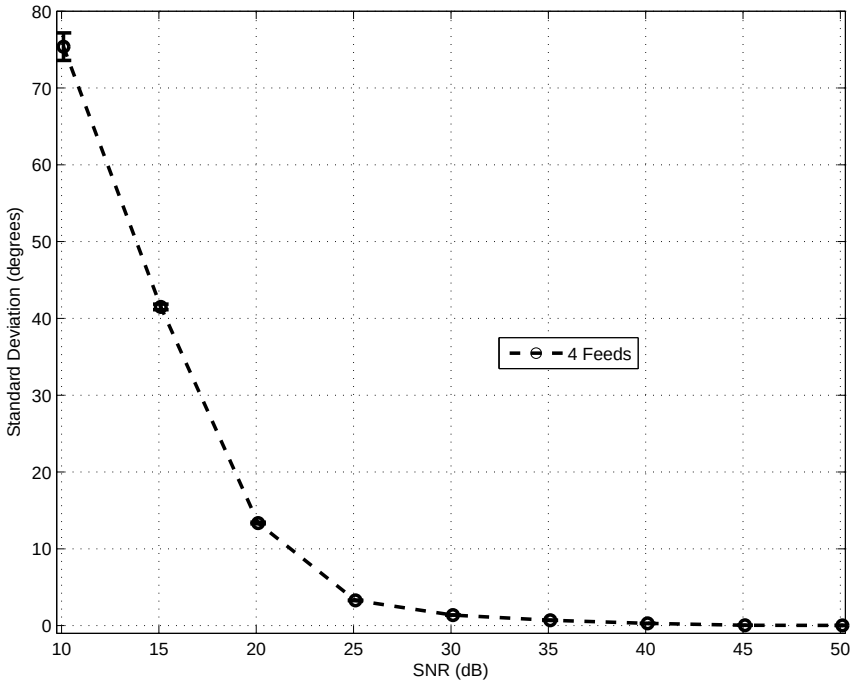

Figure 4.34: Standard deviation of AOA estimation error vs. SNR for a $f_c = 4$ MHz incident signal with 95% confidence intervals using $N_A = 4$ feed points to synthesize a cube antenna pattern.

the pattern of a cube antenna. The goal is to determine the relationship between the number of feed points used in a HFDF system and the resulting estimation errors. By minimizing the number of feed points necessary to perform AOA estimation, the amount of modification required on the aircraft and the complexity of the HFDF system may be reduced. The primary results used to compare system performance are standard deviation of the average estimation error and the average estimation error as a function of SNR over the range of simulated azimuth angles.

The standard deviation of the average estimation error resulting from combining $N_A = 4$, $N_A = 8$, and $N_A = 16$ feed points to synthesize the pattern of a cube antenna is shown in Fig. 4.36. The lowest standard deviation is achieved when $N_A = 16$ feed points are used to synthesize the pattern, especially between $SNR = 10$ dB and $SNR = 20$ dB. The standard deviation of the estimation error is approximately the

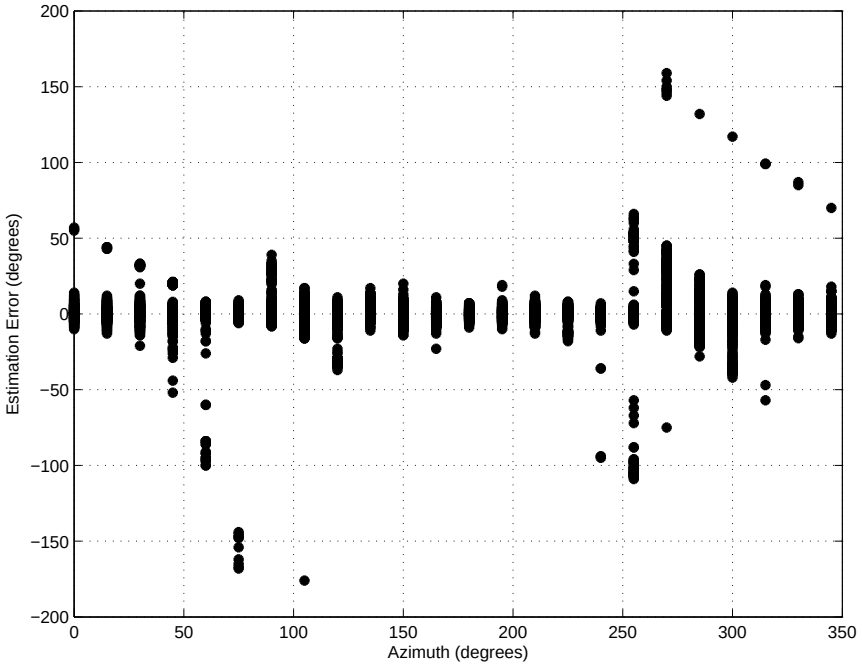

Figure 4.35: Azimuth estimation error vs. true azimuth angle for a $f_c = 4$ MHz incident signal with $SNR = 20$ dB using $N_A = 4$ feed points to synthesize a cube antenna pattern.

same when $N_A = 4$ or $N_A = 8$ feed points are used to synthesize the cube antenna pattern, with the only noticeable separation occurring at $SNR = 20$ dB.

The average estimation error as a function of azimuth angle and SNR for simulated HFDF systems comprised of $N_A = 4$, $N_A = 8$, and $N_A = 16$ feed points is shown in Fig. 4.37. The range of the average estimation error provides further evidence that the HFDF system using $N_A = 16$ feed points to synthesize the cube antenna pattern produces the minimum error of the 3 simulated HFDF systems. While the simulated system comprised of $N_A = 4$ feed points synthesizing the pattern shows greater overall estimation error at the lowest SNR values simulated, the magnitude of the errors is greatest for the HFDF system comprised of $N_A = 8$ feed points. The magnitude of the errors when $N_A = 8$ feed points are used to synthesize the pattern of a cube antenna are likely greater than when $N_A = 4$ feed points are used due to the higher directive gain of the synthesized loops when $N_A = 4$ feed points are used to synthesize the pattern of the cube antenna.

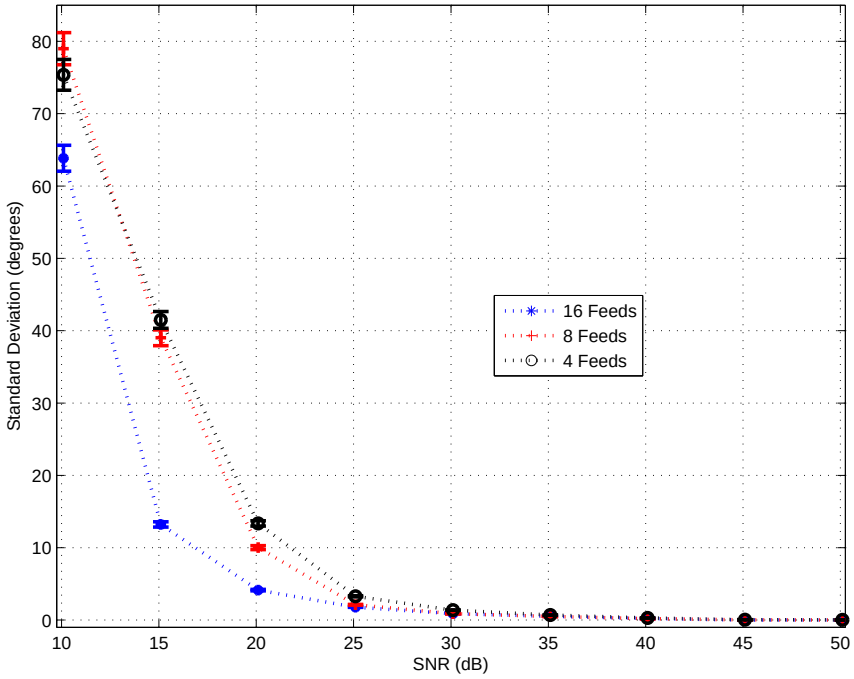

Figure 4.36: Standard deviation of azimuth estimation error vs. SNR for a $f_c = 4$ MHz incident signal. Standard deviation based on average estimation error over 200 iterations of 24 azimuth angles.

4.7 Results and Analysis of an 11 MHz Synthesized Array HFDF System

This section presents the results and analysis of HFDF system performance using combinations of $N_A = 4$, $N_A = 8$, and $N_A = 16$ feed points to synthesize the radiation pattern of an orthogonal, 3-loop cube antenna for an $f_c = 11$ MHz incident signal. The patterns are synthesized by linearly combining the radiated far-field voltages of the individual feed points. The results of simulations in this section are based on the far-field radiated voltage, not the received voltage. The incident signals, steering vectors, and array manifolds are based directly on the complex, far-field, radiated voltages provided by BRC, as it is not possible to directly apply the reciprocity theorem outlined in Chapter III to the synthesized data. The resulting synthesized patterns of each loop are contained in Appendix A.

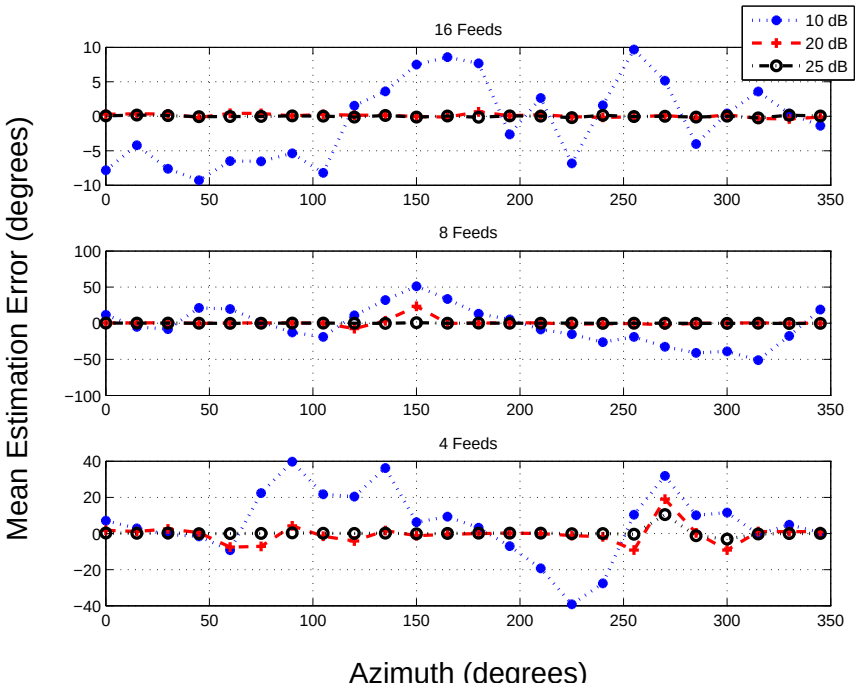

Figure 4.37: Average estimation error vs. SNR for a $f_c = 4$ MHz incident signal. Results based on multiple values of SNR. NOTE: Error scales (y-axis) are different for each plot.

4.7.1 AOA Results Using 16 Feed Points to Synthesize a Cube Antenna Pattern. This section contains the results and analysis of HFDF system simulations using synthesized cube antenna patterns resulting from the linear combination of $N_A = 16$ feed points and an $f_c = 11$ MHz incident signal. The synthesized patterns associated with this linear combination of feed points are contained in Appendix A.

The top plot of Fig. 4.38 shows the average AOA estimation error as a function of SNR. The estimation error averaged over 200 Monte Carlo iterations at each of the 24 simulated azimuth angles is plotted for each simulated SNR. As the SNR increases, the average estimation error converges to 0°. At the lowest SNR value, $SNR = 10$ dB, the average estimation errors are distributed between $-50°$ and $+20°$. The bottom plot of Fig. 4.38 shows the average estimation error versus SNR where the estimation error is averaged over 200 Monte Carlo iterations and 24 azimuth angles. The error bars represent the 95% confidence interval of the average estimation error. Average estimation error is approximately 0° for all values greater than $SNR = 25$ dB.

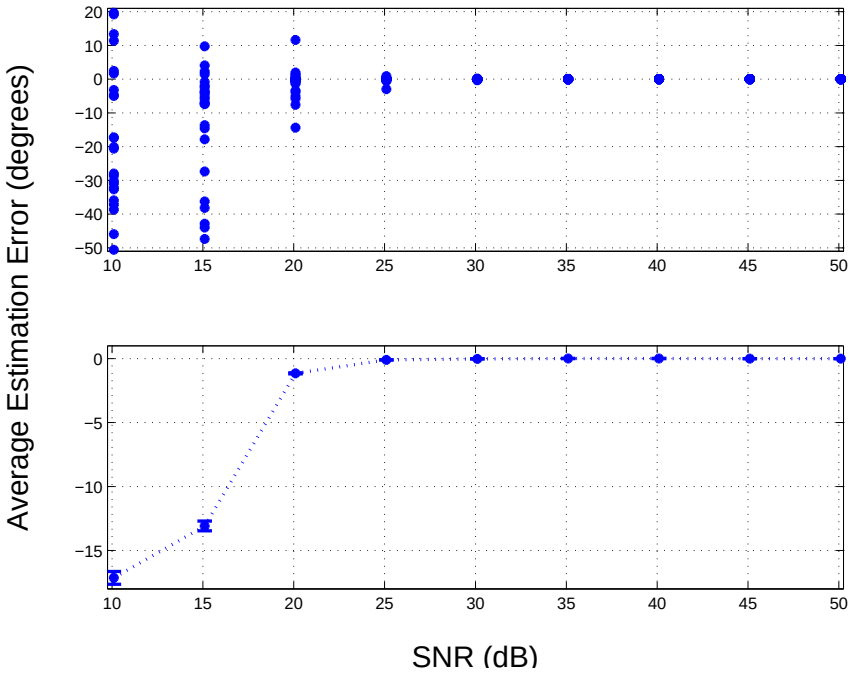

Figure 4.38: Azimuth estimation error vs. SNR for an $f_c = 11$ MHz incident signal using $N_A = 16$ feed points to synthesize a cube antenna pattern. Top: Average estimation error of 24 azimuth angles based on 200 Monte Carlo iterations. Bottom: Estimation error averaged over 200 Monte Carlo iterations and 24 azimuth angles with 95% confidence intervals.

The standard deviation of the AOA estimation error resulting from an $f_c = 11$ MHz incident signal on a simulated HFDF system with a synthesized pattern using $N_A = 16$ feeds is shown in Fig. 4.39. The threshold SNR is determined to be approximately $SNR = 20$ dB to $SNR = 25$ dB. The standard deviation is approximately 0° for all values greater than $SNR = 30$ dB. The large standard deviations at $SNR = 10$ dB and $SNR = 15$ dB SNR indicate that the estimation errors at these SNR values are distributed over a wide range of values.

The distribution of the estimation errors as a function of azimuth with $SNR = 20$ dB is shown in Fig. 4.40. Large magnitude errors appear between azimuth angles of 100° and 200°, resulting in the standard deviation of the azimuth estimation error to be near 10°. Most of the errors are between $\pm 20^\circ$.

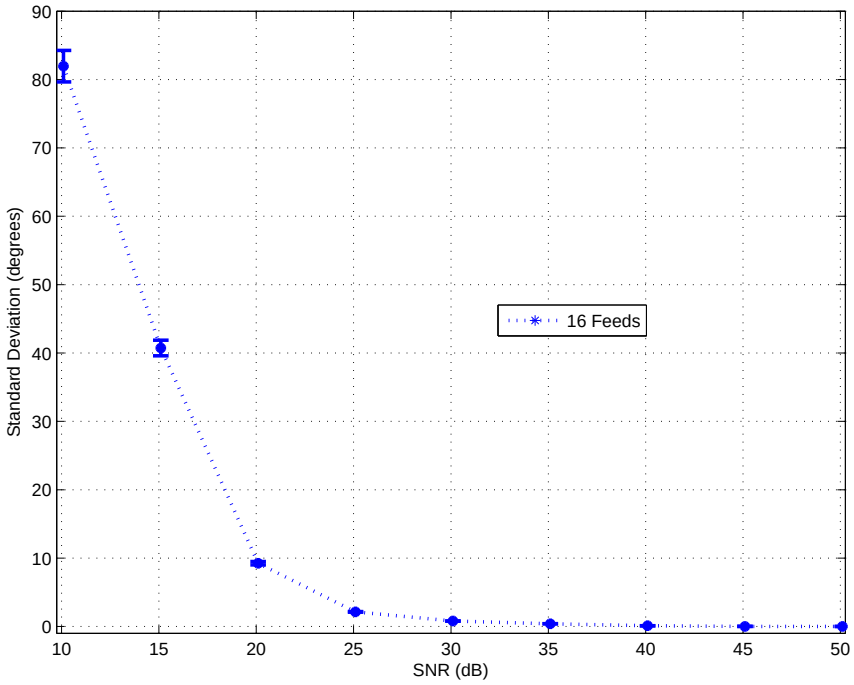

Figure 4.39: Standard deviation of AOA estimation error vs. SNR for an $f_c = 11$ MHz incident signal with 95% confidence intervals using $N_A = 16$ feed points to synthesize a cube antenna pattern.

4.7.2 AOA Results Using 8 Feed Points to Synthesize a Cube Antenna Pattern.

The results and analysis of HFDF system simulations using synthesized cube antenna patterns resulting from the linear combination of $N_A = 8$ feed points and an $f_c = 11$ MHz incident signal are contained in this section. The synthesized patterns associated with this linear combination of feed points are contained in Appendix A.

The top plot of Fig. 4.41 shows the average AOA estimation error as a function of SNR. The estimation error averaged over 200 Monte Carlo iterations at each of the 24 simulated azimuth angles is plotted for each simulated SNR. As the SNR increases, the average estimation error converges to 0°. The average estimation errors at $SNR = 10$ dB cover a large range of values, from $-60°$ to $+80°$. This distribution of errors is much greater than the results using $N_A = 16$ feed points to synthesize the pattern. The bottom plot of Fig. 4.41 shows the average estimation error versus SNR where the estimation error is averaged over 200 Monte Carlo iterations and 24

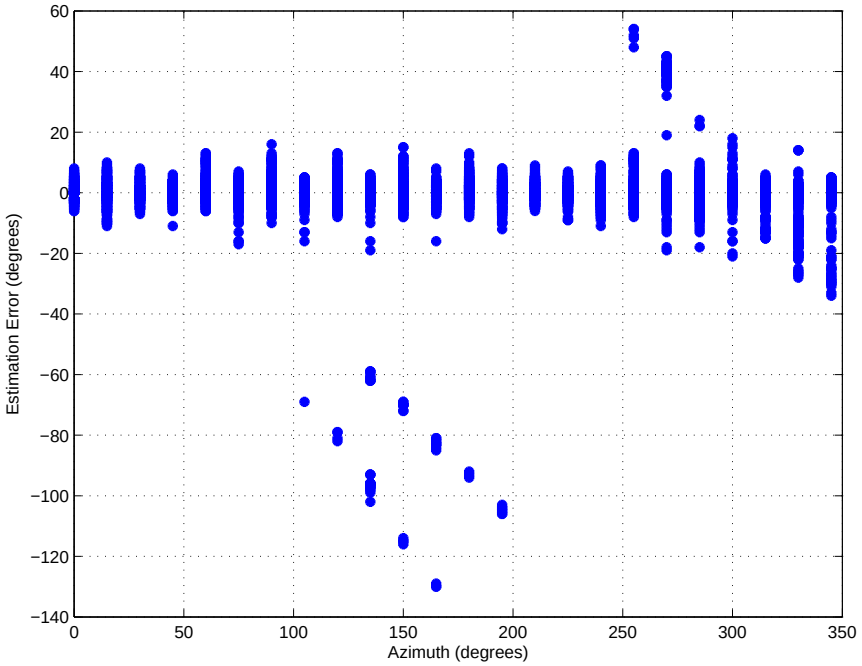

Figure 4.40: Azimuth estimation error vs. true azimuth angle for an $f_c = 11$ MHz incident signal with $SNR = 20$ dB using $N_A = 16$ feed points to synthesize a cube antenna pattern.

azimuth angles. The error bars represent the 95% confidence interval of the average estimation error. Average estimation error is approximately 0° for all values beyond $SNR = 20$ dB but the average error values at $SNR = 10$ and $SNR = 15$ dB are nearly the same magnitude (sign is different) as the errors present when $N_A = 16$ feed points are used to synthesize the cube antenna pattern.

The standard deviation of the AOA estimation error resulting from an $f_c = 11$ MHz incident signal on a simulated HFDF system with a synthesized pattern using $N_A = 8$ feeds is shown in Fig. 4.42. The threshold SNR is determined to be approximately $SNR = 20$ dB to $SNR = 25$ dB. The reduction in standard deviation between $SNR = 15$ dB to $SNR = 20$ dB is greater than 25°. The significant reduction in standard deviation between $SNR = 10$ dB and $SNR = 20$ dB is a result of the reduction in the range of average estimation errors over these SNR values. The standard deviation at $SNR = 10$ dB using $N_A = 8$ feed points is approximately 5° less than when $N_A = 16$ feed points are used, indicating that the distribution of

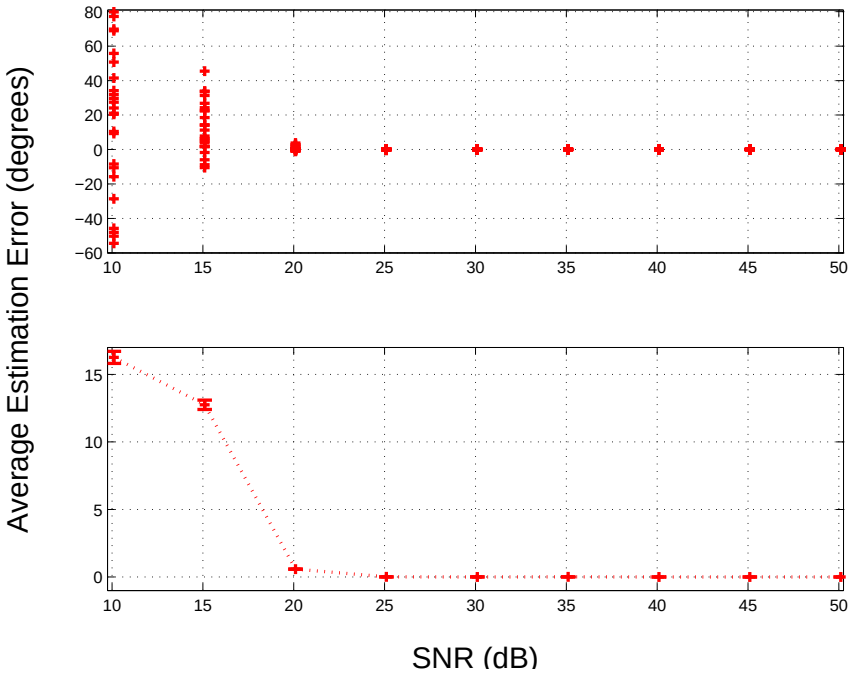

Figure 4.41: Azimuth estimation error vs. SNR for an $f_c = 11$ MHz incident signal using $N_A = 8$ feed points to synthesize a cube antenna pattern. Top: Average estimation error of 24 azimuth angles based on 200 Monte Carlo iterations. Bottom: Estimation error averaged over 200 Monte Carlo iterations and 24 azimuth angles with 95% confidence intervals.

estimation errors over the 200 iterations and 24 azimuth angles is slightly less when $N_A = 8$ feed points are used. The standard deviation is approximately 0° for all values greater than $SNR = 35$ dB.

The distribution of the estimation errors as a function of azimuth with $SNR = 20$ dB is shown in Fig. 4.43. The estimation errors are somewhat evenly distributed around 0° for most azimuth angles resulting in an average error near 0°. Most of the errors are between ±25°. There are a few larger estimation errors present, some approaching 180°, though not as many large magnitude errors using $N_A = 8$ feed points compared to the results using $N_A = 16$ feed points to synthesize the cube antenna pattern. This is a result of the pattern being nearly uniform across all azimuth angles resulting in similar responses for multiple azimuth AOAs. The largest errors present using $N_A = 8$ feed points occur near 0° and 180° azimuth.

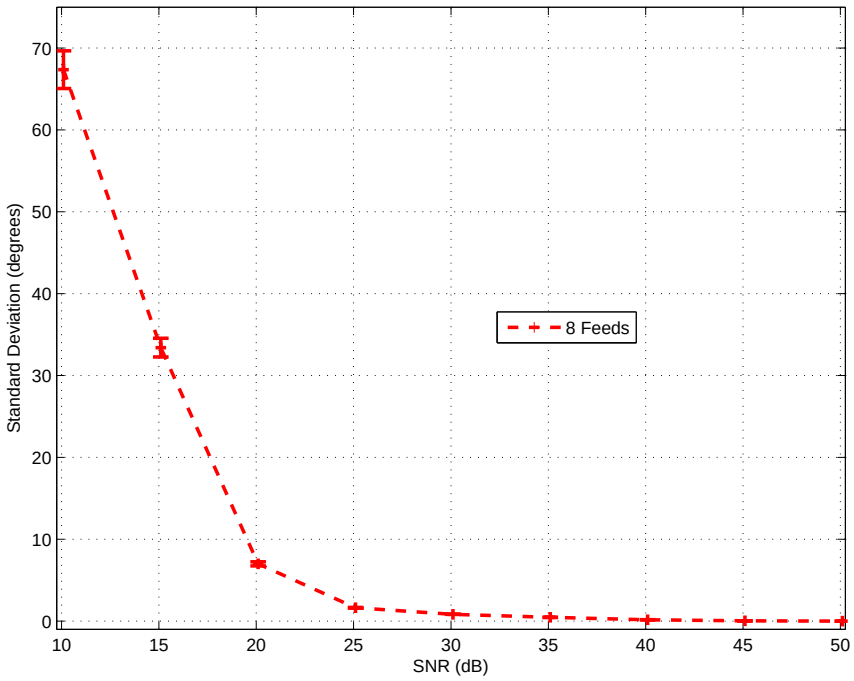

Figure 4.42: Standard deviation of AOA estimation error vs. SNR for an $f_c = 11$ MHz incident signal with 95% confidence intervals using $N_A = 8$ feed points to synthesize a cube antenna pattern.

4.7.3 AOA Results Using 4 Feed Points to Synthesize a Cube Antenna Pattern.

This section contains the results and analysis of HFDF system simulations using synthesized cube antenna patterns resulting from the linear combination of $N_A = 4$ feed points and an $f_c = 11$ MHz incident signal. The synthesized patterns associated with this linear combination of feed points are contained in Appendix A.

The top plot of Fig. 4.44 shows the average AOA estimation error as a function of SNR. The estimation error averaged over 200 Monte Carlo iterations at each of the 24 simulated azimuth angles is plotted for each simulated SNR. As the SNR increases, the average estimation error converges to 0°, though it does not appear to reach 0° until values are greater than $SNR = 35$ dB. The average estimation errors at $SNR = 10$ dB are distributed between $-80°$ and $+60°$. This range of average errors is similar to the error distribution when $N_A = 8$ feed points are used to synthesize the pattern, though for $N_A = 4$ feed points the errors tend to be negative. Similar to the

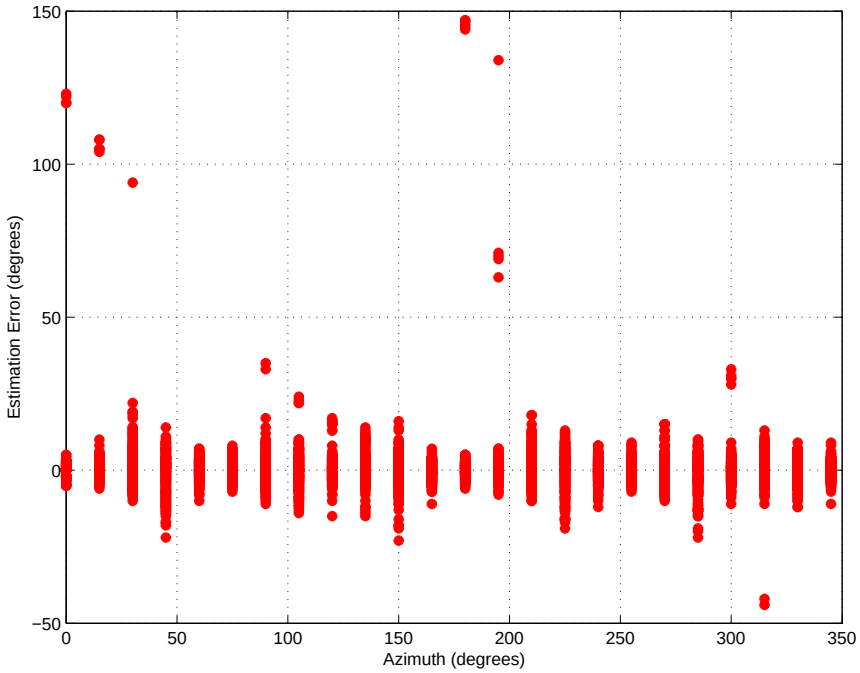

Figure 4.43: Azimuth estimation error vs. true azimuth angle for an $f_c = 11$ MHz incident signal with $SNR = 20$ dB using $N_A = 8$ feed points to synthesize a cube antenna pattern.

distribution of average errors for the synthesized pattern using $N_A = 8$ feed points, there are errors outside the mean of the distribution for values up to $SNR = 30$ dB. The bottom plot of Fig. 4.44 shows the average estimation error versus SNR where the estimation error is averaged over 200 Monte Carlo iterations and 24 azimuth angles. The error bars represent the 95% confidence interval of the average estimation error. Average estimation error approaches 0° when the value is above $SNR = 30$ dB.

The standard deviation of the AOA estimation error resulting from an $f_c = 11$ MHz incident signal on a simulated HFDF system with a synthesized pattern using $N_A = 4$ feeds is shown in Fig. 4.45. The threshold SNR is determined to be approximately $SNR = 25$ dB to $SNR = 30$ dB. The standard deviation at $SNR = 10$ dB is approximately the same as when $N_A = 16$ feed points are used to synthesize the cube antenna pattern. The standard deviation is approximately 0° for all values greater than $SNR = 35$ dB.

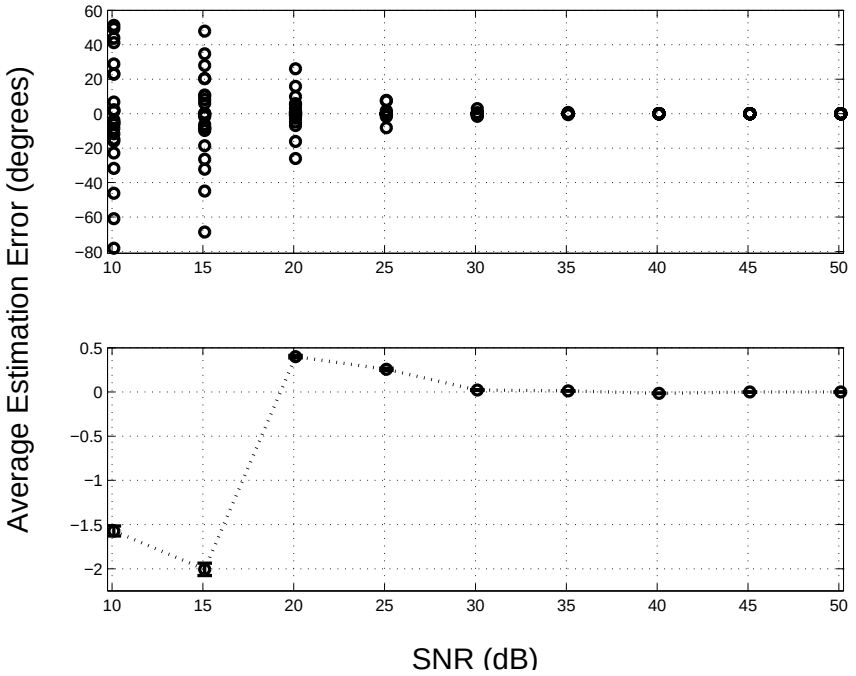

Figure 4.44: Azimuth estimation error vs. SNR for an $f_c = 11$ MHz incident signal using $N_A = 4$ feed points to synthesize a cube antenna pattern. Top: Average estimation error of 24 azimuth angles based on 200 Monte Carlo iterations. Bottom: Estimation error averaged over 200 Monte Carlo iterations and 24 azimuth angles with 95% confidence intervals.

The distribution of the estimation errors as a function of azimuth with $SNR =$ 20 dB is shown in Fig. 4.46. The estimation errors are widely distributed across all azimuth angles. There are several angles resulting in large estimation errors approaching $\pm 180°$. These larger errors effect the average error calculation by skewing the average away from $0°$.

4.7.4 Comparison of AOA Estimation Performance Using 4, 8, and 16 Feed Points. This section contains a comparison of the AOA estimation results obtained when $N_A = 4$, $N_A = 8$, and $N_A = 16$ feed points are linearly combined to synthesize the pattern of a cube antenna. The goal is to determine the relationship between the number of feed points used to synthesize the cube antenna pattern and the AOA estimation errors. Minimizing the number of feed points used will reduce the amount

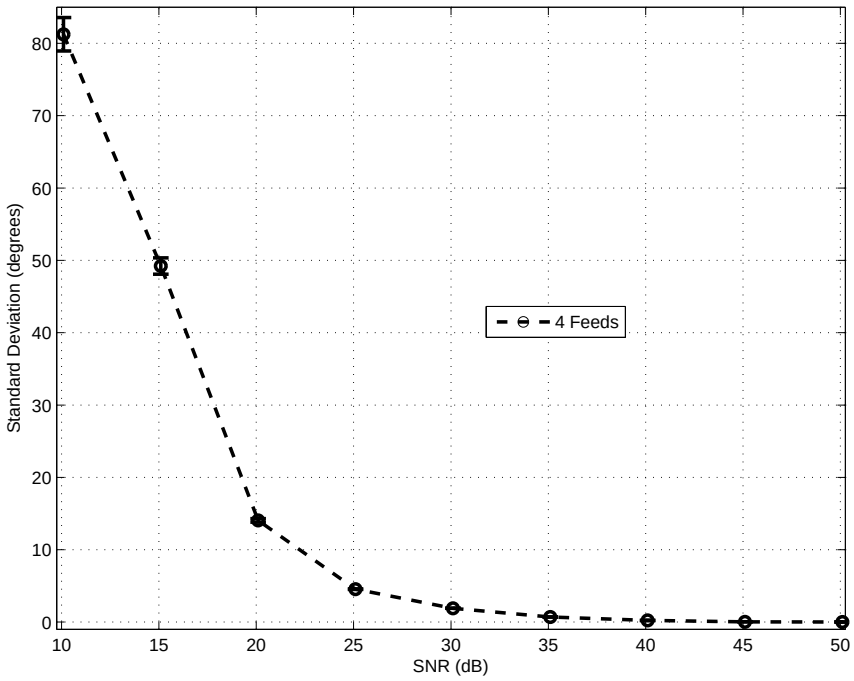

Figure 4.45: Standard deviation of AOA estimation error vs. SNR for an $f_c = 11$ MHz incident signal with 95% confidence intervals using $N_A = 4$ feed points to synthesize a cube antenna pattern.

of modification required on the aircraft and reduce the complexity of the DF system. The primary results used to compare system performance are standard deviation of the estimation error and the average estimation error over the range of simulated azimuth angles for multiple SNR values.

The standard deviation of the average estimation errors resulting from combining $N_A = 4$, $N_A = 8$, and $N_A = 16$ feed points to synthesize the pattern of a cube antenna is shown in Fig. 4.47. Between $SNR = 10$ dB and $SNR = 20$ dB, the minimum standard deviation is achieved when $N_A = 8$ feed points are used to synthesize the pattern.

The average estimation error as a function of azimuth angle and SNR for simulated HFDF systems comprised of $N_A = 4$, $N_A = 8$, and $N_A = 16$ feed points is shown in Fig. 4.48. The range of the average estimation error provides further evidence that the HFDF system using $N_A = 16$ feed points to synthesize the cube antenna pattern

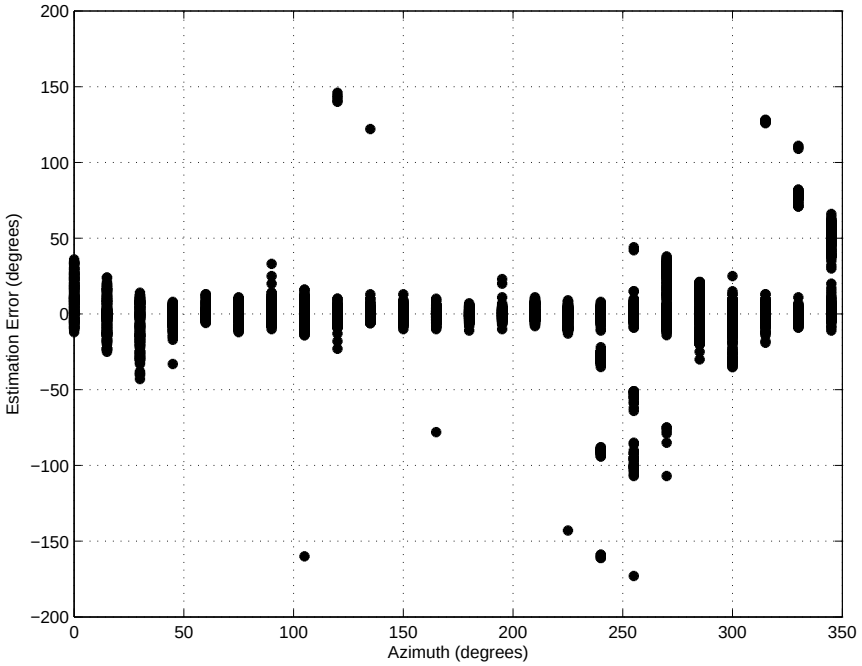

Figure 4.46: Azimuth estimation error vs. true azimuth angle for an $f_c = 11$ MHz incident signal with $SNR = 20$ dB using $N_A = 4$ feed points to synthesize a cube antenna pattern.

produces the minimum estimation error of the 3 simulated systems. At the lowest SNR value, the simulated HFDF system comprised of $N_A = 4$ feed points synthesizing the cube antenna pattern results in a lower average estimation error over most azimuth angles but as the SNR increases, the simulated HFDF system using $N_A = 8$ feed points to synthesize the pattern produces lower average estimation error.

4.8 Summary of Synthesized Array AOA Estimation Results

The results using $N_A = 4$, $N_A = 8$, and $N_A = 16$ feed points to synthesize the pattern of a 3-loop cube antenna demonstrate that accurate AOA estimation of HF signals from an airborne platform using the MLM algorithm is difficult to achieve. As is the case with the individual feed model, the synthesized array simulations are of a "best-case"' scenario. Given the ideal parameters used in the simulation, large AOA estimation errors are present, particularly at the lowest SNR values simulated. The distribution of the errors covers a large range with numerous, large magnitude

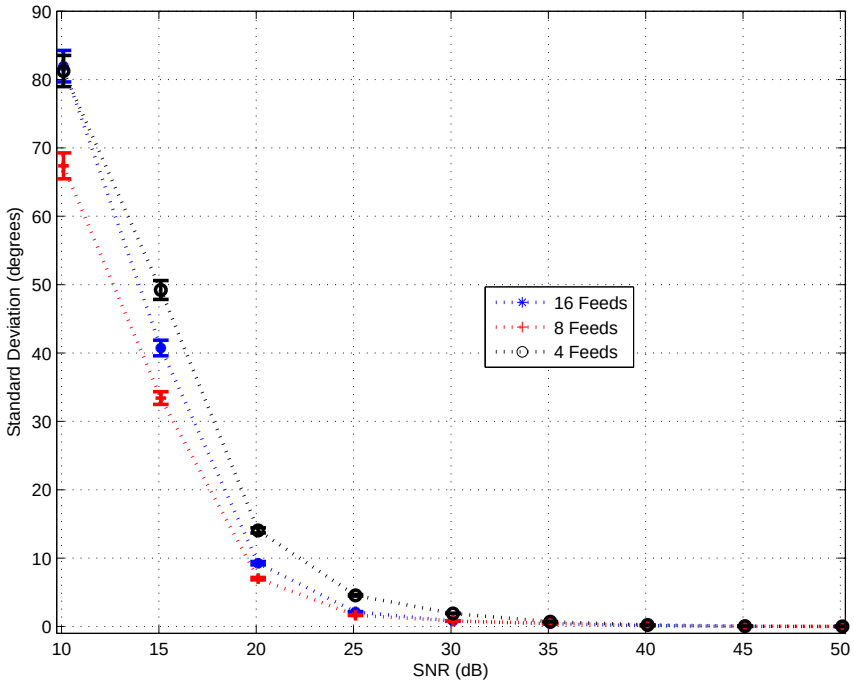

Figure 4.47: Standard deviation of azimuth estimation error vs. SNR for an $f_c = 11$ MHz incident signal. Standard deviation based on average estimation error over 200 iterations of 24 azimuth angles.

estimation errors occurring at several azimuth angles. The performance of the HFDF systems does not seem to benefit greatly when more feed points are used to synthesize the pattern, as the model using an $N_A = 8$ feed point match resulted in a lower standard deviation of errors at $f_c = 11$ MHz. At $SNR = 13$ dB, accurate AOA estimation is not achieved by any of the simulated synthesized systems. Average estimation error does not approach 0° until $SNR = 25$ dB to $SNR = 30$ dB is achieved, which may be unrealistic in an operational setting. Additionally, the SNR has been improved by coherently integrating over 1024 samples of the incident signal, resulting in a 30.1 dB increase in SNR compared to the per-sample SNR. The directive gain patterns of the 3 loops, particularly the xy-loop, are nearly uniform over all azimuth angles. This uniformity may result in similar system responses at multiple AOAs.

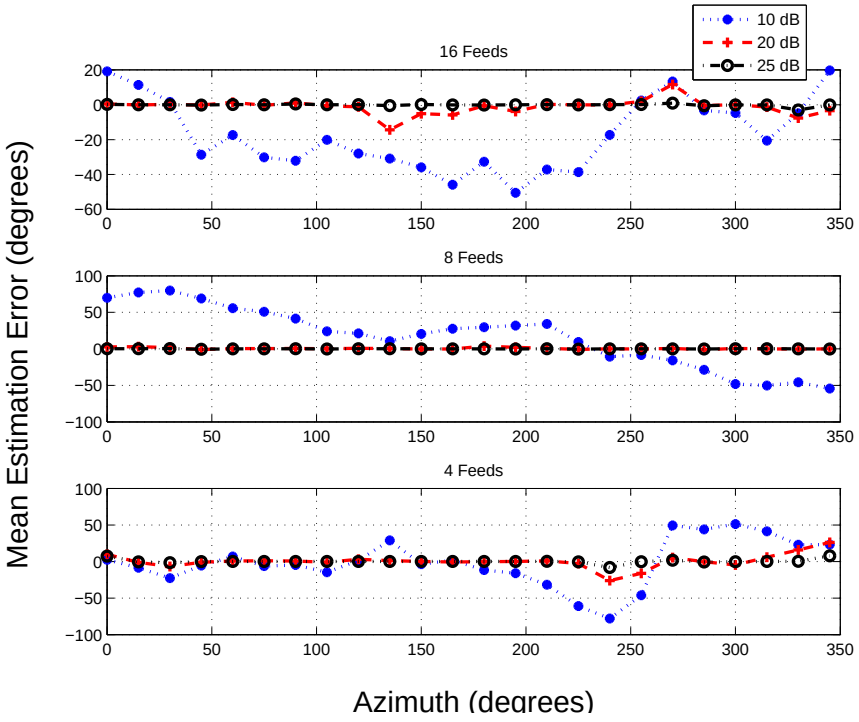

Figure 4.48: Average estimation error vs. SNR for an $f_c = 11$ MHz incident signal. Results based on multiple values of SNR. NOTE: Error scales (y-axis) are different for each plot.

V. Conclusions and Recommendations

The primary purpose of this research was to determine if an ensemble of Structurally Integrated (SI) antennas can function in a high frequency direction finding (HFDF) system on a large, airborne platform. The accuracy of azimuth-only angle of arrival (AOA) estimation using incident signals with center frequencies of $f_c = 4$ MHz and $f_c = 11$ MHz was the primary focus of this research. The maximum likelihood method (MLM) DF algorithm was used to generate the AOA estimates. Two potential methods for combining and processing the ensemble of SI antenna outputs for HFDF purposes have been explored. One method used a receive channel for each feed point. The second method used the antenna ensemble to synthesize the pattern of a 3-loop cube antenna, also called a vector antenna, and only required three receiver channels. A secondary goal was to determine the relationship between the number of feed points used in the HFDF system and the resulting azimuth-only estimation error. The effect of input impedance and feed point location on HFDF system performance was explored as well.

5.1 Conclusions

Using an ensemble of SI antennas with superesolution estimation techniques demonstrate potential for extending accurate DF techniques to the high frequency (HF) range. Current military DF capability at HF is generally not publicly available, though as of 2002, a low-band DF subsystem was still being developed [2]. All simulations conducted for this research were based on a "best-case" scenario with the ensemble response to the simulated AOA being known exactly, resulting in a perfectly calibrated array manifold. A sufficient number of Monte Carlo iterations were used to generate statistically significant AOA estimates. Additionally, 1024 samples of the complex incident signal were coherently integrated, effectively increasing the per-sample signal-to-noise ratio (SNR) by approximately 30 dB.

The DF accuracy demonstrated under this research shows the difficulty of performing accurate DF in the HF range. Using an ensemble of $N_A = 16$ SI antenna feed

points, with each feed point having an independent receiver channel, average azimuth AOA estimation errors of less than 1° were achieved at the relatively low $SNR = 10$ dB for an incident signal at $f_c = 4$ MHz. When the ensemble was reduced to $N_A = 8$ SI antenna feed points, the estimation accuracy decreased to an average error within $\pm 2°$ of the true AOA at $SNR = 10$ dB. However, for $N_A = 4$ SI antenna feed points the azimuth-only AOA estimation was very poor, even when potentially unrealistic $SNR \geq 35$ dB conditions were simulated.

The trend of increased azimuth AOA error with decreasing N_A held true for $f_c = 11$ MHz incident signals as well. Using $N_A = 16$ SI antenna feed points with independent receiver channels resulted in AOA estimates within 0.1° with $SNR = 10$ dB. Using $N_A = 8$ SI antenna feed points resulted in a decrease in accuracy with the estimates within 0.15° of the true AOA. An ensemble of $N_A = 4$ SI antenna feed points resulted in poor estimation accuracy, with large-magnitude errors appearing at several AOAs.

Simulations using random configurations of $N_A = 4$ individual feed points showed that diversity of feed point location must be considered, in addition to the magnitude of the input impedance when generating an ensemble of structurally integrated antennas. At both center frequencies simulated in this research, including a feed point with vertical displacement, i.e. on the tail of the aircraft, in an ensemble of $N_A = 4$ SI antenna feed points resulted in more accurate AOA estimates than the ensemble consisting of the $N_A = 4$ SI antenna feed points with the highest input impedance used as the sole criteria for selection.

Based on simulation results, it is possible to perform HFDF using an ensemble of SI antennas, though the number of antennas required to achieve the desired level of accuracy will depend on operational objectives. The more feed points available for use in the HFDF system, the more accurate the estimates will be, especially as the frequency increases.

The AOA estimation accuracy was poor when the radiated far-field voltages were combined to synthesize the pattern of a 3-loop cube antenna, regardless of frequency and number of feed points used. Linearly combining the voltages of the feed points is an unnecessary step resulting in suboptimal arrays.

5.2 Recommendations

The next research step should include finding a suitable set of collocated SI feed points which allow accurate DF for the desired range of center frequencies, 2-32 MHz. Based on the results of this research and the research of Newman [27], the location of the feed points is more critical at the lowest frequencies, when the aircraft is electrically small. The dimensions of the aircraft are on the order of, or larger than, a wavelength for frequencies above $f_c = 8$ MHz and locating the SI feed points exactly at the maximum of the characteristic current or voltage will not be as critical at these higher frequencies because more characteristic modes will be effective radiators. The desired accuracy of the AOA estimates will dictate the number of SI feed points required, but in general, including more SI feed points will result in a more accurate AOA estimate.

The results of this research should be verified using surrogate measurements. A multichannel HF receiver and set of HF antennas are available at AFIT for this purpose. The frequency manager should be able to provide the location and operating frequency of any local HF emitters so the accuracy of the surrogate AOA measurements may be verified. This step was originally planned for this research effort, but due to time constraints and unforeseen difficulty in developing the steering vectors and array manifolds for the available antennas, it was not completed.

The only source of interference in this research is complex, additive, white Gaussian noise with a noise power based on the desired SNR. Future research should include characterization of the expected noise power and radio frequency interference in the operational environment.

This research assumes that azimuth AOA is the desired output of the DF system and so elevation AOA was set to 90° for all simulations, that is, groundwave transmission was simulated. This is unrealistic when attempting to perform DF of HF signals. Signals in the HF range are often reflected from the ionosphere and are known as skywaves. Research into the accuracy of the system when skywaves are received by the system is needed and will include estimates of elevation and azimuth AOA.

The system model should also be extended to include incident AOAs not included in the array manifold. The results based on these AOAs will demonstrate the effect of the discrete array manifold on estimation accuracy. The model should also be extended to include multiple incident signals in the environment, which may require using an estimation technique such as multiple signal classification (MUSIC) or estimation of signal parameter via rotational invariance techniques (ESPRIT). The computational burden may be reduced by using MUSIC or ESPRIT as the MLM algorithm involves a time-intensive search of the array manifold to find the steering vector most correlated with the incident signal.

This research effort only examined the estimation accuracy achieved using ϕ-polarized incident signals because aircraft do not provide many vertical surfaces for installing θ-polarized feed points. In an operational setting, θ-polarized or cross-polarized signals will occur and may be of operational interest. Research into methods to increase the system response to diverse signal polarizations is needed.

Appendix A. Directive Gain Patterns Used for Direction Finding Simulations

This appendix contains the directive gain patterns of all individual feed points comprising the high frequency direction finding system for both $f_c = 4$ MHz and $f_c = 11$ MHz. The synthesized cube antenna patterns for both $f_c = 4$ MHz and $f_c = 11$ MHz are also included.

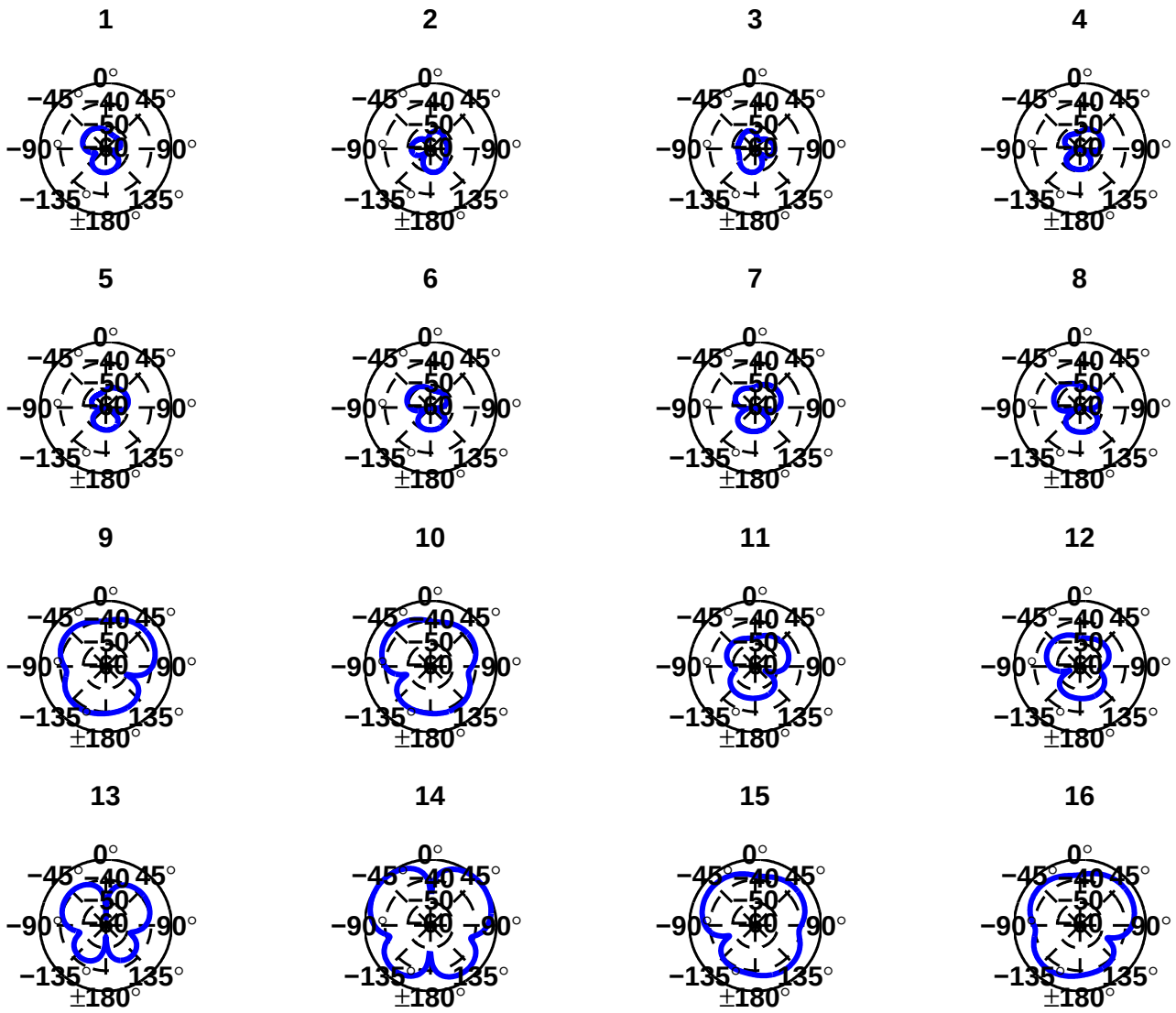

Figure A.1: $f_c = 4$ MHz feed point gain patterns. Feed points 10, 14, 15, 16 have the highest input impedance.

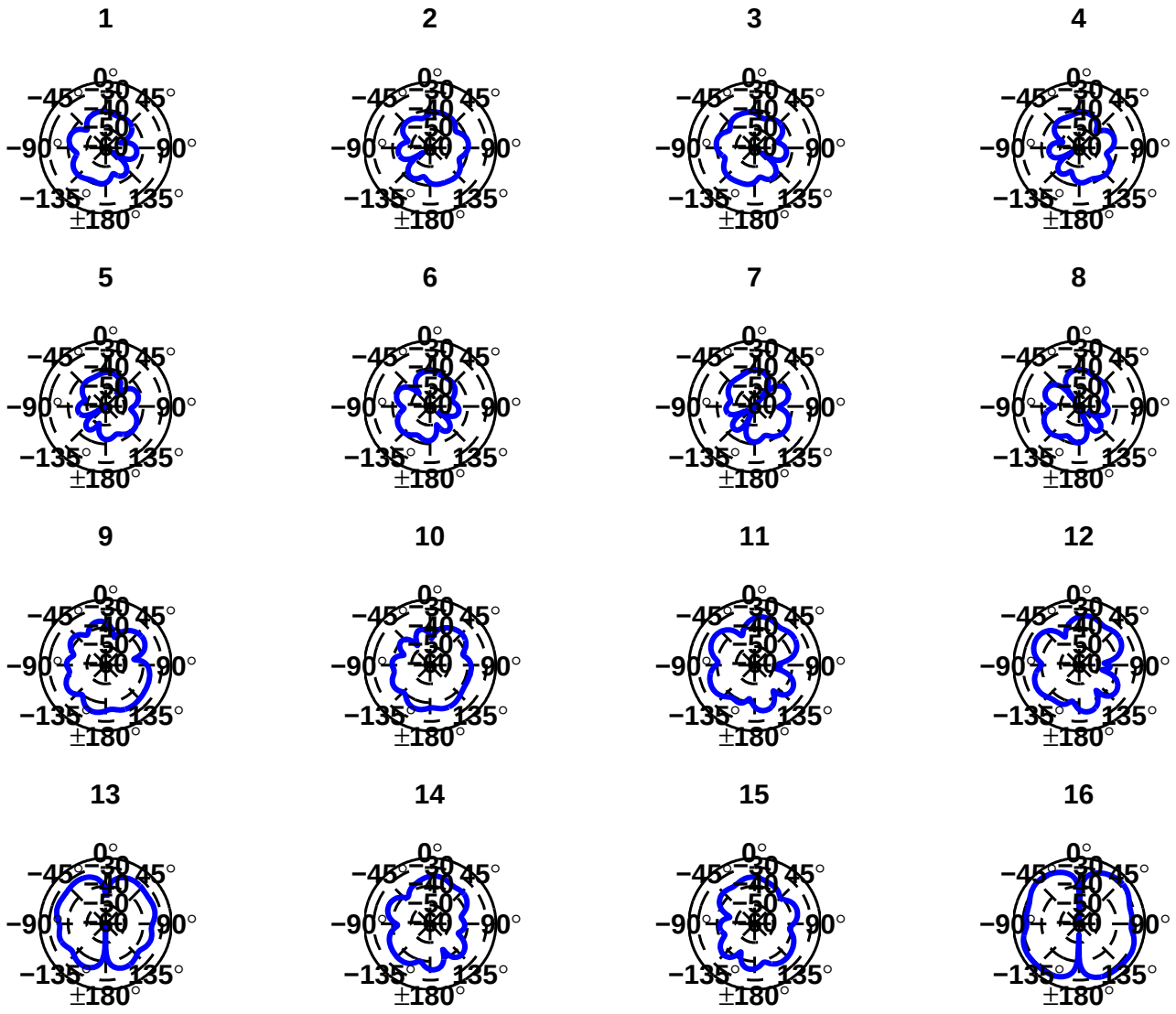

Figure A.2: $f_c = 11$ MHz feed point gain patterns. Feed points 11, 12, 13, 16 have the highest input impedance.

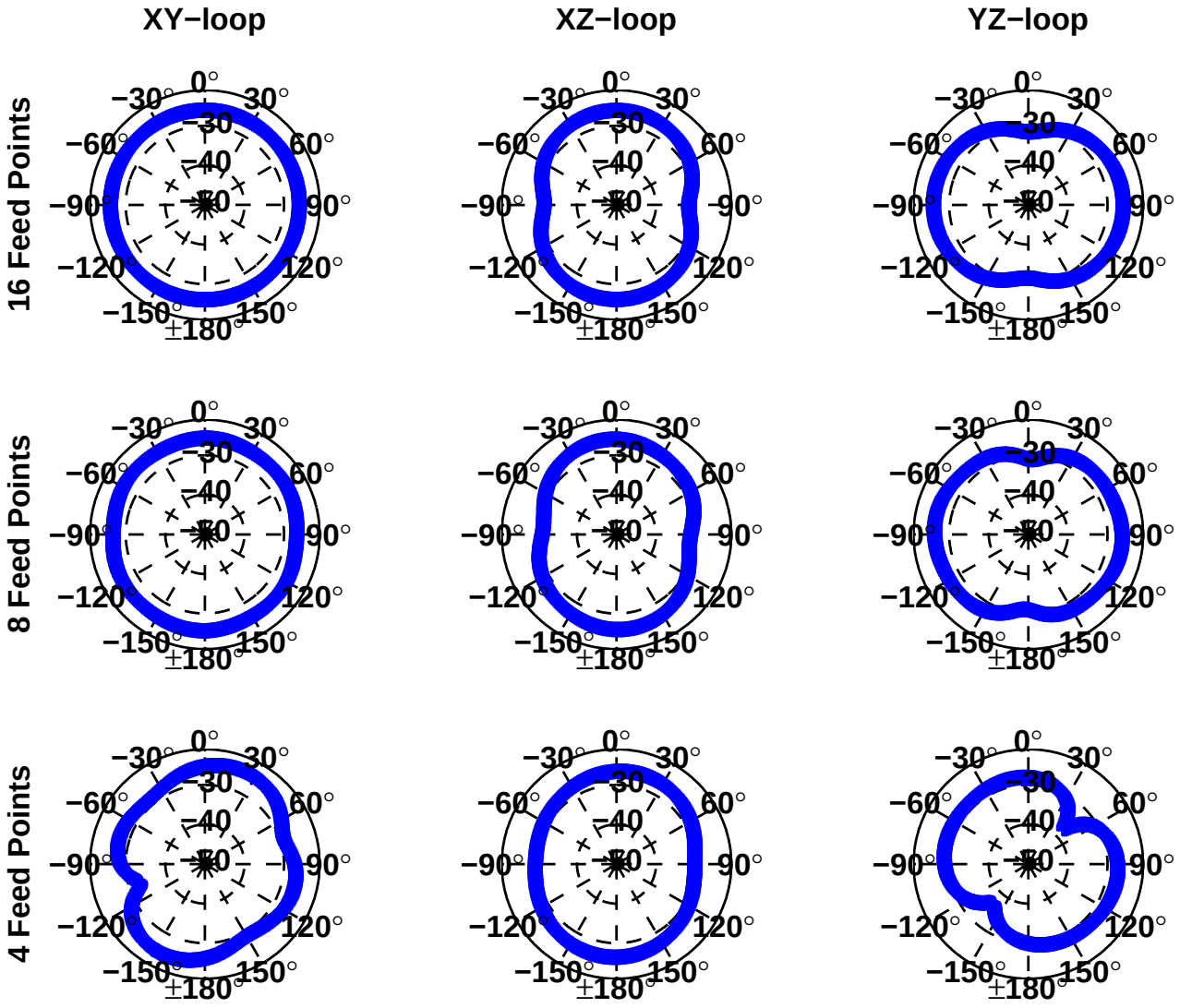

Figure A.3: $f_c = 4$ MHz synthesized cube antenna patterns. Each row contains all 3 loops for linear combinations of $N_A = 16$, $N_A = 8$, and $N_A = 4$ feed points.

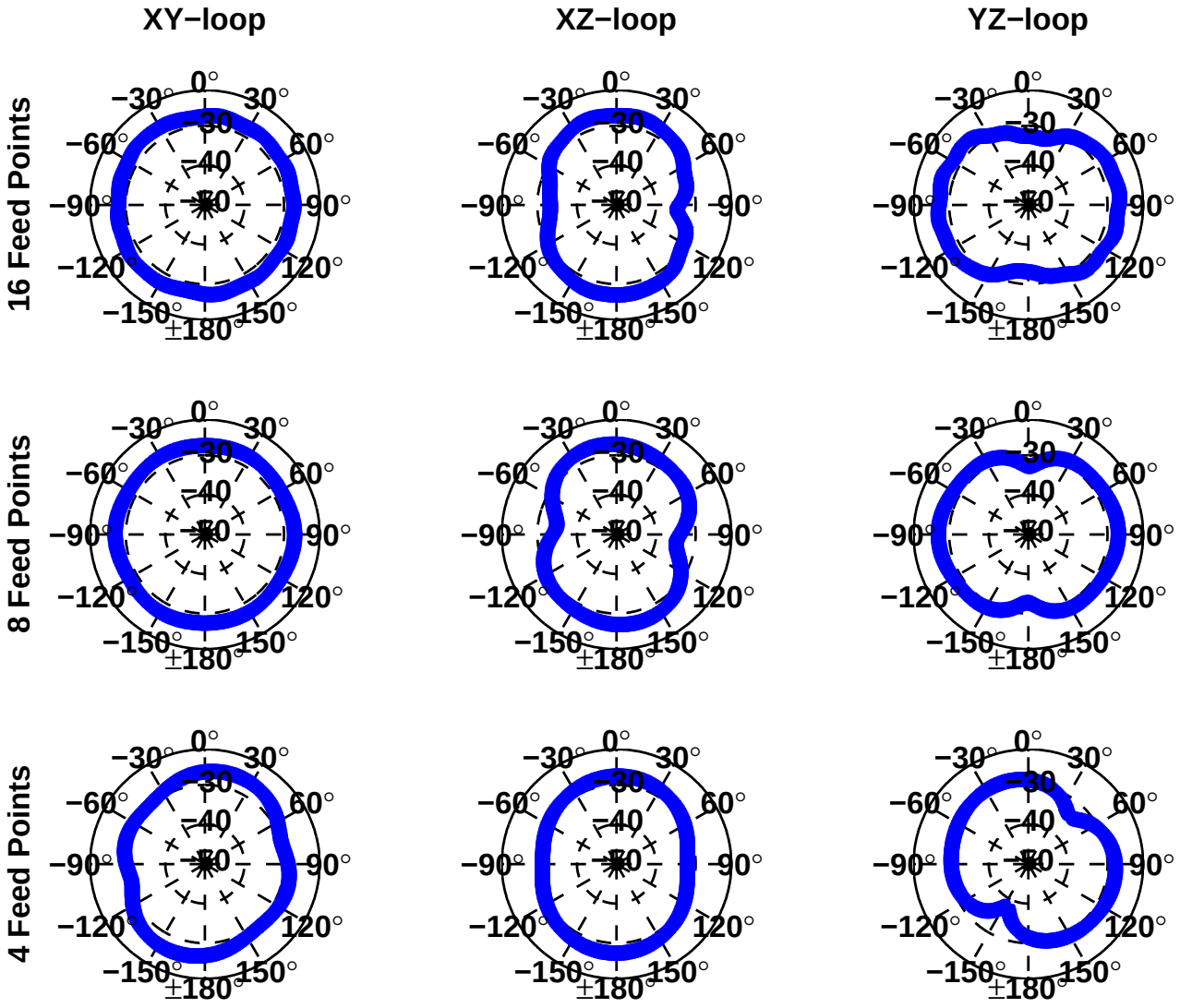

Figure A.4: $f_c = 11$ MHz synthesized cube antenna patterns. Each row contains all 3 loops for linear combinations of $N_A = 16$, $N_A = 8$, and $N_A = 4$ feed points.

Appendix B. Angle of Arrival Estimation Error Plots

This appendix contains estimation error distribution plots for multiple values of signal-to-noise ratio (SNR). These plots show the error distribution converges to 0° as the SNR increases.

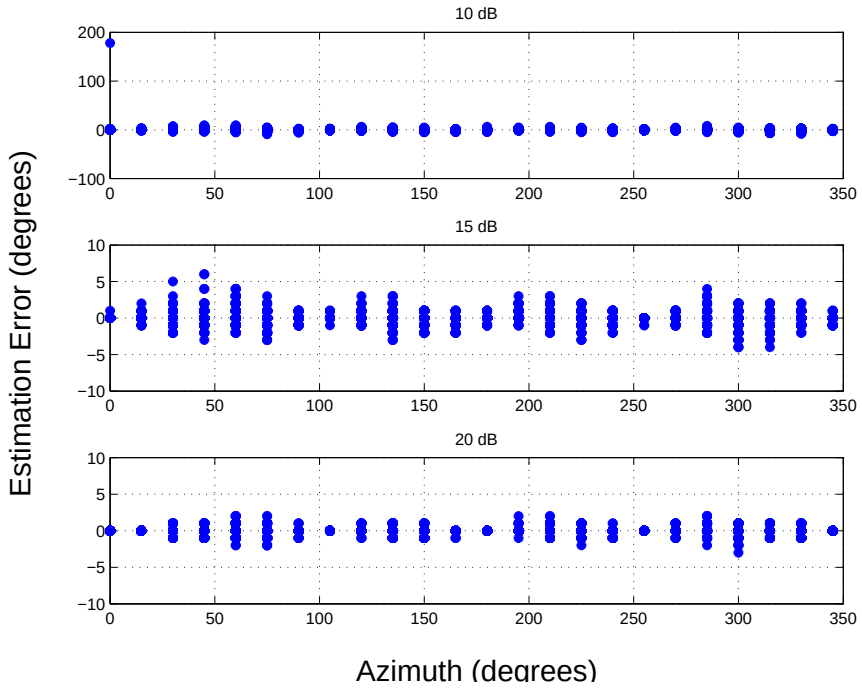

Figure B.1: $f_c = 4$ MHz Error Distribution vs. Azimuth for multiple SNR values using $N_A = 16$ individual feed points.

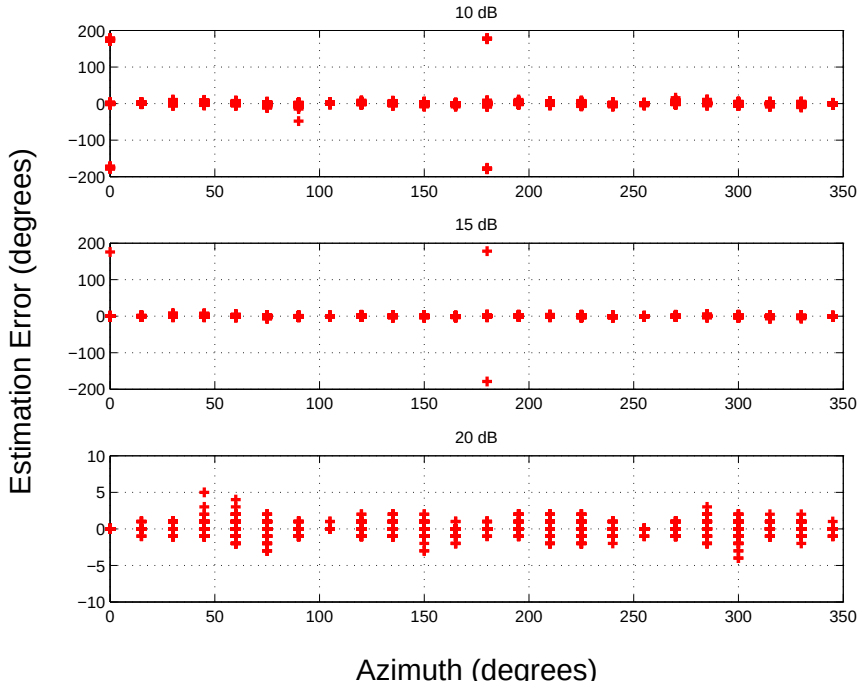

Figure B.2: $f_c = 4$ MHz Error Distribution vs. Azimuth for multiple SNR values using $N_A = 8$ individual feed points.

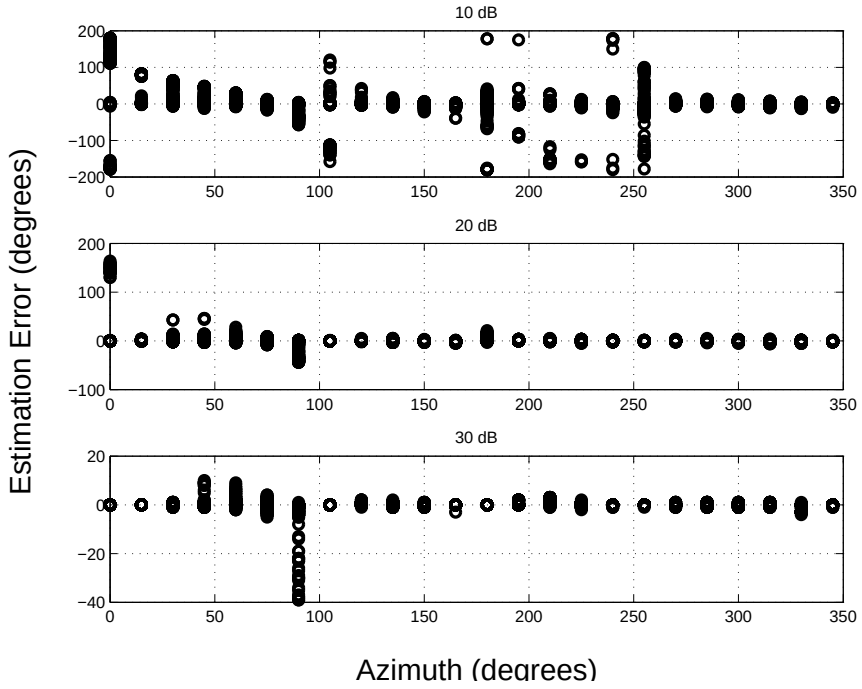

Figure B.3: $f_c = 4$ MHz Error Distribution vs. Azimuth for multiple SNR values using $N_A = 4$ individual feed points.

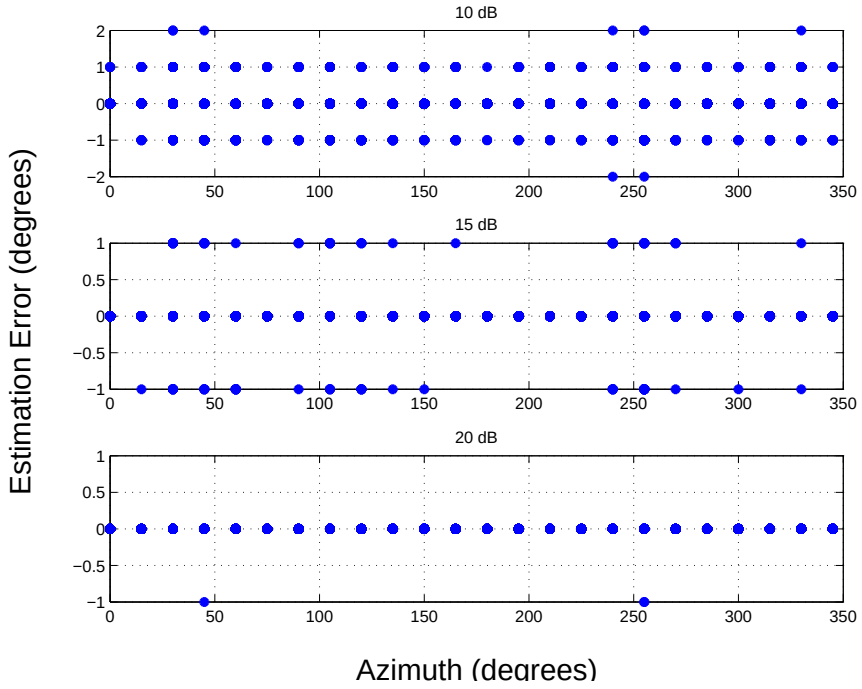

Figure B.4: $f_c = 11$ MHz Error Distribution vs. Azimuth for multiple SNR values using $N_A = 16$ individual feed points.

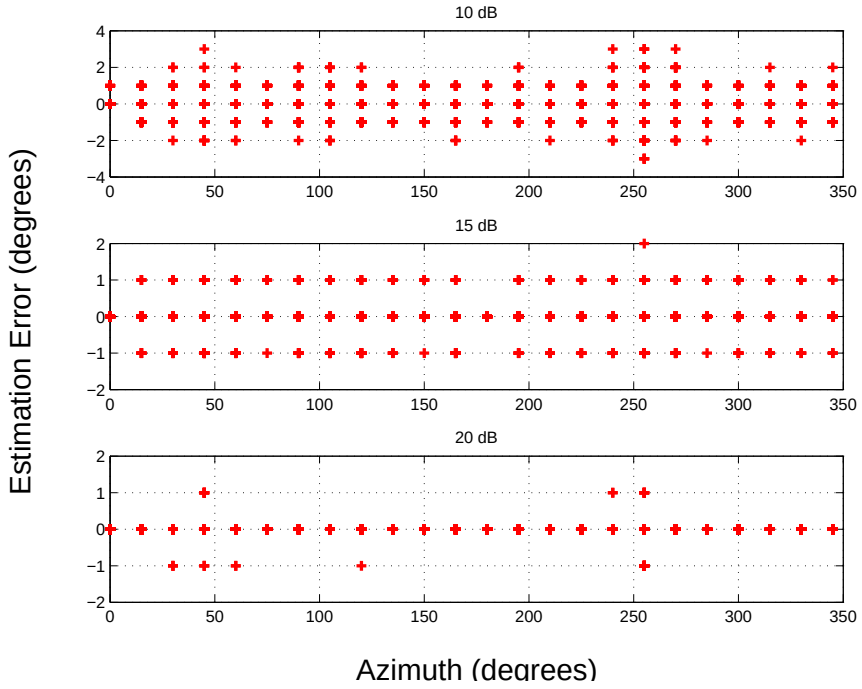

Figure B.5: $f_c = 11$ MHz Error Distribution vs. Azimuth for multiple SNR values using $N_A = 8$ individual feed points.

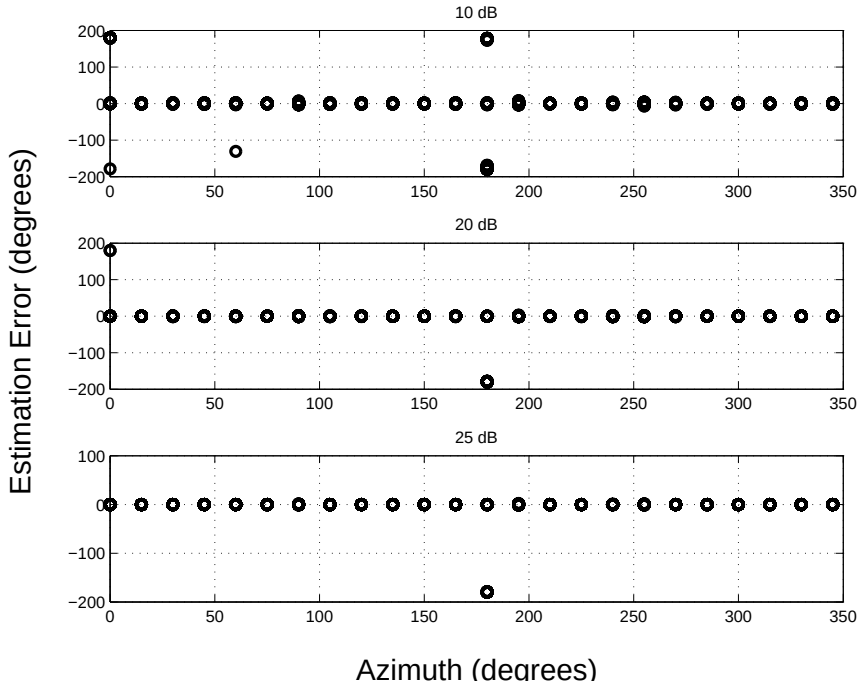

Figure B.6: $f_c = 11$ MHz Error Distribution vs. Azimuth for multiple SNR values using $N_A = 4$ individual feed points.

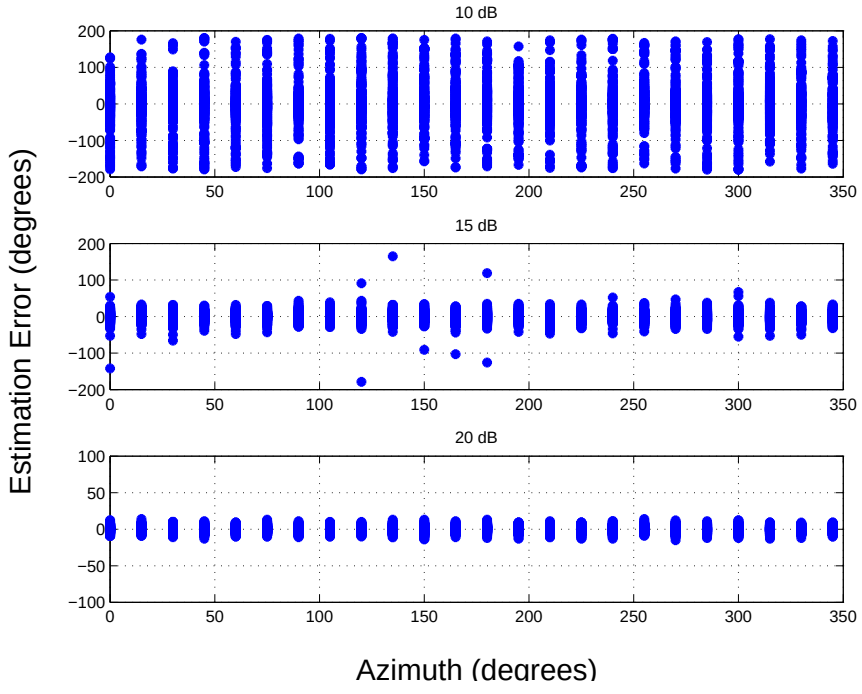

Figure B.7: $f_c = 4$ MHz Error Distribution vs. Azimuth for multiple SNR values using $N_A = 16$ feed points to synthesize a cube antenna pattern.

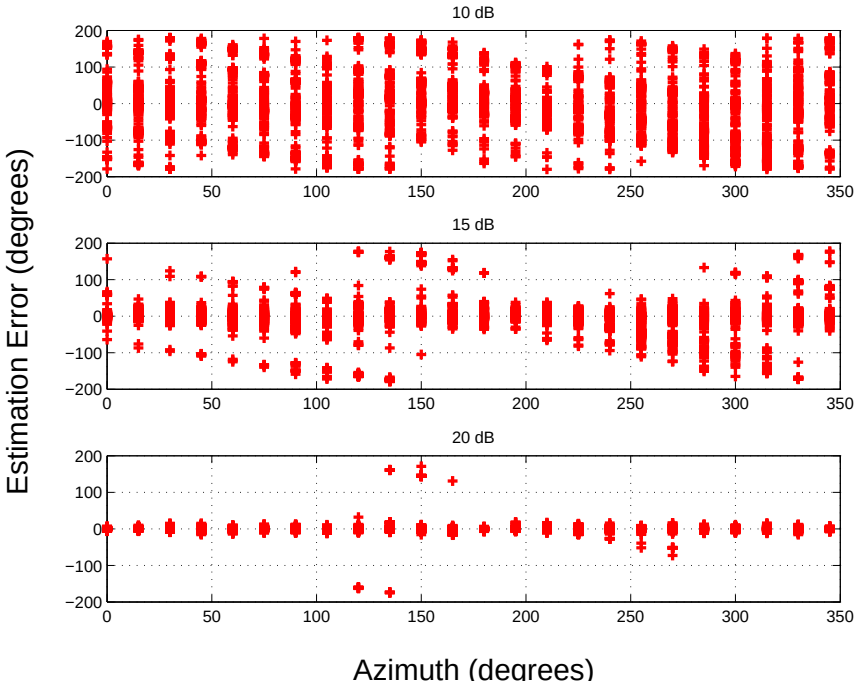

Figure B.8: $f_c = 4$ MHz Error Distribution vs. Azimuth for multiple SNR values using $N_A = 8$ feed points to synthesize a cube antenna pattern.

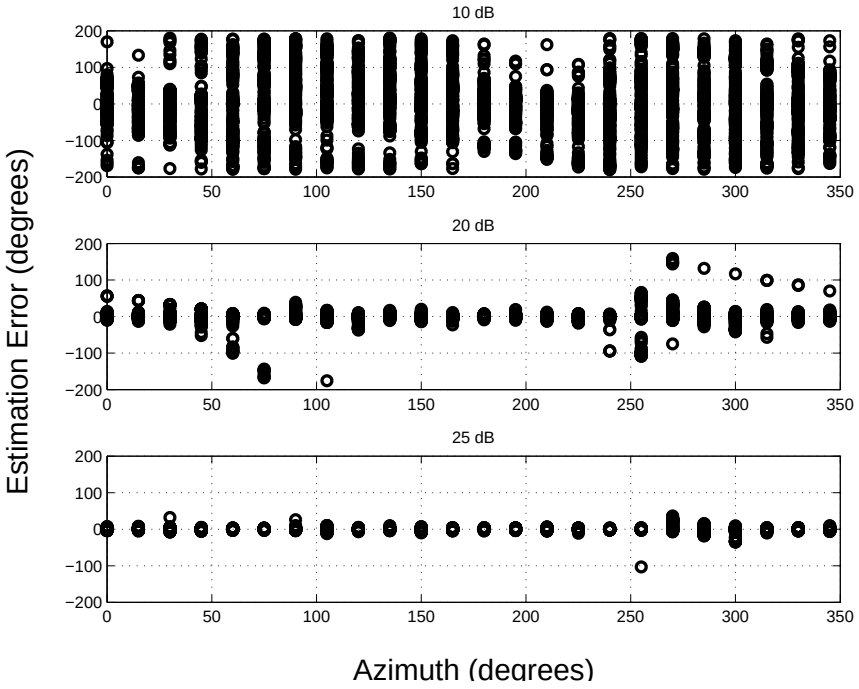

Figure B.9: $f_c = 4$ MHz Error Distribution vs. Azimuth for multiple SNR values using $N_A = 4$ feed points to synthesize a cube antenna pattern.

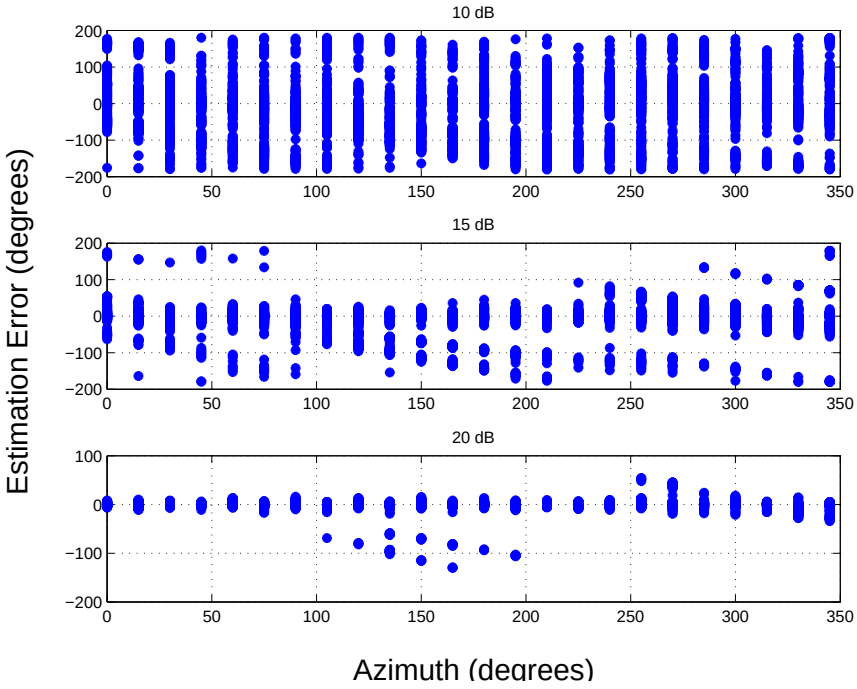

Figure B.10: $f_c = 11$ MHz Error Distribution vs. Azimuth for multiple SNR values using $N_A = 16$ feed points to synthesize a cube antenna pattern.

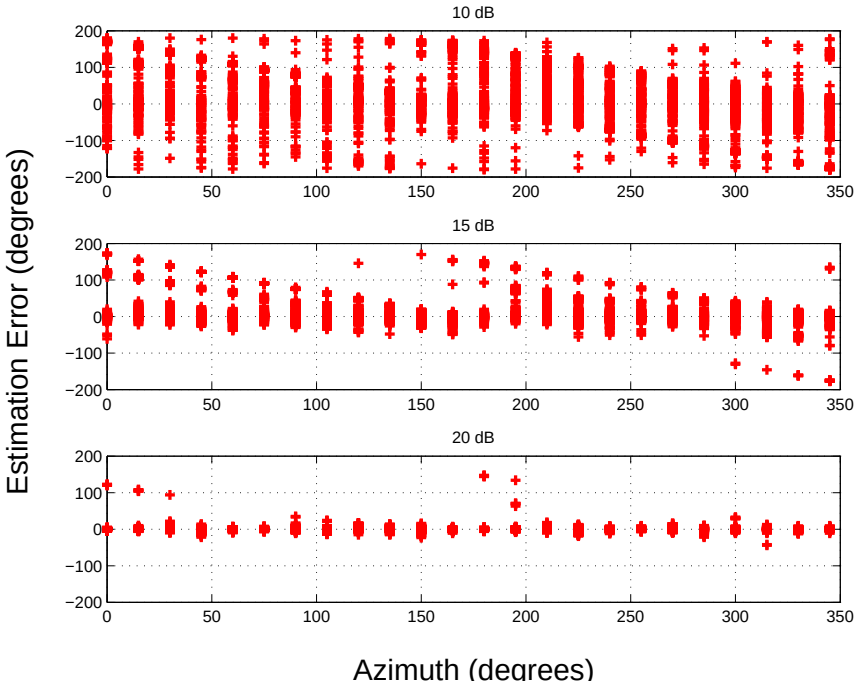

Figure B.11: $f_c = 11$ MHz Error Distribution vs. Azimuth for multiple SNR values using $N_A = 8$ feed points to synthesize a cube antenna pattern.

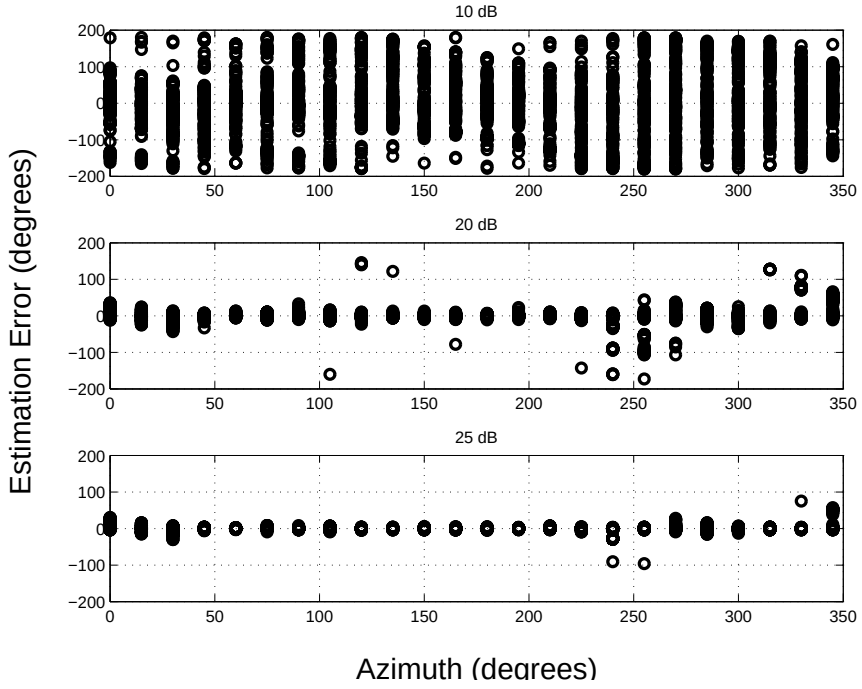

Figure B.12: $f_c = 11$ MHz Error Distribution vs. Azimuth for multiple SNR values using $N_A = 4$ feed points to synthesize a cube antenna pattern.

Appendix C. Approximate Feed Point Location on the Aircraft

This appendix contains the approximate locations of the individual feed points comprising the high frequency direction finding systems for both $f_c = 4$ MHz and $f_c = 11$ MHz. The figures are not to scale.

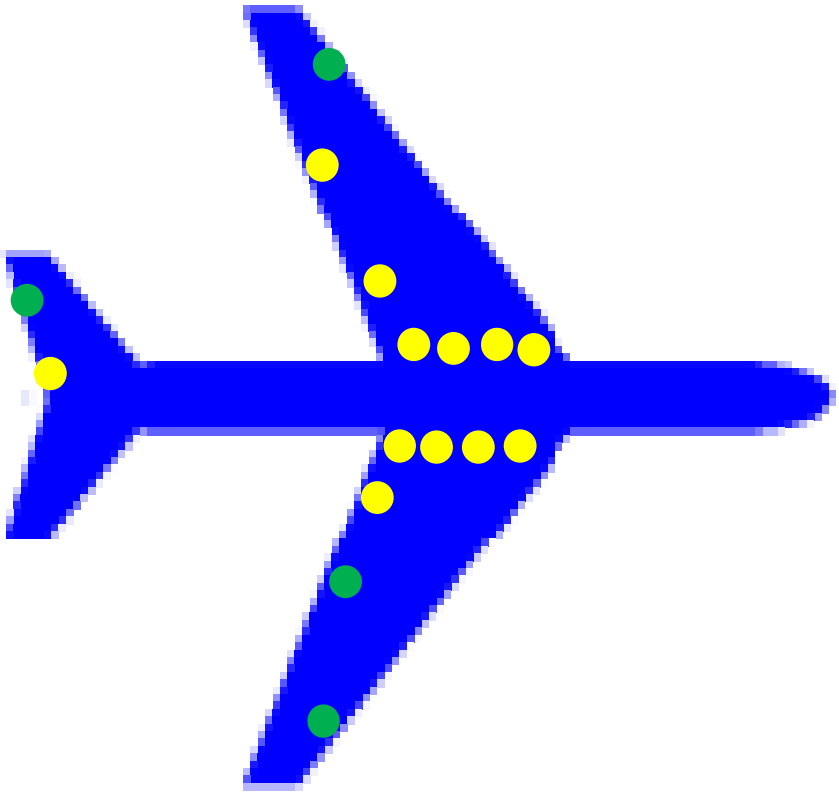

Figure C.1: $f_c = 4$ MHz highest impedence feed point locations shown in green. The feed points are labeled 10, 14, 15, 16 in the BRC data.

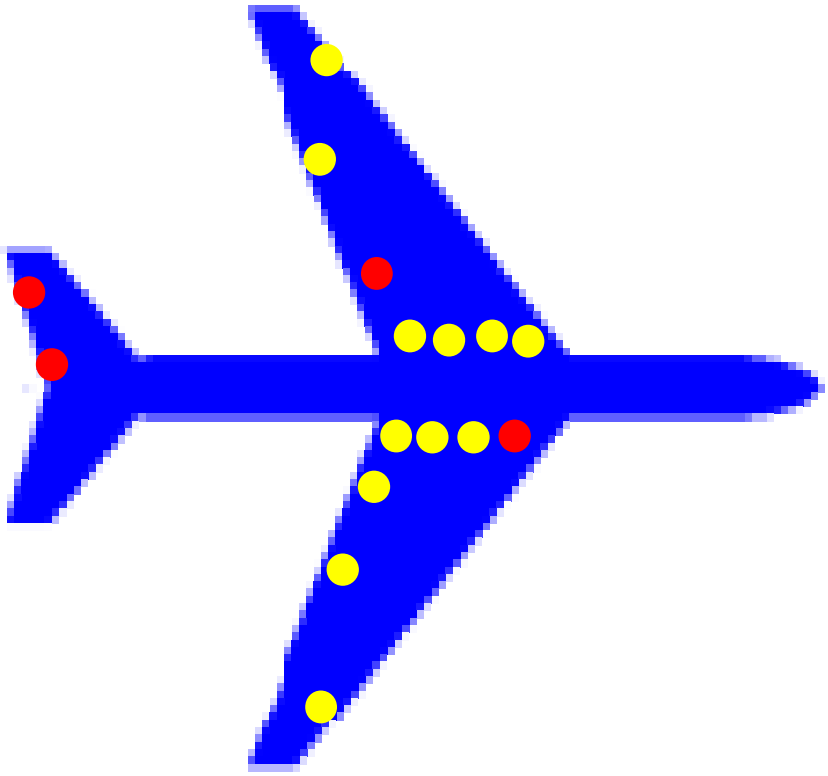

Figure C.2: $f_c = 4$ MHz feed point locations of best random configuration shown in red. The feed points are labeled 6, 11, 13, 14 in the BRC data.

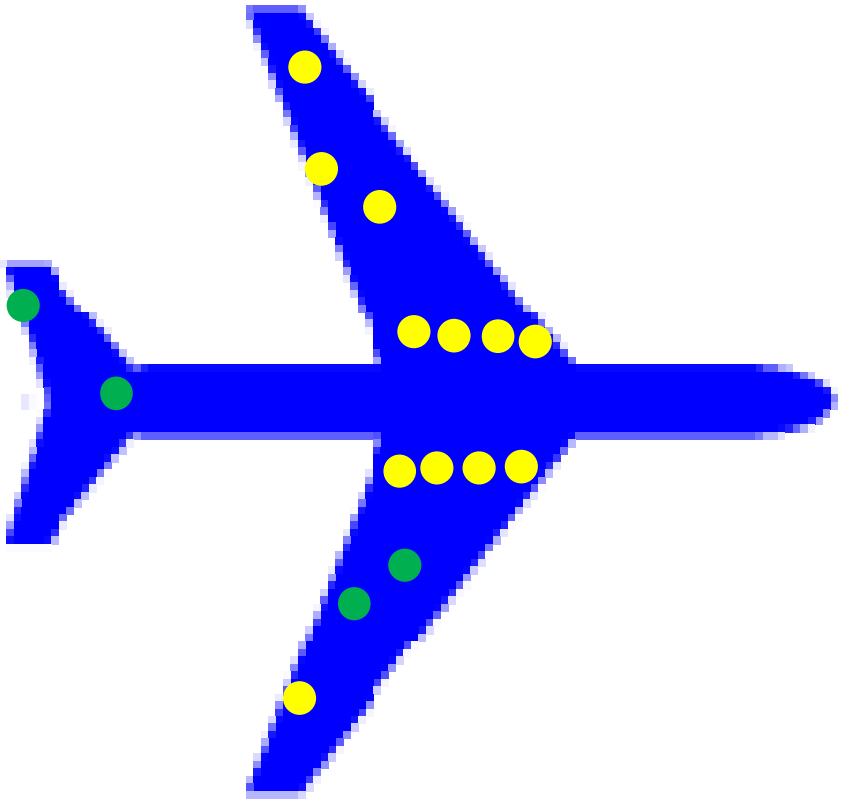

Figure C.3: $f_c = 11$ MHz highest impedence feed point locations shown in green. The feed points are labeled 11, 12, 13, 16 in the BRC data.

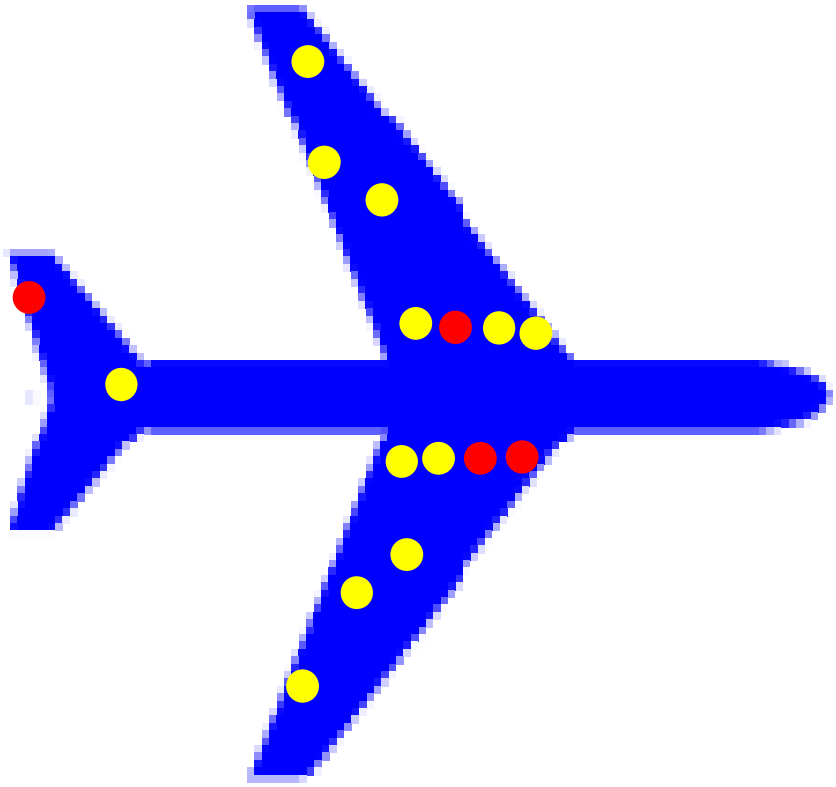

Figure C.4: $f_c = 11$ MHz feed point locations of best random configuration shown in red. The feed points are labeled 1, 3, 5, 16 in the BRC data.

Bibliography

1. "Frequency Allocations and Radio Treaty Matters; General Rules and Regulations," *Code of Federal Regulations*, Title 18, vol. 1, pt 2.102, 2009 ed.
2. R. Wall, "Pentagon OKs restart to COMINT project," *Aviation Weekly & Space Technology*, vol. 157, no. 14, pp. 32–33, 2002.
3. G. A. Akers, "Low band direction finding using an ensemble of structurally integrated antennas," Master's thesis, Air Force Institute of Technology (AU), 2000.
4. D. B. Dixon, "Low-band emitter direction finding and location on UAV-sized platforms," Master's thesis, Air Force Institute of Technology (AU), 2001.
5. R. P. Penno and K. M. Pasala, "Theory of angle estimation using a multiarm spiral antenna," *IEEE Trans. Aerosp. Electron. Syst.*, vol. 37, no. 1, pp. 123–133, 2001.
6. R. L. Kellog, E. E. Mack, and C. D. Crews, *Direction Finding Antennas and Systems*, 4th ed. New York: McGraw-Hil Companies, 2007, ch. 47, pp. 47–2–47–34.
7. R. Schmidt and R. Franks, "Multiple source DF signal processing: An experimental system," *IEEE Trans. Antennas and Propag.*, vol. 34, no. 3, pp. 281–290, 1986.
8. C. A. Balanis, "Antenna theory: a review," *Proc. IEEE*, vol. 80, no. 1, pp. 7–23, 1992.
9. P. Stoica and R. Moses, *Spectral Analysis of Signals*. Upper Saddle River, NJ: Prentice Hall, 2005.
10. S. M. Sherman, *Monopulse Principles and Techniques*. Dedham, Mass.: Artech House, 1984.
11. A. R. Baron, K. P. Davis, and C. B. Hofmann, "Passive direction finding and signal location," *Microwave Journal*, vol. 25, no. 9, pp. 59–76, 1982.
12. J. L. Butler, "Multiple beam antennas," Sanders Associates, Nashua, NH, Internal memo RF 3849, 1960.
13. D. J. Torrieri, "Statistical theory of passive location systems," *IEEE Trans. Aerosp. Electron. Syst.*, vol. 20, no. 2, pp. 183–198, 1984.
14. G. A. Akers and C. F. Corbin, "The effect of the number of modes and feed locations in angle-of-arrival estimation using a multimode antenna," in *Proc. 2010 Nat. Aerospace & Electronics Conf.*, Dayton, OH, July 2010.
15. T. Van, J. Berrie, P. Yan, M. Brewer, T. Van, and D. Latypov, "Direction finding approaches for high frequency applications," BerrieHill Research Corporation, Task No. ART TO-015, Final Report, 2009.

16. J. V. N. Granger, "Wing-cap and tail-cap aircraft antennas," Stanford Research Institute, Technical Report no. 6, 1950.

17. ——, "Shunt-excited flat-plate antennas with applications to aircraft structures," *Proc. IRE*, vol. 38, no. 3, pp. 280–287, 1950.

18. R. Tanner, "Shunt and notch-fed HF aircraft antennas," *IEEE Trans. Antennas Propag.*, vol. 6, no. 1, pp. 35–43, 1958.

19. G. Marrocco and L. Mattioni, "Naval structural antenna systems for broadband HF communications," *IEEE Trans. Antennas Propag.*, vol. 54, no. 4, pp. 1065–1073, 2006.

20. G. Marrocco, L. Mattioni, and V. Martorelli, "Naval structural antenna systems for broadband HF communications part II: Design methodology for real naval platforms," *IEEE Trans. Antennas Propag.*, vol. 54, no. 11, pp. 3330–3337, 2006.

21. R. Garbacz and R. Turpin, "A generalized expansion for radiated and scattered fields," *IEEE Trans. Antennas Propag.*, vol. 19, no. 3, pp. 348–358, 1971.

22. R. Harrington and J. Mautz, "Theory of characteristic modes for conducting bodies," *IEEE Trans. Antennas Propag.*, vol. 19, no. 5, pp. 622–628, 1971.

23. ——, "Computation of characteristic modes for conducting bodies," *IEEE Trans. Antennas Propag.*, vol. 19, no. 5, pp. 629–639, 1971.

24. B. Friedlander, *Classical and Modern Direction-of-Arrival Estimation*, 1st ed. Burlington, MA: Academic Press, 2009, ch. 1, pp. 1–51.

25. T. Van, "Received voltage derived from the reciprocity theorem," BerrieHill Research Corporation, Research note, 2010.

26. M. A. Richards, *Fundamentals of Radar Signal Processing.* New York: McGraw-Hill Companies, 2005, ch. 1, pp. 33–35.

27. E. H. Newman, "Small antenna location synthesis using characteristic modes," *IEEE Trans. Antennas Propag.*, vol. 27, no. 4, pp. 530–531, 1979.

REPORT DOCUMENTATION PAGE

Form Approved
OMB No. 0704–0188

1. REPORT DATE *(DD–MM–YYYY)*	2. REPORT TYPE	3. DATES COVERED *(From — To)*
24–03–2011	Master's Thesis	August 2009-March 2011

4. TITLE AND SUBTITLE

High Frequency Direction Finding
Using Structurally Integrated Antennas
On a Large Airborne Platform

5a. CONTRACT NUMBER

5b. GRANT NUMBER

5c. PROGRAM ELEMENT NUMBER

6. AUTHOR(S)

Corbin, Clair F., 1 Lt, USAF

5d. PROJECT NUMBER

ENG 10-239 & ENG 11-239

5e. TASK NUMBER

5f. WORK UNIT NUMBER

7. PERFORMING ORGANIZATION NAME(S) AND ADDRESS(ES)

Air Force Institute of Technology
Graduate School of Engineering and Management (AFIT/EN)
2950 Hobson Way
WPAFB OH 45433-7765 DSN: 785-3636

8. PERFORMING ORGANIZATION REPORT NUMBER

AFIT/GE/ENG/11-06

9. SPONSORING / MONITORING AGENCY NAME(S) AND ADDRESS(ES)

Air Force Research Laboratory, AFMC
Attn: AFRL/RYWC (Dr. Philip Mumford)
2241 Avionics Circle, Bldg 620
WPAFB OH 45433-7734
(937)938-8553
Philip.Mumford@wpafb.af.mil

10. SPONSOR/MONITOR'S ACRONYM(S)

AFRL/RYWC

11. SPONSOR/MONITOR'S REPORT NUMBER(S)

12. DISTRIBUTION / AVAILABILITY STATEMENT

APPROVED FOR PUBLIC RELEASE; DISTRIBUTION UNLIMITED;
THIS MATERIAL IS DECLARED A WORK OF THE U.S. GOVERNMENT AND
IS NOT SUBJECT TO COPYRIGHT PROTECTION IN THE UNITED STATES

13. SUPPLEMENTARY NOTES

14. ABSTRACT

Estimating the angle of arrival (AOA) of a high frequency (HF) signal, 2-32 MHz, is challenging, especially if the antenna array is installed on a platform with dimensions on the order of one wavelength. Accurate AOA estimates are necessary for search and rescue operations and geolocating RF emitters of interest. This research examines the performance of a direction finding (DF) system using structurally integrated (SI) antennas installed on an airborne platform which allows the aircraft structure to become the receiving element. Two simulated DF systems are analyzed at 4 and 11 MHz. The relationship between the number of SI antennas used and the AOA accuracy is examined by simulating systems using 4, 8, and 16 antennas. Simulations are also performed using the SI array to synthesize the pattern of a 3-loop cube, or vector, antenna. The maximum likelihood algorithm is used to produce AOA estimates. An array of SI antennas, with a dedicated receiver channel for each antenna, produce more accurate AOA estimates at 11 MHz than at 4 MHz. The accuracy improves when more antennas are included, regardless of frequency. Synthesizing a pattern to perform AOA estimation is an unnecessary step resulting in a suboptimal array for HFDF purposes.

15. SUBJECT TERMS

Angle of arrival, high frequency, direction finding, maximum likelihood estimation, structurally integrated antennas

16. SECURITY CLASSIFICATION OF:			17. LIMITATION OF ABSTRACT	18. NUMBER OF PAGES	19a. NAME OF RESPONSIBLE PERSON
a. REPORT	b. ABSTRACT	c. THIS PAGE			Maj Geoffrey A. Akers (ENG)
U	U	U	UU	128	19b. TELEPHONE NUMBER *(include area code)* (937)255-3636x4659; email:geoffrey.akers@afit.edu